Threading-Gated Photochromism in [2]Pseudorotaxanes

Giorgio Baggi,[†] Lorenzo Casimiro,[‡¶] Massimo Baroncini,[§¶] Serena Silvi,*[‡¶] Alberto Credi,[§¶] and Stephen J. Loeb*[†]

[†] Department of Chemistry and Biochemistry, University of Windsor, Windsor, ON, N9B 3P4, Canada.
[‡] Dipartimento di Chimica "G. Ciamician", Università di Bologna, 40126 Bologna, Italy.
[§] Dipartimento di Scienze e Tecnologie Agro-alimentari, Università di Bologna, 40127 Bologna, Italy.
[¶] CLAN-Center for Light Activated Nanostructures, Università di Bologna and Consiglio Nazionale delle Ricerche, 40129 Bologna, Italy.

1. GENERAL COMMENTS

Benzo[*b*]thiophene was purchased from AK Scientific. All the other chemicals were obtained from Sigma-Aldrich and used as received. 2-methylbenzo[*b*]thiophene[S1] and 3-bromo-2-methylbenzo[*b*]thiophene[S2] were synthesized according to previously reported procedures. Solvents were dried on molecular sieves according to a previously reported procedure.[S3] Deuterated solvents were obtained from Cambridge Isotope Laboratories and used as received. Column chromatography was performed using Silicycle Ultra Pure Silica Gel (230–400 mesh). Qualitative thin layer chromatography was performed using Silicycle SiliaPlate aluminum backed TLC plates (200 μm thickness).

Solution ^1H, ^{13}C, ^1H-^1H COSY, EXSY and NOESY/ROESY NMR spectra were recorded on a Brüker Avance III console equipped with an 11.7 T magnet, $\nu_o(^1H) = 500$ MHz and $\nu_o(^{13}C) = 125.7$ MHz; chemical shifts are quoted in ppm relative to tetramethylsilane by using the residual solvent peak as a reference. All peak positions are listed in ppm relative to TMS.

All spectroscopic measurements were performed in quartz cuvettes on air-equilibrated CH_2Cl_2 (Uvasol) solutions at room temperature. UV-vis spectra were recorded either with Perkin Elmer Lambda750, Perkin Elmer Lambda650, Agilent Technologies Cary 300, or Varian Cary 50 Bio spectrophotometers. Emission spectra were recorded on Varian Cary Eclipse or Edinburgh FLS980 fluorescence spectrometers. Fluorescence lifetimes were measured with a time-correlated single photon counting, using a laser diode (320 nm, 340 nm, 360 nm) as excitation source.

Irradiation experiments for UV-Vis studies were performed on air-equilibrated solutions, thoroughly stirred, at room temperature. A Hanau Q400 mercury medium pressure lamp (125 W), with an appropriate interference filter, or a fluorometer were used as sources of irradiation. Irradiation experiments for ^1H NMR studies were performed on samples (20 mM in CD_2Cl_2) contained in quartz NMR tubes, placed in a Luzchem LZC-ICH2 photoreactor equipped with 16 UV fluorescent lamps of the opportune wavelength (UVA, UVB, or UVC), for a total intensity of 4.8 mW/cm^2.

Melting point analyses were performed on a Stanford Research Systems Opti Melt MPA100. High resolution mass spectrometry (HR-MS) experiments were performed on a Xevo G2-XS time-of-flight (ToF) mass spectrometer, using either liquid injection for Electrospray Ionization (ESI) or direct contact sampling using the Atmospheric Solids Analysis Probe (ASAP). Measurements in ESI(+) sensitivity mode were carried out using solutions prepared by dilution in 50:50 water/acetonitrile with 0.1% formic acid of stock solutions of the samples in dichloromethane/acetonitrile, injected for analysis at a rate of 5 μL/min using a syringe pump. Measurements in ASAP(+) sensitivity mode were carried out using the sample as received.

All single crystal X-ray data were collected on a Bruker D8 Venture diffractometer, equipped

with a PHOTON 100 detector, Kappa goniometer, and collected using a Mo sealed tube source or a Cu high brilliance IμS microfocus source. Crystals were frozen in paratone oil inside a cryoloop and reflection data were integrated using APEX III software.

2. SYNTHESIS AND CHARACTERIZATION
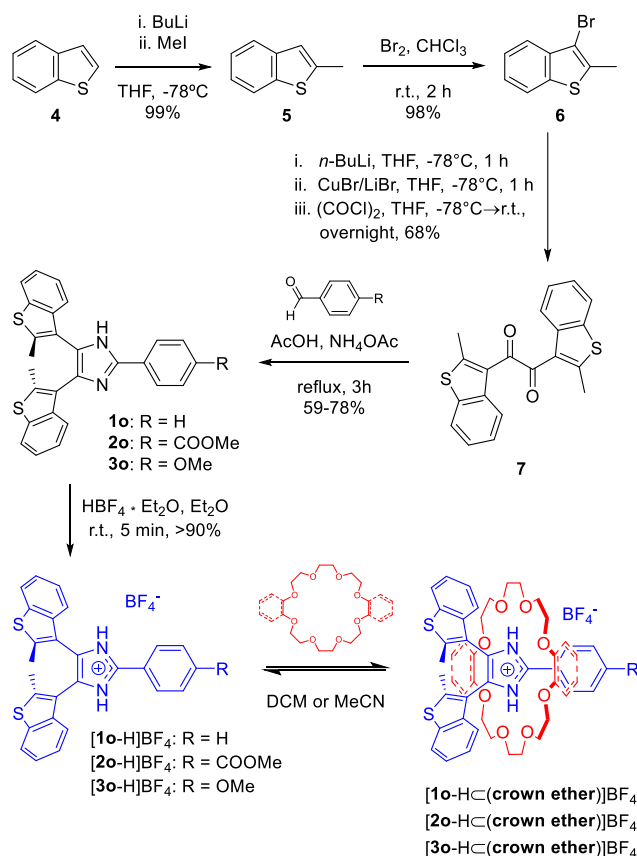
Scheme S1. Synthesis of Bis(thienyl)imidazolium Axles and [2]Pseudorotaxane Formation

Synthesis of 1,2-bis(2-methylbenzo[b]thiophen-3-yl)ethane-1,2-dione
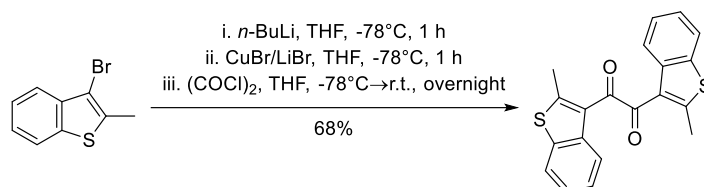

A solution of *n*-BuLi in hexane (1.6 M, 13.75 mL, 22 mmol) was added dropwise to a solution of 3-bromo-2-methylbenzo*[b]*thiophene (5.0 g, 22 mmol) in anhydrous and degassed THF (35 mL) cooled to −78° C in an acetone/dry ice bath, and the mixture was stirred at the same temperature of one hour. Meanwhile, CuBr (3.15 g, 22 mmol) and LiBr (1.91g, 22 mmol) were mixed in anhydrous and degassed THF (100 mL), the mixture was stirred until a homogenous solution was obtained, and subsequently cooled to −78° C in an acetone/dry ice bath. The suspension of 3-lithium-2-methylbenzo*[b]*thiophene was cannula-transferred to the cooled CuBr/LiBr solution, and the mixture was stirred at −78° C for one hour. A solution of oxalyl chloride (0.858 mL, 10 mmol) in anhydrous and degassed THF (20 mL) was cooled to −78° C in an acetone/dry ice bath and cannula-transferred to the reaction mixture. The acetone/dry ice bath was removed, and the mixture was stirred overnight. The reaction mixture was carefully quenched with 1M HCl(aq) (100 mL), and the organic layers were evaporated under reduced pressure. The aqueous mixture was

extracted with EtOAc (3 × 100 mL), the organic layers were washed with brine, dried over MgSO$_4$, filtered and evaporated to dryness. The residue was purified by column chromatography (SiO$_2$, hexanes/DCM 1:1, R_f = 0.61) to yield a yellow solid (2.38 g, 68%). M.p.: 168° C. ^{1}H NMR (500 MHz, CDCl$_3$) δ 8.46 (d, J = 8.1 Hz, 2H), 7.80 (d, J = 7.8 Hz, 2H), 7.45 (ddd, J = 8.1, 7.1, 1.3 Hz, 2H), 7.39 (ddd, J = 7.8, 7.1, 1.3 Hz, 2H), 2.74 (s, 6H). ^{13}C NMR (126 MHz, CDCl$_3$) δ 189.39, 156.84, 138.63, 137.23, 127.33, 126.16, 125.26, 124.19, 121.77, 17.38. HR-MS (ASAP-TOF): calcd for $[M/2]^+$, $[C_{10}H_7O_1S_1]^+$, m/z = 175.0218, found m/z = 175.0218.

Synthesis of 1o
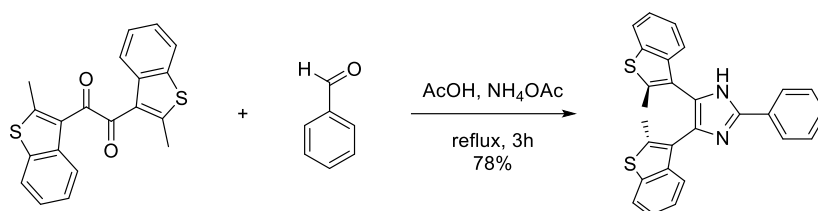
1,2-Bis(2-methylbenzo[b]thiophen-3-yl)ethane-1,2-dione (350.5 mg, 1.0 mmol), benzaldehyde (0.508 mL, 5.0 mmol), and NH$_4$OAc (2.31 g, 30.0 mmol) were mixed in glacial acetic acid (4 mL) and the mixture was refluxed for 3 hours. The reaction mixture was cooled to room temperature and water (20 mL) was added causing the precipitation of a pale yellow powder. The pH of the mixture was brought to 8-9 with NH$_4$OH$_{(aq)}$ and the suspension was left in the ultrasonic bath for 1 hour. The pale yellow solid was filtered, washed exhaustively with water, and air-dried. The crude was purified by column chromatography (SiO$_2$, DCM/EtOAc/AcOH 7:2:1, R_f = 0.28) to yield the pure product as an off-white solid (342 mg, 78%). M.p.: 222° C. ^{1}H NMR (500 MHz, CD$_2$Cl$_2$) δ 9.82 (br s, 1H), 7.98 (d, J = 7.4 Hz, 2H), 7.76 (br m, 3H), 7.64 (br m, 1H), 7.50 (t, J = 7.4 Hz, 2H), 7.43 (t, J = 7.4 Hz, 1H), 7.28 (br m, 4H), 2.02 (s, 6H). ^{13}C NMR (126 MHz, CD$_2$Cl$_2$) δ 147.35, 140.61 (br), 139.94 (br), 138.77, 136.28 (br), 130.77, 129.55, 129.44, 125.74, 124.97 (br), 124.56 (br), 123.66 (br), 122.44 (br), 14.92. HR-MS (ESI-TOF): calcd for $[M + H]^+$, $[C_{27}H_{21}N_2S_2]^+$, m/z = 437.1141, found m/z = 437.1140.

Synthesis of [1o–H]BF$_4$
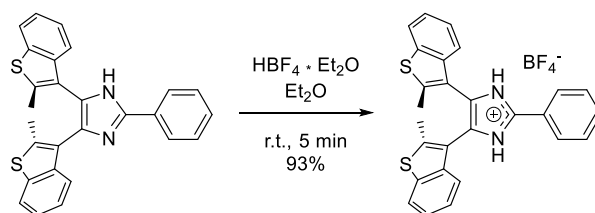
Compound **1** (43.9 mg, 0.10 mmol) was dissolved in Et$_2$O (10 mL) and HBF$_4$·Et$_2$O (15 μL, 0.11 mmol) was added in one portion to the stirred solution, causing the precipitation of a solid. The white powder was filtered, washed exhaustively with Et$_2$O, and air dried (49 mg, 93%). M.p.:

decomposition above 165° C. ^{1}H NMR (500 MHz, CD$_2$Cl$_2$) δ 8.03 (dd, J = 6.9, 1.0 Hz, 2H), 7.75 (dd, J = 7.9, 1.3 Hz, 2H), 7.67 (tt, J = 7.4, 1.0 Hz, 1H), 7.61 (dd, J = 7.4, 6.9 Hz, 2H), 7.40 (d, J = 8.0 Hz, 2H), 7.30 (ddd, J = 8.0, 7.6, 1.3 Hz, 2H), 7.24 (t, J = 7.6 Hz, 2H), 2.24 (s, 6H). ^{13}C NMR (126 MHz, CD$_2$Cl$_2$) δ 146.78, 144.94, 138.79, 138.71, 133.79, 130.61, 127.84, 126.76, 125.60, 125.30, 123.00, 122.70, 121.65, 118.64, 15.20. HR-MS (ESI-TOF): calcd for [**M** + H]$^+$, [C$_{27}$H$_{21}$N$_2$S$_2$]$^+$, m/z = 437.1141, found m/z = 437.1140.

Synthesis of 2o
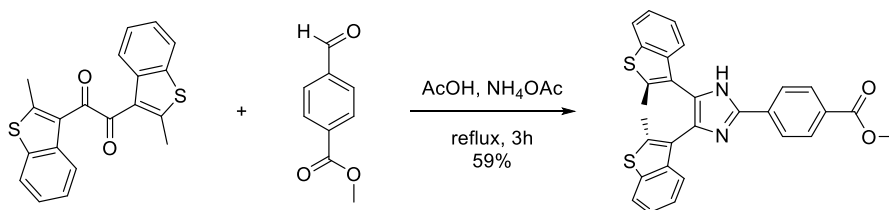
1,2-Bis(2-methylbenzo[b]thiophen-3-yl)ethane-1,2-dione (350.5 mg, 1.0 mmol), methyl 4-formylbenzoate (820.8 mg, 5.0 mmol), and NH$_4$OAc (2.31 g, 30.0 mmol) were mixed in glacial acetic acid (4 mL) and the mixture was refluxed for 3 hours. The reaction mixture was cooled to room temperature and water (20 mL) was added causing the precipitation of a pale yellow powder. The pH of the mixture was brought to 8-9 with NH$_4$OH$_{(aq)}$ and the suspension was left in the ultrasonic bath for 1 hour. The pale yellow solid was filtered, washed exhaustively with water, and air-dried. The crude was purified by column chromatography (SiO$_2$, DCM/EtOAc 19:1, R_f = 0.52) to yield the pure product as an off-white solid (290 mg, 59%). M.p.: 244° C. ^{1}H NMR (500 MHz, CD$_2$Cl$_2$) δ 9.90 (br s, 1H), 8.13 (d, J = 8.5 Hz, 2H), 8.06 (d, J = 8.5 Hz, 2H), 7.82 (d, J = 7.5 Hz, 1H), 7.79 (m, 1H), 7.74 (d, J = 7.6 Hz, 1H), 7.63 (m, 1H), 7.32 (m, 2H), 7.25 (m, 2H), 3.92 (s, 3H), 2.05 (s, 3H), 2.03 (s, 3H). ^{13}C NMR (126 MHz, CD$_2$Cl$_2$) δ 167.21, 146.45, 141.31, 140.68, 139.88, 138.95, 137.03, 134.75, 130.90, 130.87, 127.25, 125.65, 125.43, 124.95, 124.73, 124.39, 123.74, 122.94, 122.35, 52.84, 15.10. HR-MS (ESI-TOF): calcd for [**M** + H]$^+$, [C$_{29}$H$_{23}$N$_2$O$_2$S$_2$]$^+$, m/z = 495.1195, found m/z = 495.1195.

Synthesis of [2o–H]BF$_4$

Compound **2** (49.5 mg, 0.10 mmol) was dissolved in Et$_2$O (10 mL) and HBF$_4$·Et$_2$O (15 μL, 0.11 mmol) was added in one portion to the stirred solution, causing the precipitation of a solid. The white powder was filtered, washed exhaustively with Et$_2$O, and air dried (58 mg, 99%). M.p.:
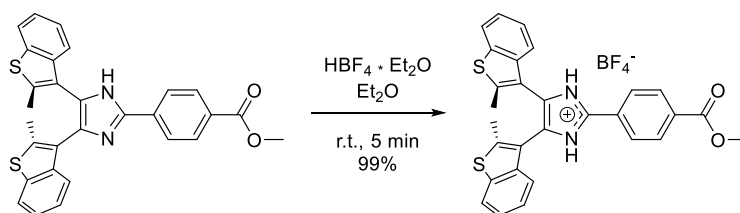
decomposition above 170° C. ^{1}H NMR (500 MHz, CD$_2$Cl$_2$) δ 8.16 (d, J = 8.6 Hz, 2H), 8.11 (d, J = 8.6 Hz, 2H), 7.74 (d, J = 8.1 Hz, 2H), 7.42 (d, J = 8.0 Hz, 2H), 7.29 (td, J = 7.6, 1.2 Hz, 2H), 7.23 (t, J = 7.6 Hz, 2H), 3.87 (s, 3H), 2.25 (s, 6H). ^{13}C NMR (126 MHz, CD$_2$Cl$_2$) δ 166.98, 145.78, 144.89, 138.95, 138.92, 134.21, 131.51, 127.96, 127.93, 127.32, 125.74, 125.46, 123.16, 121.91, 119.16, 53.48, 15.36. HR-MS (ESI-TOF): calcd for [**M** + H]$^+$, [C$_{29}$H$_{23}$N$_2$O$_2$S$_2$]$^+$, m/z = 495.1195, found m/z = 495.1194.

Synthesis of 3o
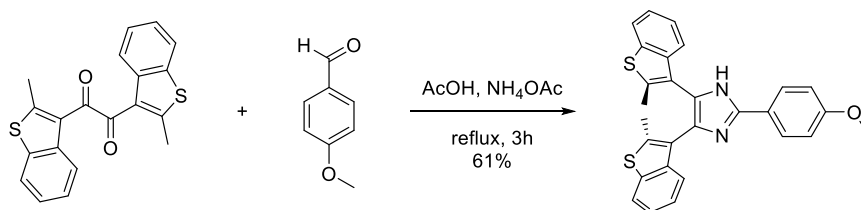
1,2-Bis(2-methylbenzo[*b*]thiophen-3-yl)ethane-1,2-dione (350.5 mg, 1.0 mmol), 4-methoxybenzaldehyde (0.608 mL, 5.0 mmol), and NH$_4$OAc (2.31 g, 30.0 mmol) were mixed in glacial acetic acid (4 mL) and the mixture was refluxed for 3 hours. The reaction mixture was cooled to room temperature and water (20 mL) was added causing the formation of a sticky brown precipitate. The pH of the mixture was brought to 8-9 with NH$_4$OH$_{(aq)}$ and the mixture was extracted with DCM (3 × 20 mL). The organic layers were washed with brine, dried over MgSO$_4$, filtered and evaporated to dryness. The residue was purified by column chromatography (SiO$_2$, DCM/EtOAc/Et$_3$N 19:1:0.1, R_f = 0.43) to yield the pure product as yellow solid (287 mg, 61%). M.p.: 229° C. ^{1}H NMR (500 MHz, CD$_2$Cl$_2$) δ 9.53 (br s, 1H), 7.91 (d, J = 8.8 Hz, 2H), 7.85 (d, J = 6.5 Hz, 1H), 7.78 (m, 1H), 7.73 (d, J = 7.0, 1H), 7.65 (m, 1H), 7.31 (m, 2H), 7.24 (m, 2H), 7.03 (d, J = 8.8 Hz, 2H), 3.88 (s, 3H), 2.06 (s, 3H), 2.03 (s, 3H). ^{13}C NMR (126 MHz, CD$_2$Cl$_2$) δ 161.17, 147.61, 140.37, 139.84, 138.91, 127.47, 124.99, 124.57, 123.48, 123.09, 122.62, 115.08, 56.13, 15.08. HR-MS (ESI-TOF): calcd for [**M** + H]$^+$, [C$_{28}$H$_{23}$N$_2$OS$_2$]$^+$, m/z = 467.1246, found m/z = 467.1248.

## Synthesis of [3o–H]BF$_4$

Compound **3** (46.7 mg, 0.10 mmol) was dissolved in Et$_2$O (10 mL) and HBF$_4$·Et$_2$O (15 μL, 0.11 mmol) was added in one portion to the stirred solution, causing the precipitation of a solid. The white powder was filtered, washed exhaustively with Et$_2$O, and air dried (55 mg, 99%). M.p.:
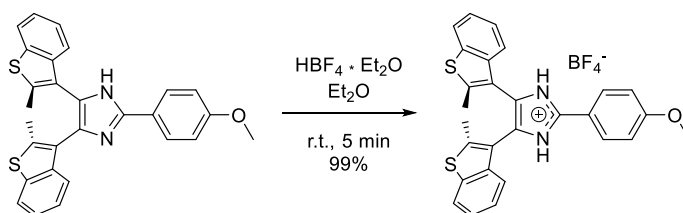
decomposition above 160° C. ^{1}H NMR (500 MHz, CD$_2$Cl$_2$) δ 7.89 (d, J = 8.9 Hz, 2H), 7.72 (d, J = 7.9 Hz, 2H), 7.45 (d, J = 8.0 Hz, 2H), 7.27 (t, J = 7.6 Hz, 2H), 7.21 (t, J = 7.6 Hz, 2H), 7.03 (d, J = 8.9 Hz, 2H), 3.90 (s, 3H), 2.01 (s, 6H). ^{13}C NMR (126 MHz, CD$_2$Cl$_2$) δ 164.00, 147.06, 144.40, 138.87, 138.79, 129.60, 126.38, 125.49, 125.20, 122.95, 121.79, 119.24, 115.99, 115.50, 56.46, 15.18. HR-MS (ESI-TOF): calcd for [**M** + H]$^+$, [C$_{28}$H$_{23}$N$_2$OS$_2$]$^+$, m/z = 467.1246, found m/z = 467.1249.

3. NMR CHARACTERIZATION

1H NMR - 7
CDCl3
500 MHz

8.47 8.47 8.46 8.45 8.45 7.81 7.81 7.80 7.79 7.79 7.46 7.46 7.45 7.45 7.44 7.43 7.43 7.41 7.40 7.39 7.39 7.38 7.38   2.74

2.00   2.04   1.99 2.12   6.33

δ (ppm)
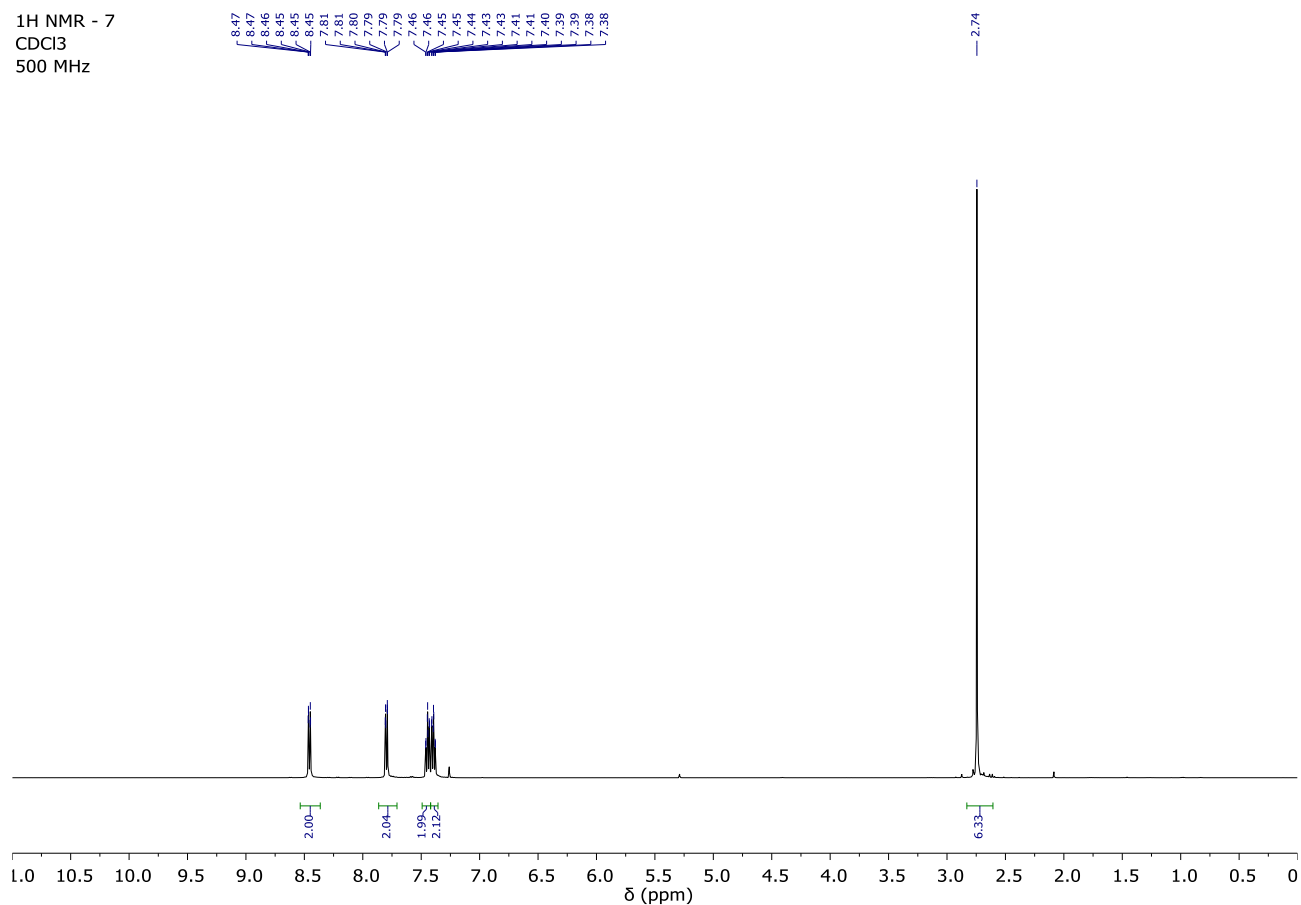
13C NMR - 7
CDCl3
126 MHz

189.39   156.84   138.63 137.23   127.33 126.16 125.26 124.19 121.77   17.38

δ (ppm)
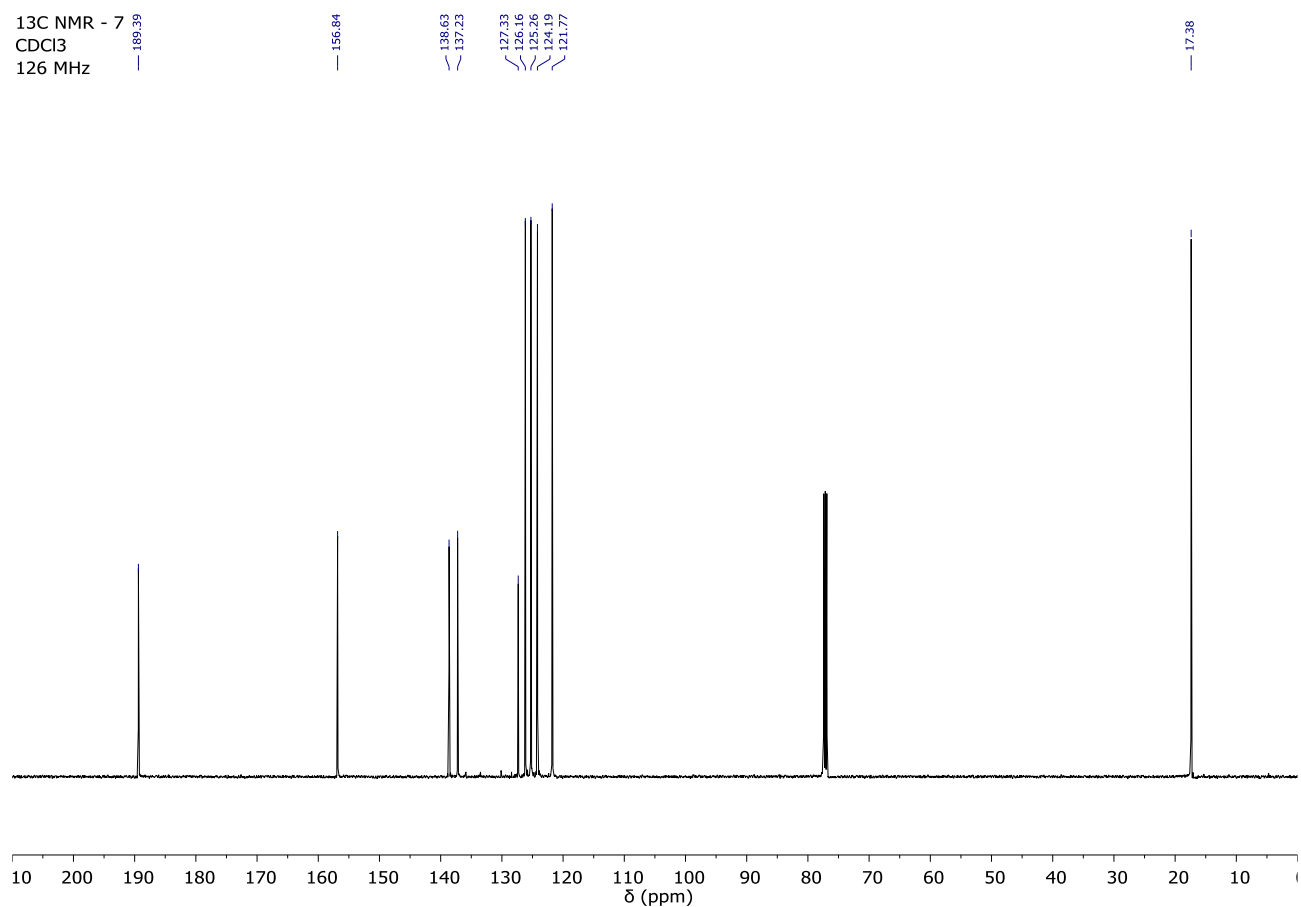
Figure S1. ^{1}H NMR (top) and ^{13}C NMR (bottom) spectra of **7** (CDCl$_3$).

S11
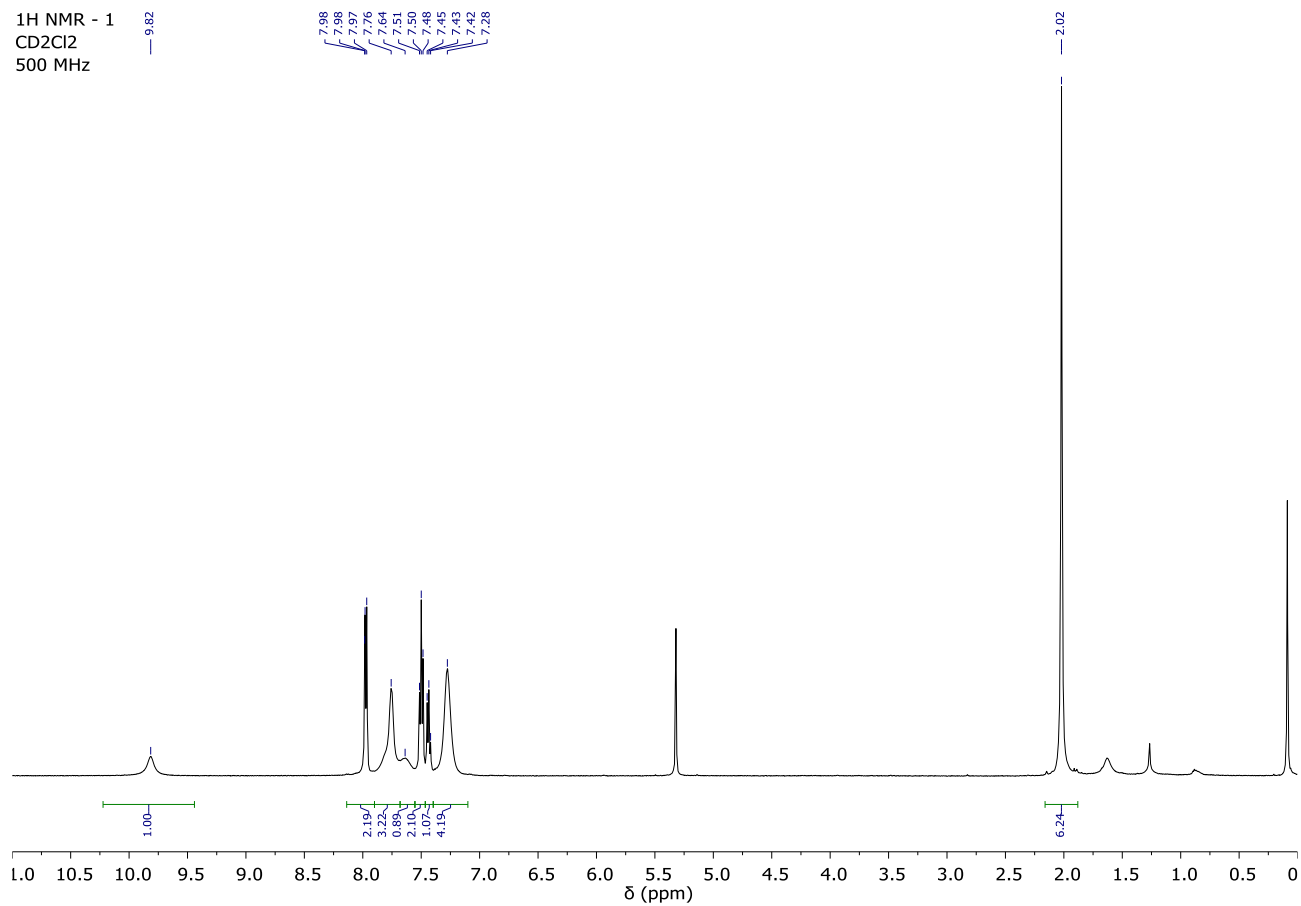
Figure S2. ^{1}H NMR (top) and ^{13}C NMR (bottom) spectra of **1o** (CD$_2$Cl$_2$).

1H NMR - [1-H]BF4
CD2Cl2
500 MHz

8.04 8.04 8.03 8.02 7.76 7.74 7.74 7.69 7.68 7.67 7.66 7.66 7.65 7.63 7.62 7.61 7.60 7.60 7.41 7.40 7.31 7.30 7.29 7.28 7.26 7.24 7.22

2.24

2.09 2.02 1.05 2.06 2.00 2.06 2.03

6.27

δ (ppm)
3.0 12.5 12.0 11.5 11.0 10.5 10.0 9.5 9.0 8.5 8.0 7.5 7.0 6.5 6.0 5.5 5.0 4.5 4.0 3.5 3.0 2.5 2.0 1.5 1.0 0.5 0

13C NMR - [1-H]BF4
CD2Cl2
126 MHz

146.78 144.94 138.79 138.71 133.79 130.61 127.84 126.76 125.60 125.30 123.00 122.70 121.65 118.64

15.20

δ (ppm)
00 190 180 170 160 150 140 130 120 110 100 90 80 70 60 50 40 30 20 10

Figure S3. ^{1}H NMR (top) and ^{13}C NMR (bottom) spectra of [**1o**–H]BF$_4$ (CD$_2$Cl$_2$).

1H NMR - 2
CD2Cl2
500 MHz

9.90
8.15
8.14
8.14
8.13
8.07
8.06
8.06
8.05
8.05
7.83
7.82
7.80
7.79
7.78
7.74
7.73
7.64
7.62
7.33
7.32
7.31
7.31
7.27
7.26
7.25
7.23
7.22

3.92

2.05
2.03

0.97

2.06
2.10
0.96
1.04
1.05
1.02

2.07
2.09

3.22

3.19
3.05

13C NMR - 2
CD2Cl2
126 MHz

167.21

146.45
141.31
140.68
139.88
138.95
137.03
134.75
130.90
130.87
127.25
125.65
125.43
124.95
124.73
124.39
123.74
122.94
122.35

52.84

15.10
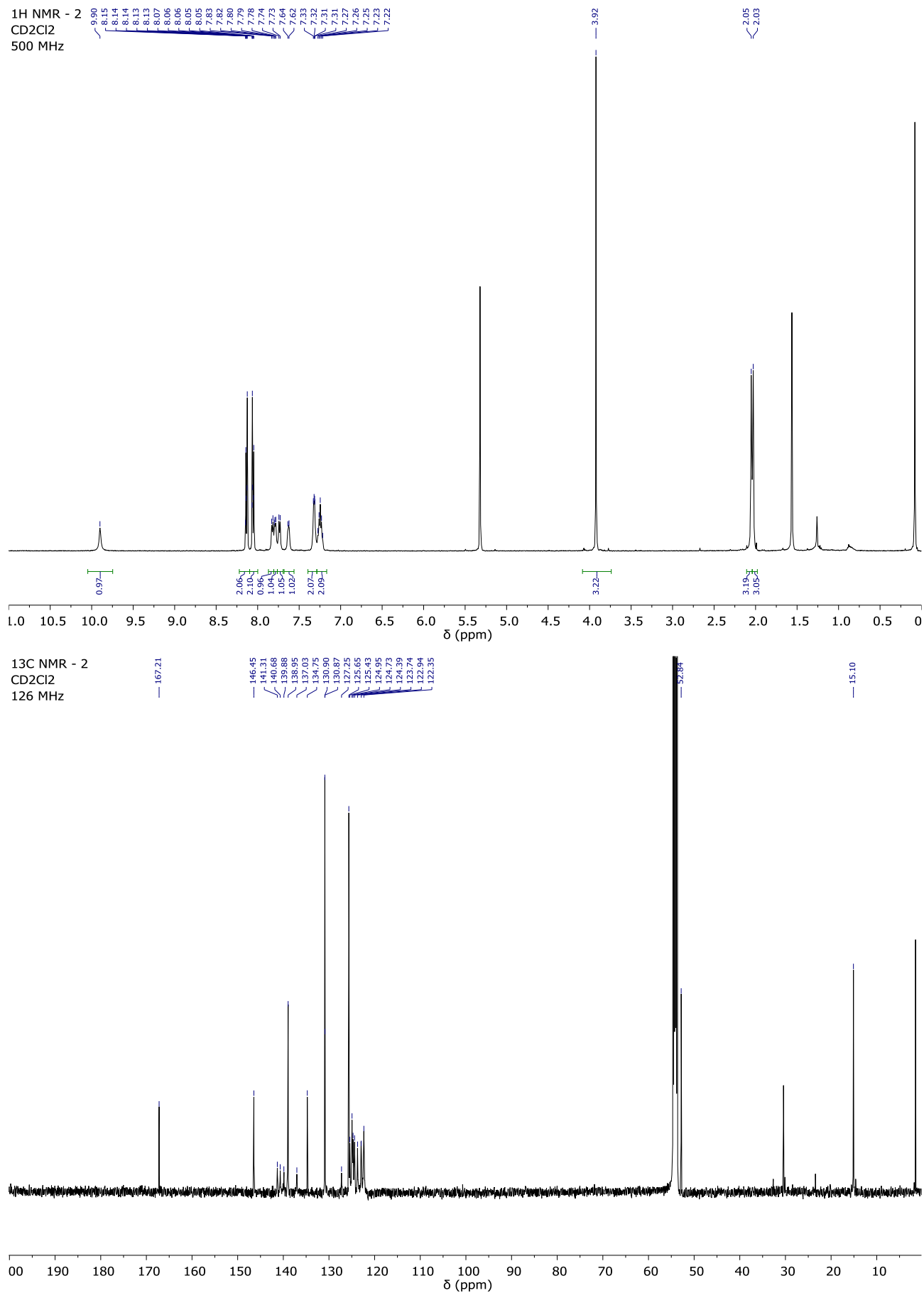
Figure S4. ^{1}H NMR (top) and ^{13}C NMR (bottom) spectra of **2o** (CD$_2$Cl$_2$).

1H NMR - [2-H]BF4
CD2Cl2
500 MHz

8.17, 8.17, 8.16, 8.15, 8.13, 8.12, 8.12, 8.11, 8.11, 7.75, 7.75, 7.74, 7.73, 7.73, 7.43, 7.41, 7.30, 7.29, 7.28, 7.27, 7.27, 7.25, 7.23, 7.22

3.87

2.25

δ (ppm)

13C NMR - [2-H]BF4
CD2Cl2
126 MHz

166.98

145.78, 144.89, 138.95, 138.92, 134.21, 131.51, 127.96, 127.93, 127.32, 125.74, 125.46, 123.16, 121.91, 119.16

53.48

15.36

δ (ppm)

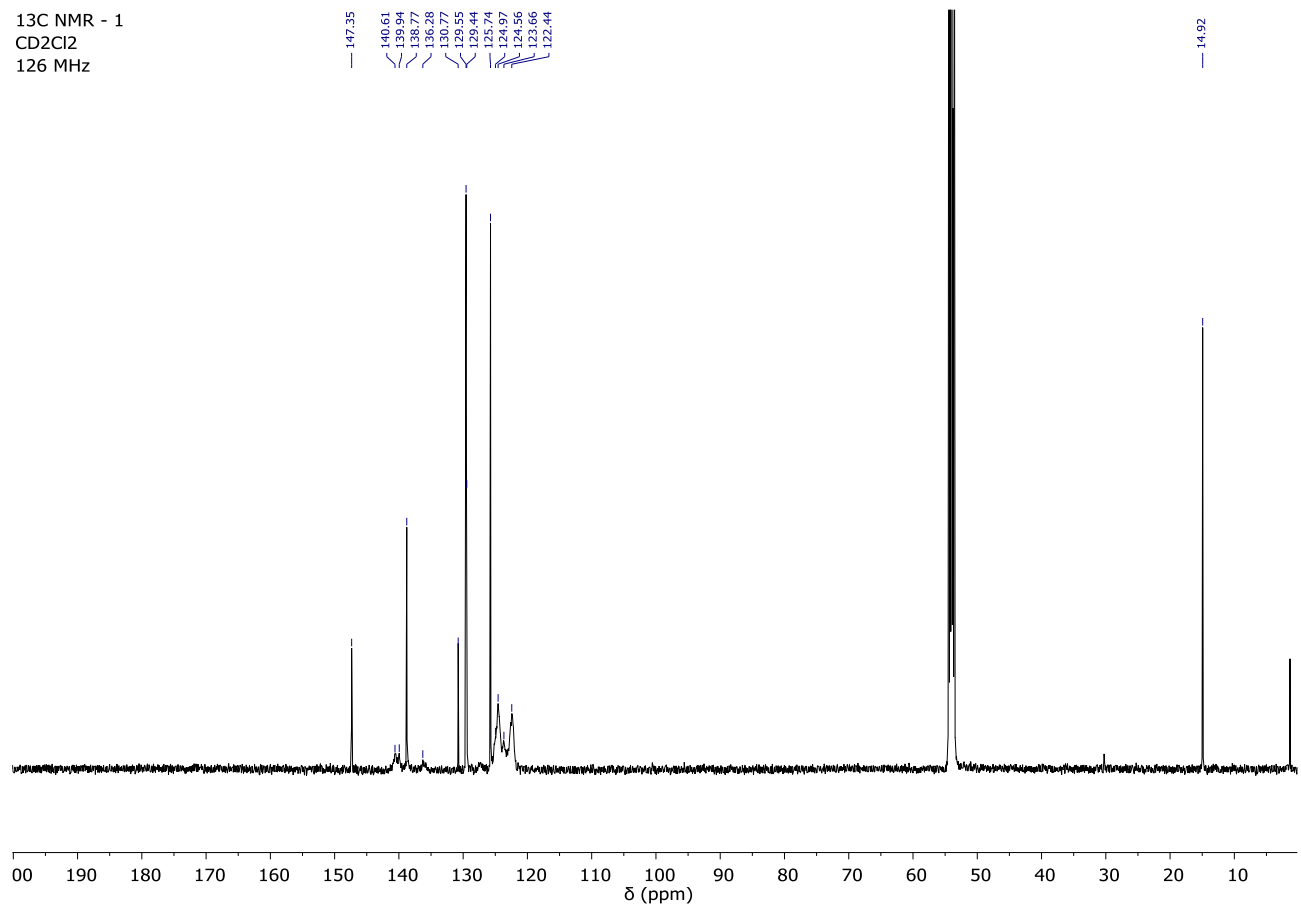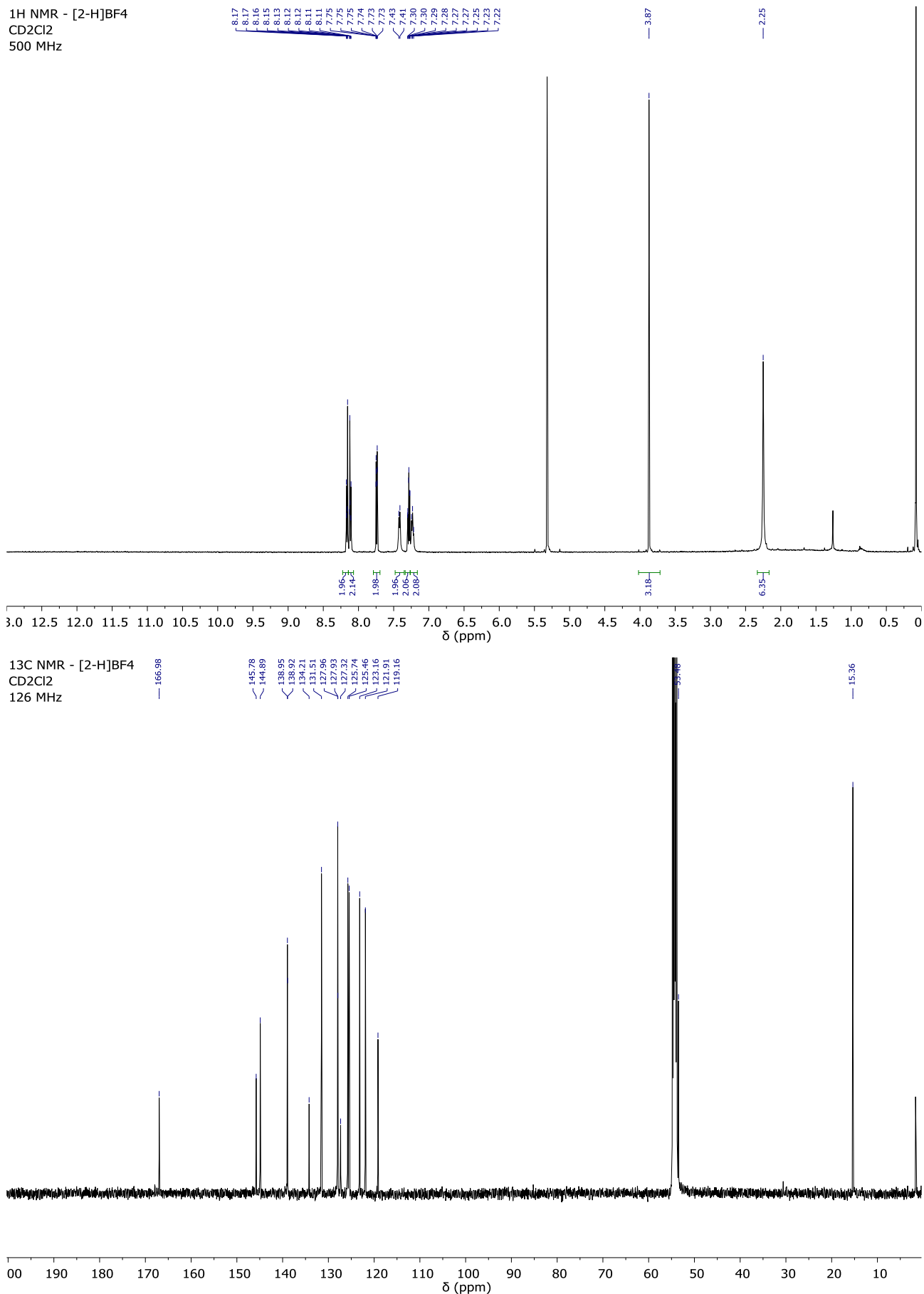**Figure S5.** ^{1}H NMR (top) and ^{13}C NMR (bottom) spectra of [**2o**–H]BF$_4$ (CD$_2$Cl$_2$).
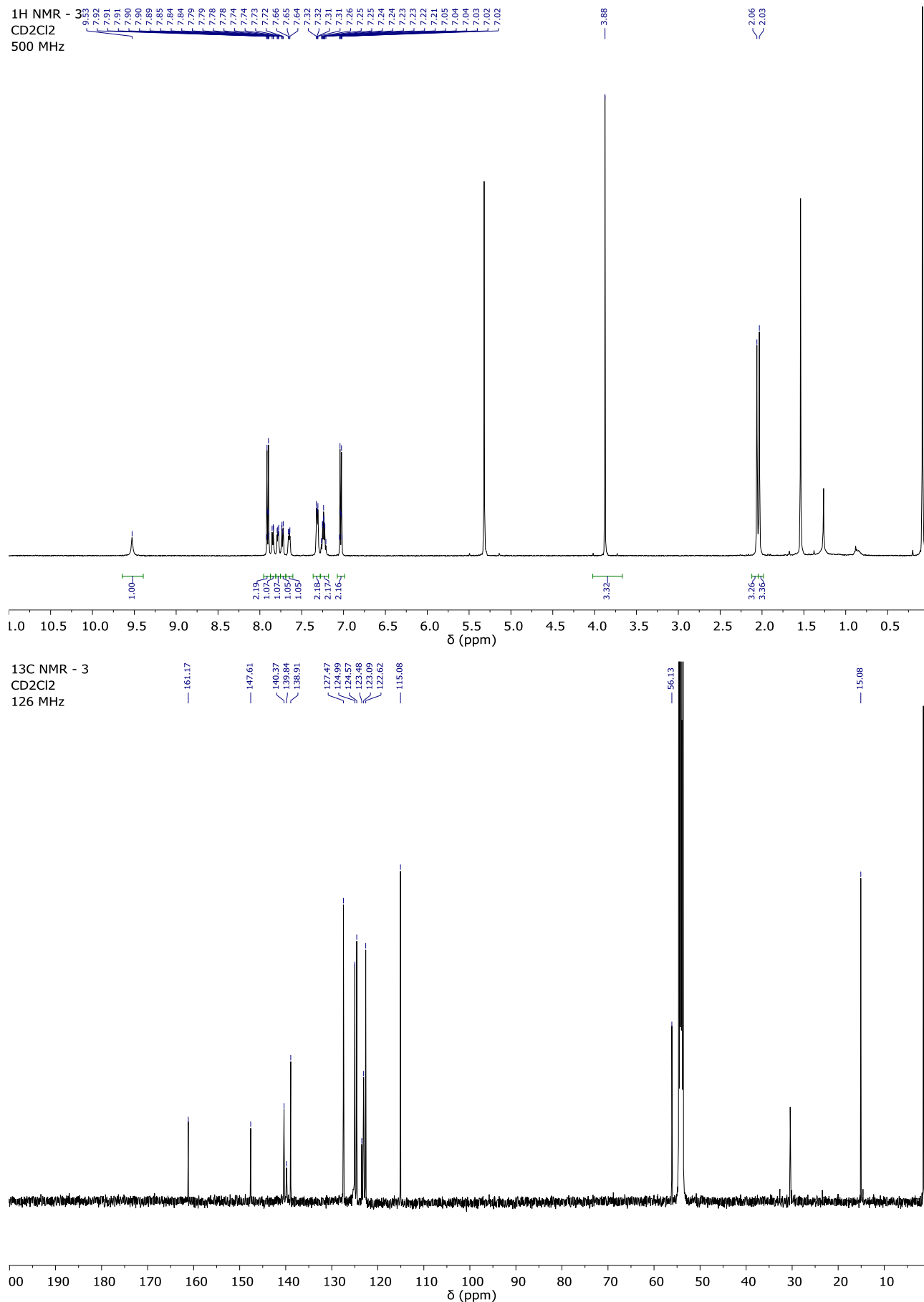
Figure S6. ^1H NMR (top) and ^{13}C NMR (bottom) spectra of **3o** (CD$_2$Cl$_2$).

1H NMR - [3-H]BF4
CD2Cl2
500 MHz

7.90
7.89
7.88
7.73
7.72
7.46
7.44
7.29
7.28
7.28
7.26
7.21
7.19
7.04
7.03
7.02

3.90

2.01

2.10
2.02
2.07
2.15
2.05
2.09

3.47

6.35

12.5 12.0 11.5 11.0 10.5 10.0 9.5 9.0 8.5 8.0 7.5 7.0 6.5 6.0 5.5 5.0 4.5 4.0 3.5 3.0 2.5 2.0 1.5 1.0 0.5 0
δ (ppm)
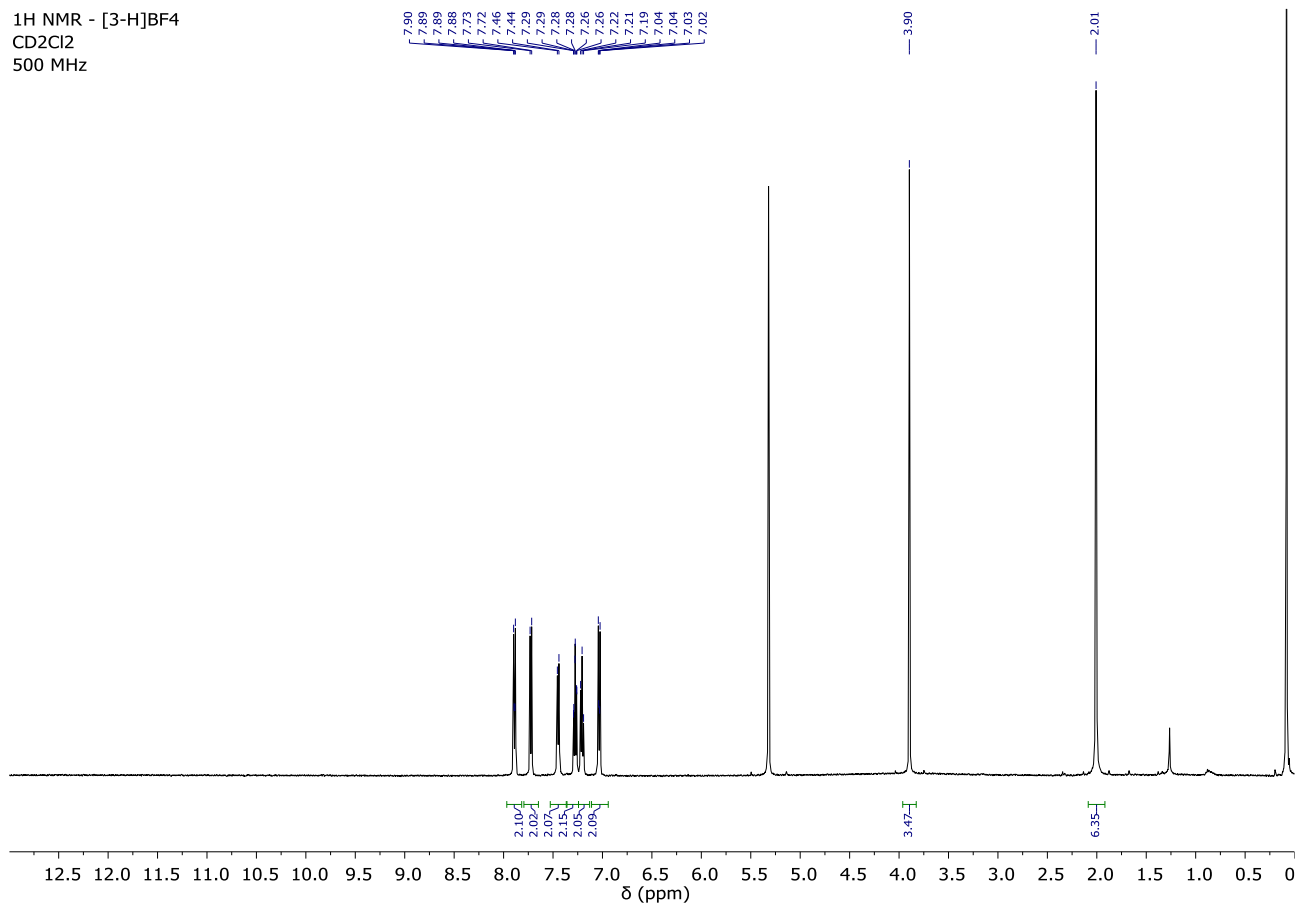
13C NMR - [3-H]BF4
CD2Cl2
126 MHz

164.00

147.06
144.40
138.87
138.79

129.60
126.38
125.49
125.20
122.95
121.79
119.24
115.99
115.50

56.46

15.18

00 190 180 170 160 150 140 130 120 110 100 90 80 70 60 50 40 30 20 10
δ (ppm)

Figure S7. ^{1}H NMR (top) and ^{13}C NMR (bottom) spectra of [**3o**–H]BF$_4$ (CD$_2$Cl$_2$).

4. SINGLE CRYSTAL X-RAY DIFFRACTION STUDIES

Crystals were frozen in paratone oil inside a cryoloop under a cold stream of $N_{2(g)}$. Single crystal X-ray data sets were collected on a Brüker D8 Venture diffractometer equipped with a PHOTON 100 detector, Kappa goniometer, and collected using a Mo sealed tube source or a Cu high brilliance IµS microfocus source. Reflection data were integrated using Bruker APEX III software. The raw area detector data frames were reduced and corrected for absorption effects using the SAINT+ and SADABS programs.[S4] Decay w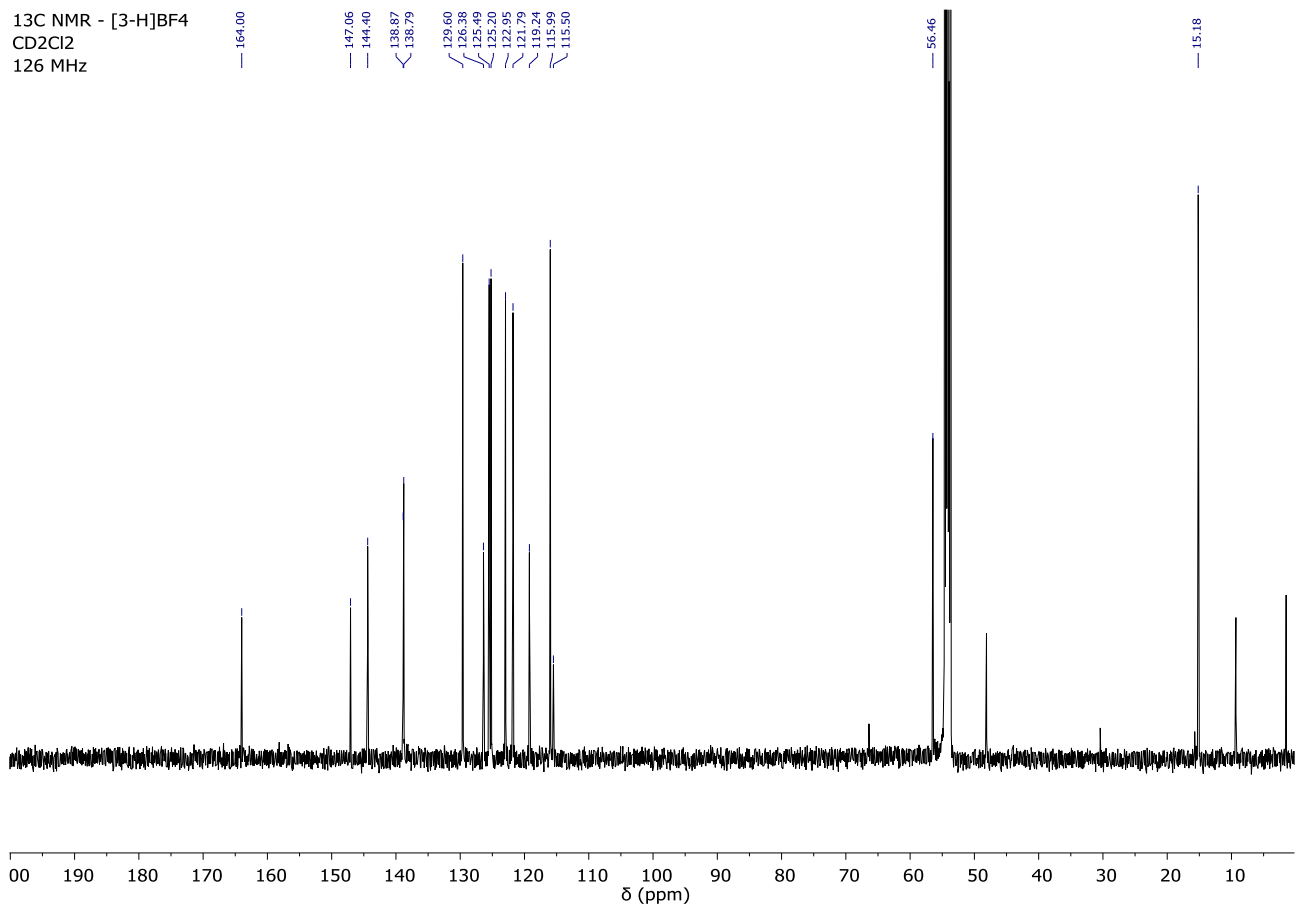as monitored using 50 standard data frames measured at the beginning and end of data collection. Final unit cell parameters were determined by least-squares refinement taken from the data set. Diffraction data and unit-cell parameters were consistent with the assigned space groups. Lorentzian polarization corrections and empirical absorption corrections, based on redundant data at varying effective azimuthal angles, were applied to the data sets. Using Olex2,[S5] the structures were solved with the ShelXS[S6] structure solution program using Direct Methods, completed by subsequent Fourier syntheses and refined using full-matrix least-squares methods against $|F^2|$ data with the XL[S6] refinement package. All non-hydrogen atoms were refined anisotropically and hydrogen atoms placed in idealized positions and refined using a riding model. Scattering factors and anomalous dispersion coefficients are contained in the SHELXTL program library[S6] and figures drawn with Diamond (Crystal Impact).[S7] Details of the structures can be obtained from the Cambridge Crystallographic Data Centre at www.ccdc.cam.ac.uk for CCDC accession numbers 1877446-1877448. Details pertinent to individual data collections and solutions are provided in Tables S1-3.

Single crystal X-ray structure of [1o–H]BF4

Crystals of [**1**-H]BF4 were obtained by slow diffusion of hexanes into an ethyl acetate solution of the compound and were of good quality. The unit cell contained four molecules of positively charged [**1o**–H]$^+$, each one counterbalanced by one tetrafluoroborate anion ($C_{108}H_{84}B_4F_{16}N_8S_8$). The structure was solved in the monoclinic space group $P2_1/c$ with Z = 4. The asymmetric unit consists of one [**1o**–H]$^+$ cation and one BF4$^-$ anion. One of the benzothiophene moieties of [**1o**–H]$^+$ was disordered over two positions with approximately 94:6 occupancy, corresponding to the typical parallel and antiparallel conformations, respectively, of bis(thienyl)ethenes; in addition, the BF4$^-$ anion was disordered over two positions with approximately 79:21 occupancy. All non-hydrogen atoms were refined anisotropically and all hydrogen atoms were placed in idealized positions and refined using a riding model. 1,2- and 1,3-distances of PART 2 of the disordered benzothiophene moiety (S1A, C13A, C14A, C15A, C16A, C17A, C18A, C19A, C20A, C21A) were restrained to be equivalent to the ones of PART 1 (S1, C13, C14, C15, C16, C17A, C18, C19, C20, C21) using the command SAME. The thermal parameters of all the atoms of the disordered tetrafluoroborate anion

were restrained to be approximately equivalent using the command SIMU. The anisotropic displacement parameters of some atoms of the disordered benzothiophene moiety in PART 2 (C13A, C14A, C15A, C18A, C19A, C21A) were constrained to be equal to those of the corresponding atoms in PART 1 (C13, C14, C15, C18, C19, C21) using the command EADP. A summary of the crystal data, solution and refinement parameters are presented in Table S1.

Table S1. Crystal Data, Solution and Refinement Parameters for [**1o**–H]BF$_4$.

CCDC number	1877446	**V (Å^3)**	2477.57(19)
Formula	C$_{27}$H$_{21}$BF$_4$N$_2$S$_2$	**Z**	4
Formula weight	524.39	**ρ, g cm^{-3}**	1.406
Crystal system	Monoclinic	**μ, mm^{-1}**	0.265
Space group	$P2_1/c$ (#14)	**Reflections used**	6152
T (K)	170.00	**variables**	420
a (Å)	9.1113(4)	**restraints**	146
b (Å)	14.2082(7)	**R1 [$I > 2\sigma(I)$]$^{[a]}$**	0.0467
c (Å)	19.2241(8)	**R1 (all data)**	0.0676
α (°)	90	**R2w [$I > 2\sigma(I)$]$^{[b]}$**	0.1022
b (°)	95.410(2)	**R2w (all data)**	0.1128
γ (°)	90	**GOF on F^2**	1.065

[a] R1 = Σ ||F_o| - |F_c|| / Σ |F_o|; [b] R2w = [Σ[$w(F_o^2 - F_c^2)^2$] / Σ[$w(F_o^2)^2$]]$^{1/2}$, [b]where $w = q[\sigma^2(F_o^2) + (aP)^2 + bP]^{-1}$.

Single crystal X-ray structure of [2o–H]BF$_4$·2Et$_2$O

Crystals of [**2o**–H]BF$_4$·2Et$_2$O were obtained by slow diffusion of diethyl ether into an acetonitrile solution of the compound and were of good quality. The unit cell contained two molecules of positively charged [**2o**–H]$^+$, each one counterbalanced by one tetrafluoroborate anion, and a total of four molecules of diethyl ether (C$_{74}$H$_{86}$B$_2$F$_8$N$_4$O$_8$S$_4$). The structure was solved in the triclinic space group P-1 with Z = 4 (Z' = 2). The asymmetric unit consists of one [**2o**–H]$^+$ cation, one BF$_4^-$ anion, and two diethyl ether molecules. One of the diethyl ether molecules was partially disordered over two positions with approximately 85:15 occupancy; in addition, the BF$_4^-$ anion was disordered over two positions with approximately 89:11 occupancy. All non-hydrogen atoms were refined anisotropically and all hydrogen atoms were placed in idealized positions and refined using a riding model. 1,2- and 1,3-distances of PART 2 of the disordered diethyl ether molecule (O1S, C4SA, C5SA) were restrained to be equivalent to the ones of PART 1 (O1S, C4S, C5S) using the command SAME. 1,2- and 1,3-distances of PART 2 of the disordered tetrafluoroborate anion (B1, F1A, F2A, F3A, F4A) were restrained to be equivalent to the ones of PART 1 (B1, F1, F2, F3, F4) using the command SAME. The thermal parameters of all the atoms of the disordered diethyl ether molecule

were restrained to be approximately equivalent using the command SIMU. The anisotropic displacement parameters of the fluorine atoms of the disordered tetrafluoroborate anion and one carbon atom of the disordered diethyl ether molecule in PART 2 (F1A, F2A, F3A, F4A, C4SA) were constrained to be equal to those of the corresponding atoms in PART 1 (F1, F2, F3, F4, C4S) using the command EADP. A summary of the crystal data, solution and refinement parameters are presented in Table S2.

Table S2. Crystal Data, Solution and Refinement Parameters for [**2o**–H]BF$_4$·2Et$_2$O.

CCDC number	1877447	**V (Å^3)**	1827.82(17)
Formula	C$_{18.5}$H$_{21.5}$B$_{0.5}$F$_2$NO$_2$S	**Z**	4
Formula weight	365.33	**ρ, g cm^{-3}**	1.328
Crystal system	Triclinic	**μ, mm^{-1}**	0.208
Space group	*P*-1 (#2)	**Reflections used**	11201
T (K)	130.01	**variables**	485
a (Å)	8.0211(4)	**restraints**	74
b (Å)	11.5905(6)	**R1 [*I* > 2σ(*I*)]$^{[a]}$**	0.0488
c (Å)	20.2484(11)	**R1 (all data)**	0.0627
α (°)	93.738(2)	**R2*w* [*I* > 2σ(*I*)]$^{[b]}$**	0.1175
b (°)	92.017(2)	**R2*w* (all data)**	0.1281
γ (°)	103.011(2)	**GOF on *F*^{2}**	1.042

[a] R1 = Σ ||F$_o$| - |F$_c$|| / Σ |F$_o$|; [b] R2*w* = [Σ[*w*(F$_o^2$ - F$_c^2$)^2] / Σ[*w*(F$_o^2$)^2]]$^{1/2}$, [b]where *w* = *q*[σ^2(F$_o^2$) + (*aP*)^2 + *bP*]$^{-1}$.

Only the anti-parallel conformation of the bis(benzothienyl)imidazolium moiety is displayed in the crystal structure of [**2o**–H]BF$_4$·2Et$_2$O (Figure S8a). Furthermore, in this crystal structure the two imidazolium NH groups prefer hydrogen bonding to the oxygen atom of one diethyl ether solvent molecule each (N–H···O 2.743 Å, 171.48°; and 2.771 Å, 171.13°) rather than interacting with the tetrafluoroborate counter-anion, as observed in the previous example. Interestingly, the two diethyl ether molecules adopt a spatial arrangement around the axle resembling two fragments of a crown ether ring (Figure S8b). Charge-assisted anion-π interactions between imidazolium units and tetrafluoroborate anions generate 1D arrays of alternating [**2o**–H]$^+$ cations and BF$_4^-$ counter-anions, which, together with π-π stacking between adjacent benzothiophene moieties and intercalated methoxycarbonyl units, dictate the formation of two types of 1D channels fully occupied by diethyl ether solvent molecules.
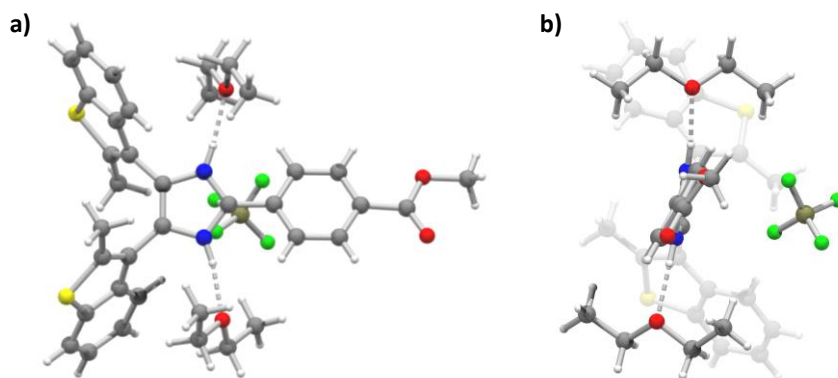
Figure S8. Single-crystal X-ray structure of [**2o**-H]BF$_4$·2Et$_2$O, a) side view and b) frontal view. Color key: C dark grey, N blue, O red, S yellow, B olive green, F bright green, H white; covalent bonds = grey, H-bonds = grey dashed.

Single crystal X-ray structure of [1o–H⊂DB24C8]BF$_4$·Et$_2$O

Crystals of [**1o**–H⊂**DB24C8**]BF$_4$·Et$_2$O were obtained by slow diffusion of diethyl ether into an acetonitrile solution of [**1o**–H]BF$_4$ and excess of **DB24C8** and were of good quality. The unit cell contained four molecules of positively charged [**1o**–H]$^+$, each one threaded into a molecule of **DB24C8** and counterbalanced by one tetrafluoroborate anion, and a total of four molecules of diethyl ether (C$_{220}$H$_{252}$B$_4$F$_{16}$N$_8$O$_{36}$S$_8$). The structure was solved in the monoclinic space group $P2_1/n$ with Z = 4. The asymmetric unit consists of one [**1o**–H⊂**DB24C8**]$^+$ [2]pseudorotaxane, one BF$_4^-$ anion, and one diethyl ether molecule. One of the benzothiophene moieties of [**1o**–H]$^+$ was disordered over two positions with approximately 93:7 occupancy, corresponding to the typical antiparallel and parallel conformations, respectively, of bis(thienyl)ethenes; in addition, the BF$_4^-$ anion was disordered over two positions with approximately 91:9 occupancy, and one portion of the **DB24C8** ring was disordered over two positions with approximately 71:29 occupancy. All non-hydrogen atoms were refined anisotropically and all hydrogen atoms were placed in idealized positions and refined using a riding model. 1,2- and 1,3-distances of PART 2 of the disordered benzothiophene moiety (S2A, C19A, C20A, C21A, C22A, C23A, C24A, C25A, C26A, C27A) were restrained to be equivalent to the ones of PART 1 (S2, C19, C20, C21, C22, C23, C24, C25, C26, C27) using the command SAME. 1,2- and 1,3-distances of PART 2 of the disordered tetrafluoroborate anion (B1, F1A, F2A, F3A, F4A) were restrained to be equivalent to the ones of PART 1 (B1, F1, F2, F3, F4) using the command SAME. All the atoms of PART 2 of the disordered benzothiophene moiety (S2A, C19A, C20A, C21A, C22A, C23A, C24A, C25A, C26A, C27A) were restrained to lie a common plane using the command FLAT. The thermal parameters of all the atoms of the disordered benzothiophene moiety were restrained to be approximately equivalent using the command SIMU. The thermal parameters of the atoms of the diethyl ether molecule (O1S C1S C2S C3S C4S) were subjected to a 'rigid bond' restraint with the command RIGU. The

anisotropic displacement parameters of the fluorine atoms of the disordered tetrafluoroborate anion, of one carbon atom of the disordered benzothiophene moiety, and of one oxygen atom of the disordered portion of the DB24C8 ring in PART 2 (F2A, F3A, F4A, C25A, O8A) were constrained to be equal to those of the corresponding atoms in PART 1 (F2, F3, F4, C25, O8) using the command EADP. A summary of the crystal data, solution and refinement parameters are presented in Table S3.

Table S3. Crystal Data, Solution and Refinement Parameters for [**1o**–H⊂**DB24C8**]BF_4·Et_2O.

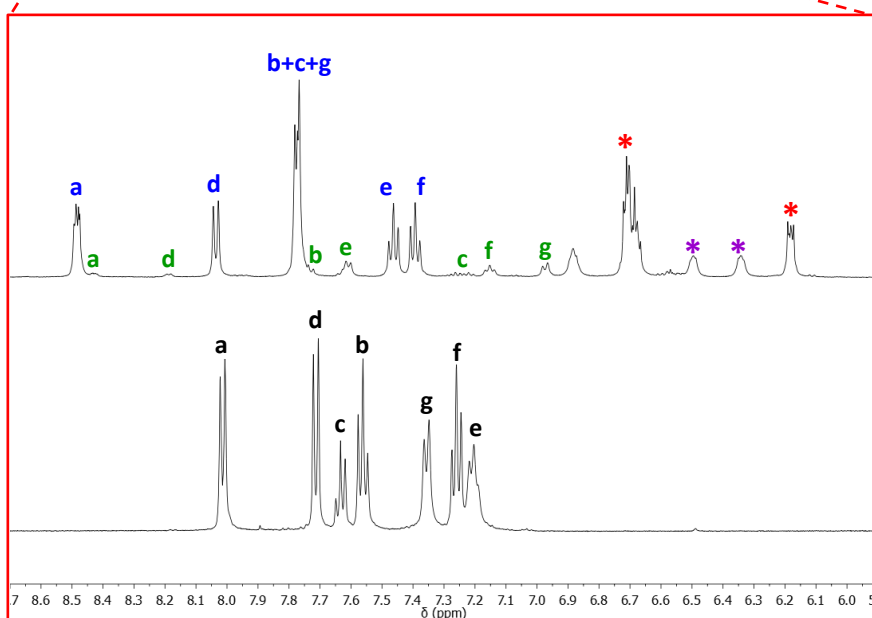|			
CCDC number	1877448	**V ($Å^3$)**	5284.8(4)
Formula	$C_{55}H_{63}BF_4N_2O_9S_2$	**Z**	4
Formula weight	1047.00	**ρ, g cm^{-3}**	1.316
Crystal system	Monoclinic	**μ, mm^{-1}**	0.173
Space group	$P2_1/n$ (#14)	**Reflections used**	13131
T (K)	173.21	**variables**	780
a (Å)	13.2818(6)	**restraints**	363
b (Å)	19.8213(8)	**R1 [$I > 2\sigma(I)$]$^{[a]}$**	0.0836
c (Å)	20.1065(9)	**R1 (all data)**	0.1100
α (°)	90	**R2w [$I > 2\sigma(I)$]$^{[b]}$**	0.2057
b (°)	93.248(2)	**R2w (all data)**	0.2252
γ (°)	90	**GOF on F^2**	1.160

[a] R1 = Σ ||F_o| - |F_c|| / Σ |F_o|; [b] R2w = [Σ[$w(F_o^2 - F_c^2)^2$] / Σ[$w(F_o^2)^2$]]$^{1/2}$, [b]where $w = q[\sigma^2(F_o^2) + (aP)^2 + bP]^{-1}$.

5. ADDITIONAL ^{1}H NMR EXPERIMENTS

[2]Pseudorotaxane formation
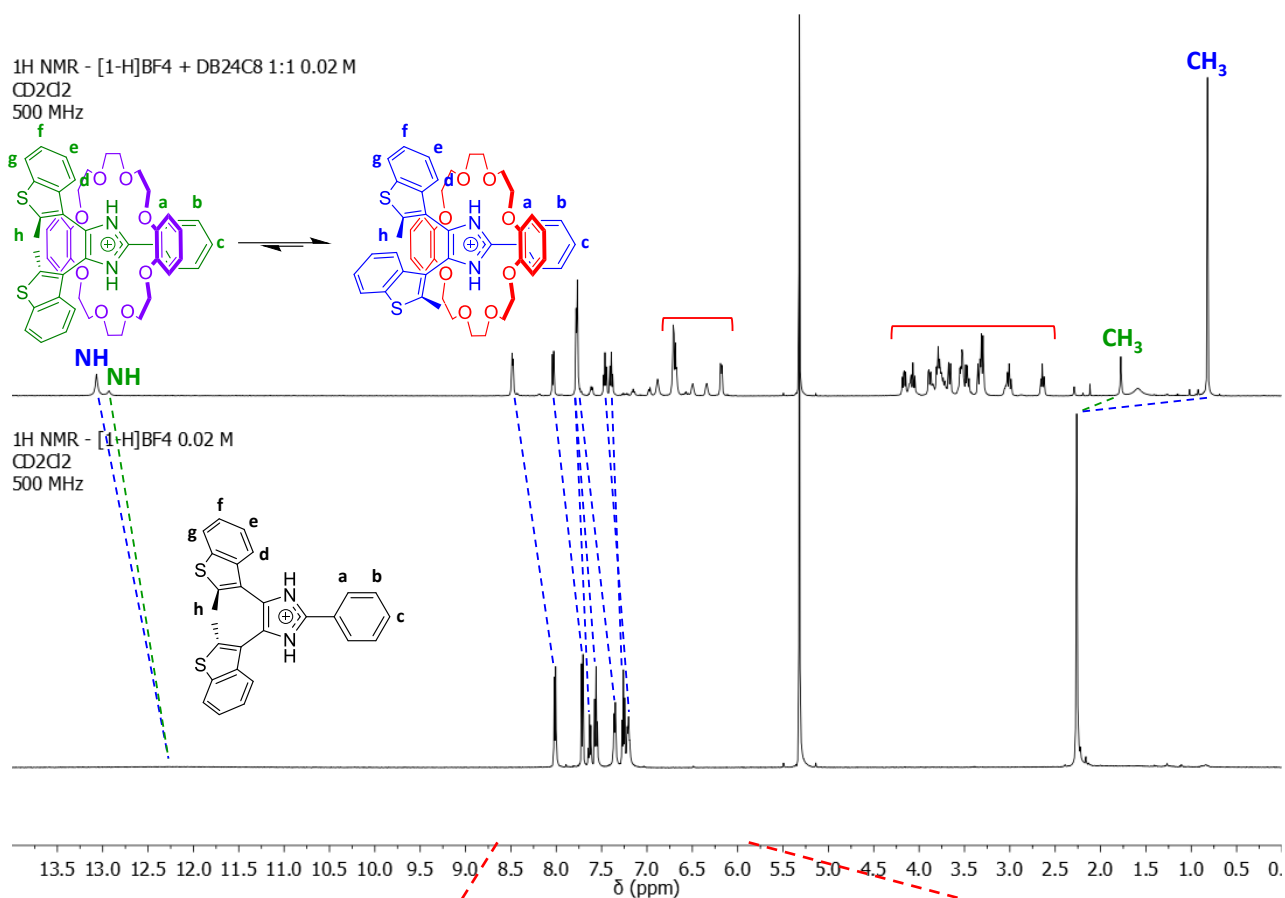
Figure S9. ^{1}H NMR spectra of [**1o**–H]BF$_4$ (bottom) and [**1o**–H⊂**DB24C8**]BF$_4$ (top) (CD$_2$Cl$_2$, 500 MHz, 298 K). The peaks of [**1o**–H]$^+$ are matched to the corresponding peaks of [**1o**–H⊂**DB24C8**]$^+$ by dashed lines. The threaded crown ether peaks are highlighted by red brackets. The axle peaks of the naked axle are labelled in black color. The axle peaks of the [2]pseudorotaxane are labelled in blue and green color, corresponding to the major parallel and the minor anti-parallel conformations of the axle, respectively; the same applies to the aromatic crown ether peaks, highlighted by red and purple asterisks, respectively.
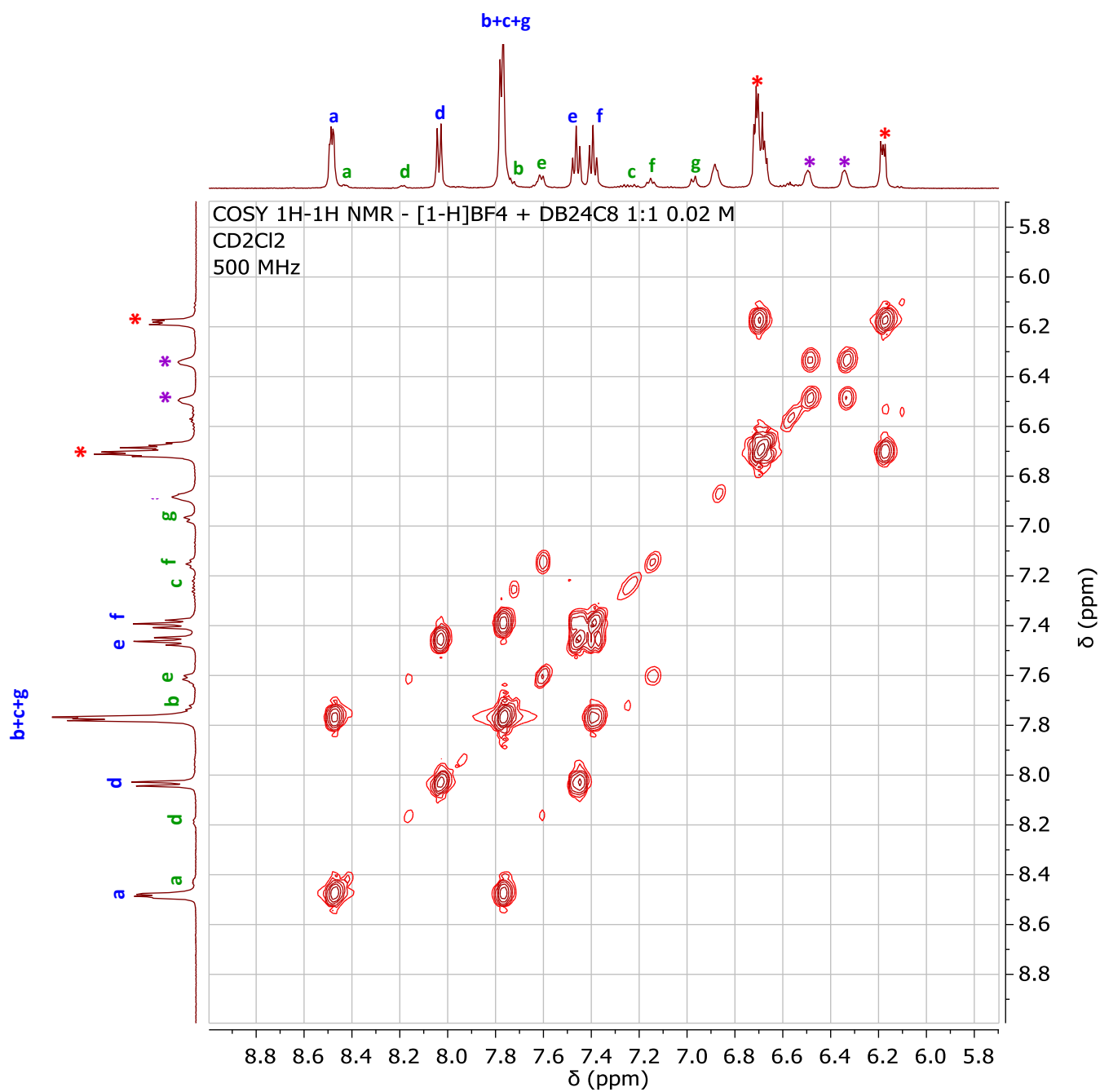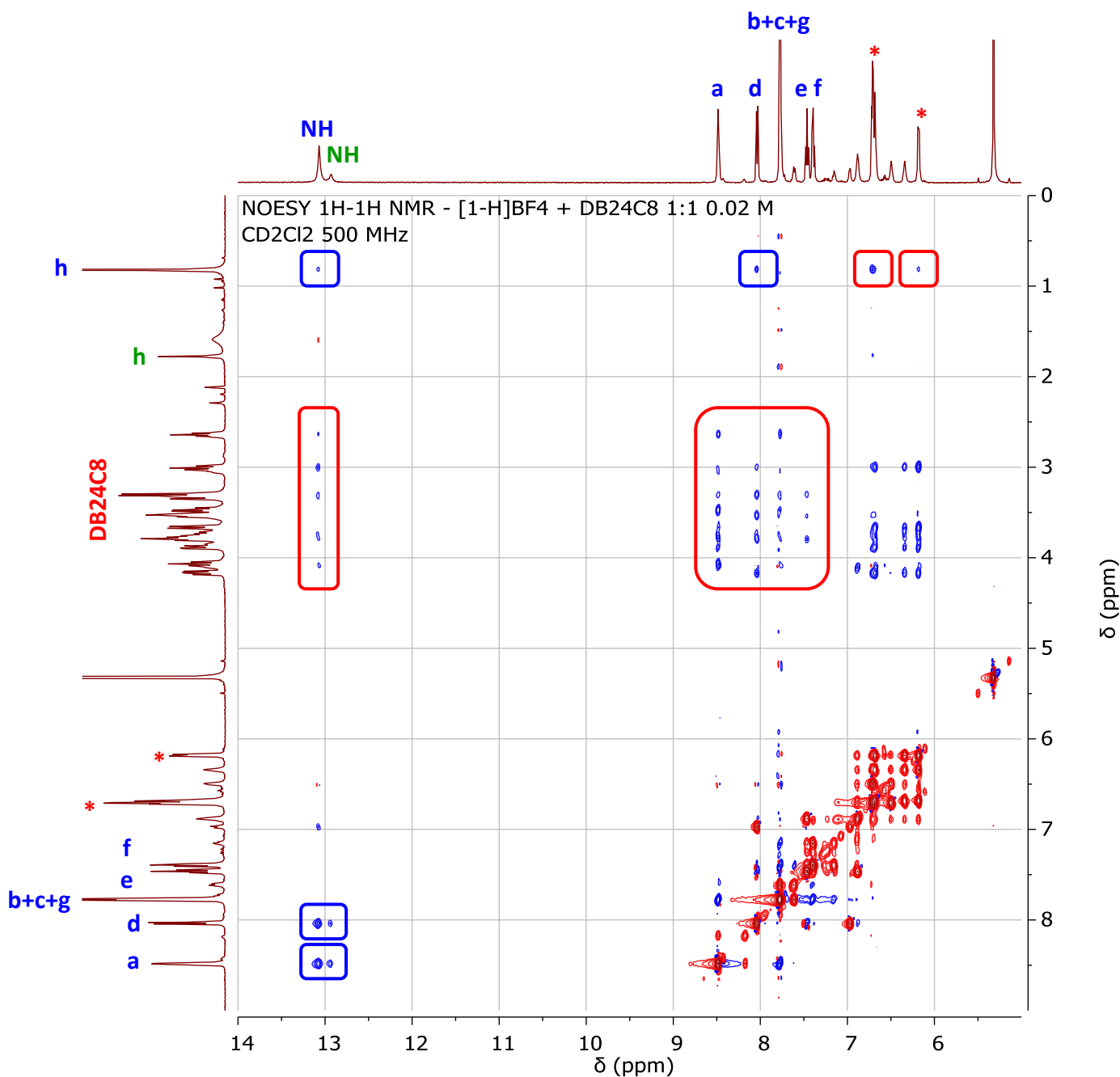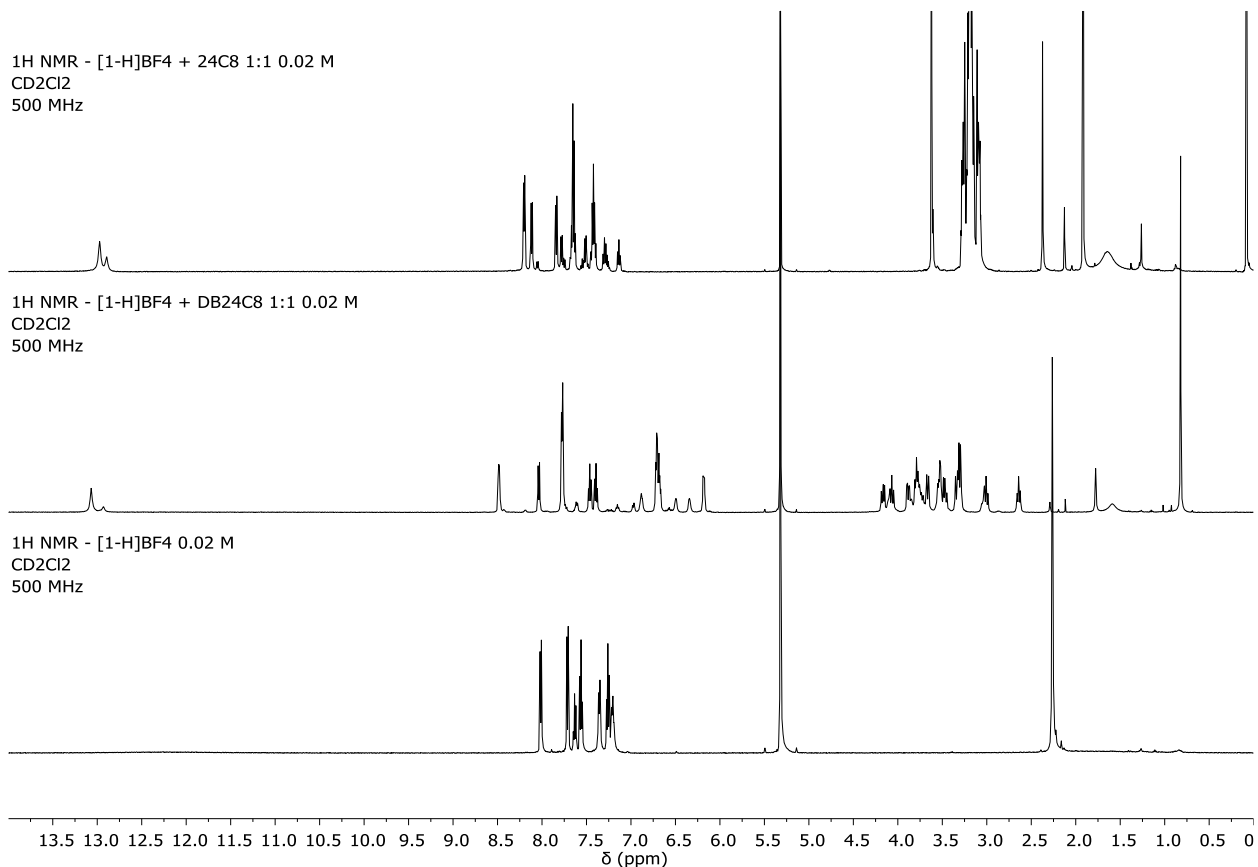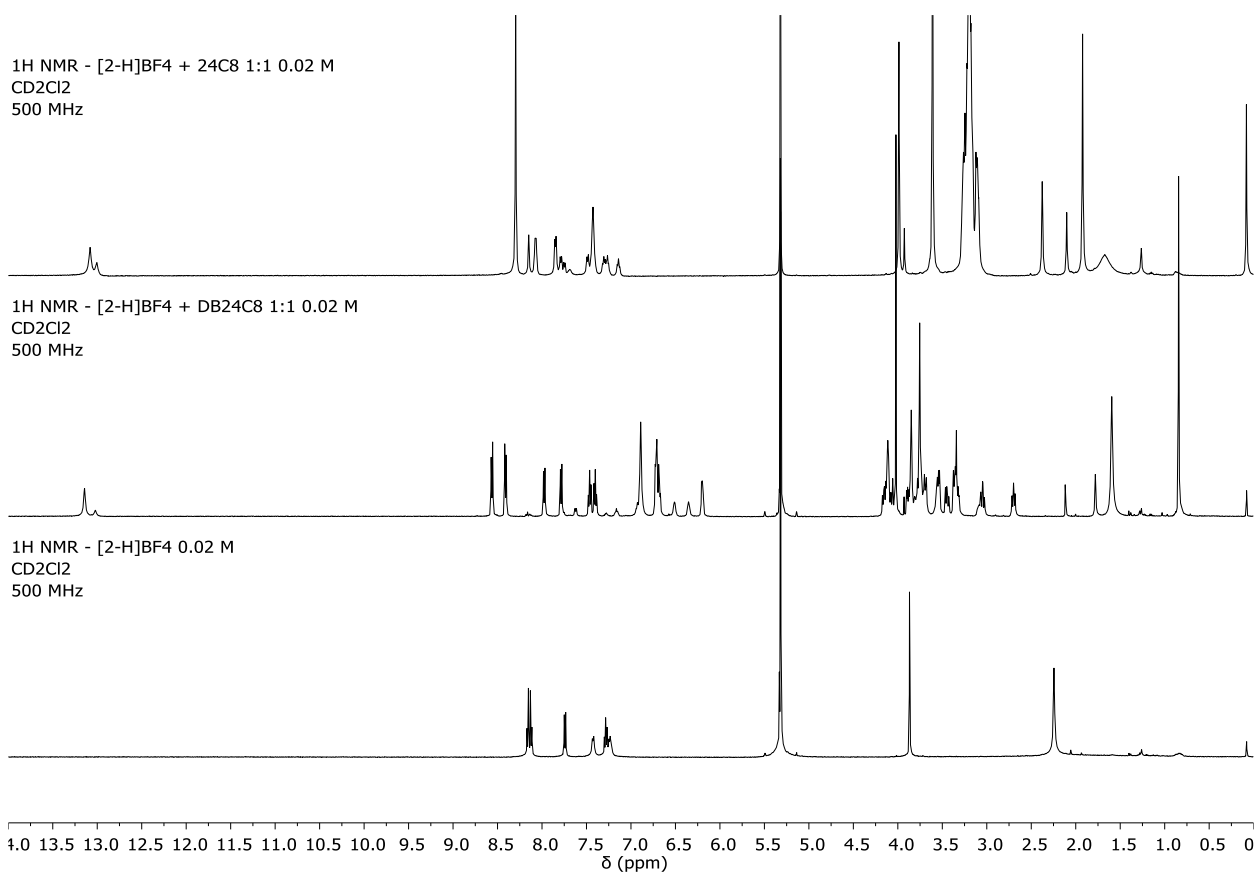
S23

COSY 1H-1H NMR - [1-H]BF4 + DB24C8 1:1 0.02 M
CD2Cl2
500 MHz
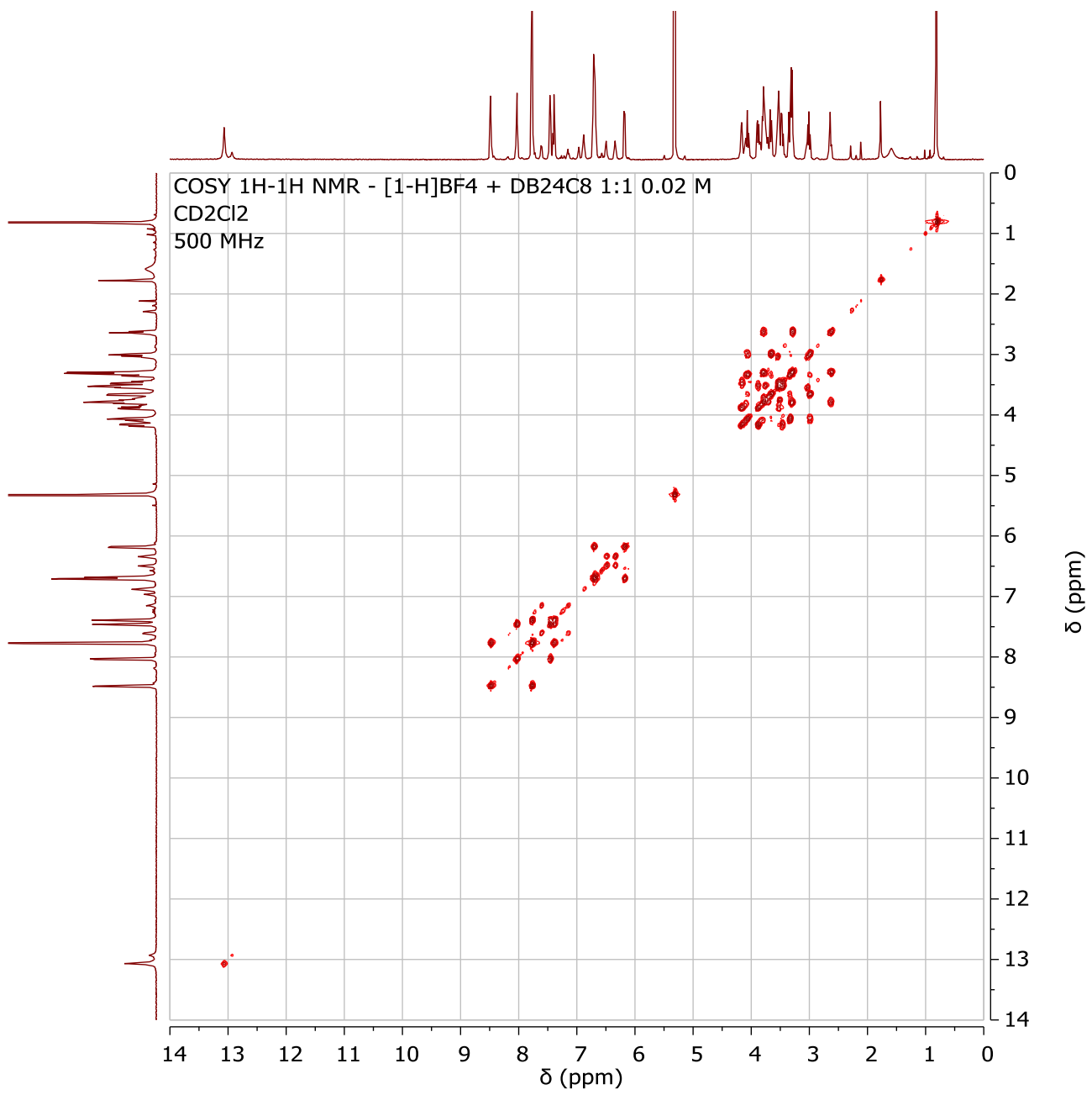
Figure S10. ^{1}H-^{1}H COSY NMR spectrum of [**1o**–H⊂**DB24C8**]BF$_4$ (CD$_2$Cl$_2$, 500 MHz, 298 K).

Figure S11. ^{1}H-^{1}H NOESY NMR spectrum of [**1o**–H⊂**DB24C8**]BF$_4$ (CD$_2$Cl$_2$, 500 MHz, 298 K). Circled in blue, cross peaks useful for peak assignment and conformational analysis (key correlations: *NH* with *h*, *d* and *a*; *h* with *d*). Circled in red, cross peaks which confirm the formation of the [2]pseudorotaxane (key correlations: *h* with *aromatic **DB24C8** protons*; *NH*, *a*, *b*, *d*, *e* with *aliphatic **DB24C8** protons*). NOE cross-peaks between aromatic **DB24C8** protons and *h* protons of the axle, and between aliphatic protons of the ring and protons N*H*, *a*, *b*, *d*, and *e* of the axle support the formation of the [2]pseudorotaxane. NOE cross-peak analysis provided insightful information about the conformations adopted by the axle: correlations between N*H* protons and *a* and *d* protons are common for both species observed in ^{1}H NMR spectra of the [2]pseudorotaxane, while correlation between *h* protons and N*H* and *d* protons, unambiguously consistent with a parallel conformation of the axle, is unique to the major species. This allowed us to perform full assignment of all peaks, and to estimate an 80:20 distribution of parallel versus anti-parallel [2]pseudorotaxane.

1H NMR - [1-H]BF4 + 24C8 1:1 0.02 M
CD2Cl2
500 MHz

1H NMR - [1-H]BF4 + DB24C8 1:1 0.02 M
CD2Cl2
500 MHz

1H NMR - [1-H]BF4 0.02 M
CD2Cl2
500 MHz

Figure S12. ^{1}H NMR spectra of [**1**–H]BF$_4$ (bottom), [**1o**–H⊂**DB24C8**]BF$_4$ (middle), and [**1o**–H⊂**24C8**]BF$_4$ (top) (CD$_2$Cl$_2$, 500 MHz, 298 K).

1H NMR - [2-H]BF4 + 24C8 1:1 0.02 M
CD2Cl2
500 MHz

1H NMR - [2-H]BF4 + DB24C8 1:1 0.02 M
CD2Cl2
500 MHz

1H NMR - [2-H]BF4 0.02 M
CD2Cl2
500 MHz

Figure S13. ^{1}H NMR spectra of [**2o**–H]BF$_4$ (bottom), [**2o**–H⊂**DB24C8**]BF$_4$ (middle), and [**2o**–H⊂**24C8**]BF$_4$ (top) (CD$_2$Cl$_2$, 500 MHz, 298 K).

1H NMR - [3-H]BF4 + 24C8 1:1 0.02 M
CD2Cl2
500 MHz

1H NMR - [3-H]BF4 + DB24C8 1:1 0.02 M
CD2Cl2
500 MHz

1H NMR - [3-H]BF4 0.02 M
CD2Cl2
500 MHz
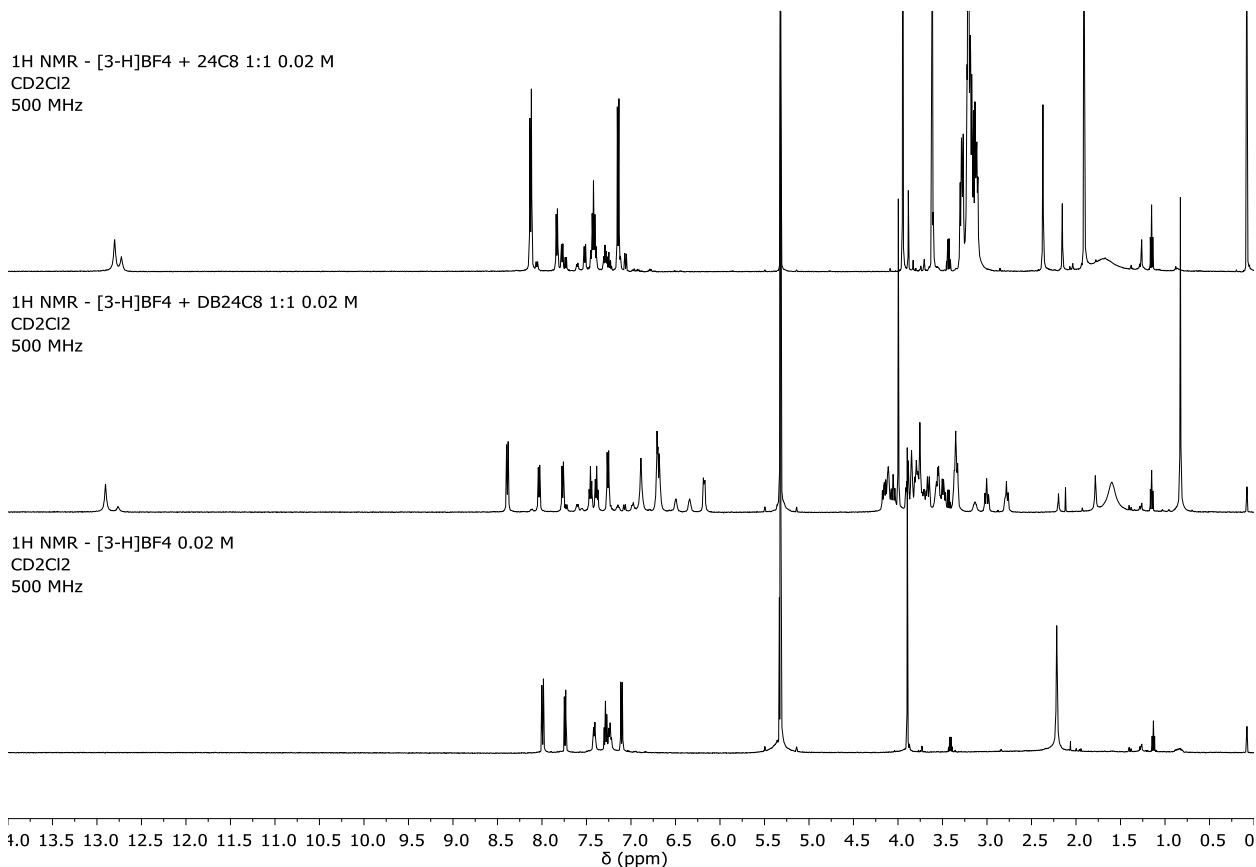
Figure S14. ^{1}H NMR spectra of [**3o**–H]BF$_4$ (bottom), [**3o**–H⊂**DB24C8**]BF$_4$ (middle), and [**3o**–H⊂**24C8**]BF$_4$ (top) (CD$_2$Cl$_2$, 500 MHz, 298 K).

1H NMR - [1-H]BF4 + 24C8 1:1 0.02 M
CD3CN
500 MHz

1H NMR - [1-H]BF4 + DB24C8 1:1 0.02 M
CD3CN
500 MHz

1H NMR - [1-H]BF4 0.02 M
CD3CN
500 MHz
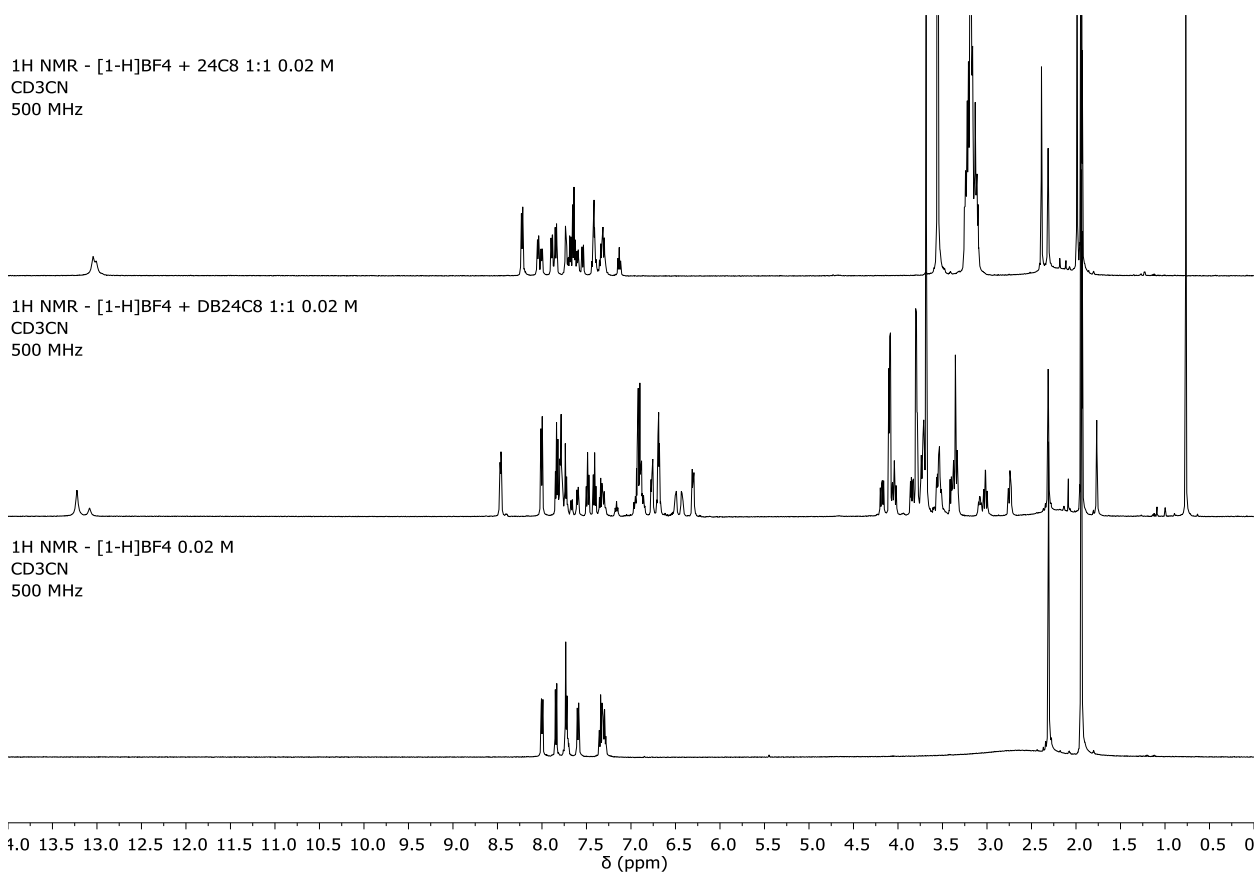
Figure S15. ^{1}H NMR spectra of [**1o**–H]BF$_4$ (bottom), [**1o**–H⊂**DB24C8**]BF$_4$ (middle), and [**1o**–H⊂**24C8**]BF$_4$ (top) (CD$_3$CN, 500 MHz, 298 K).

1H NMR - [2-H]BF4 + 24C8 1:1 0.02 M
CD3CN
500 MHz

1H NMR - [2-H]BF4 + DB24C8 1:1 0.02 M
CD3CN
500 MHz

1H NMR - [2-H]BF4 0.02 M
CD3CN
500 MHz
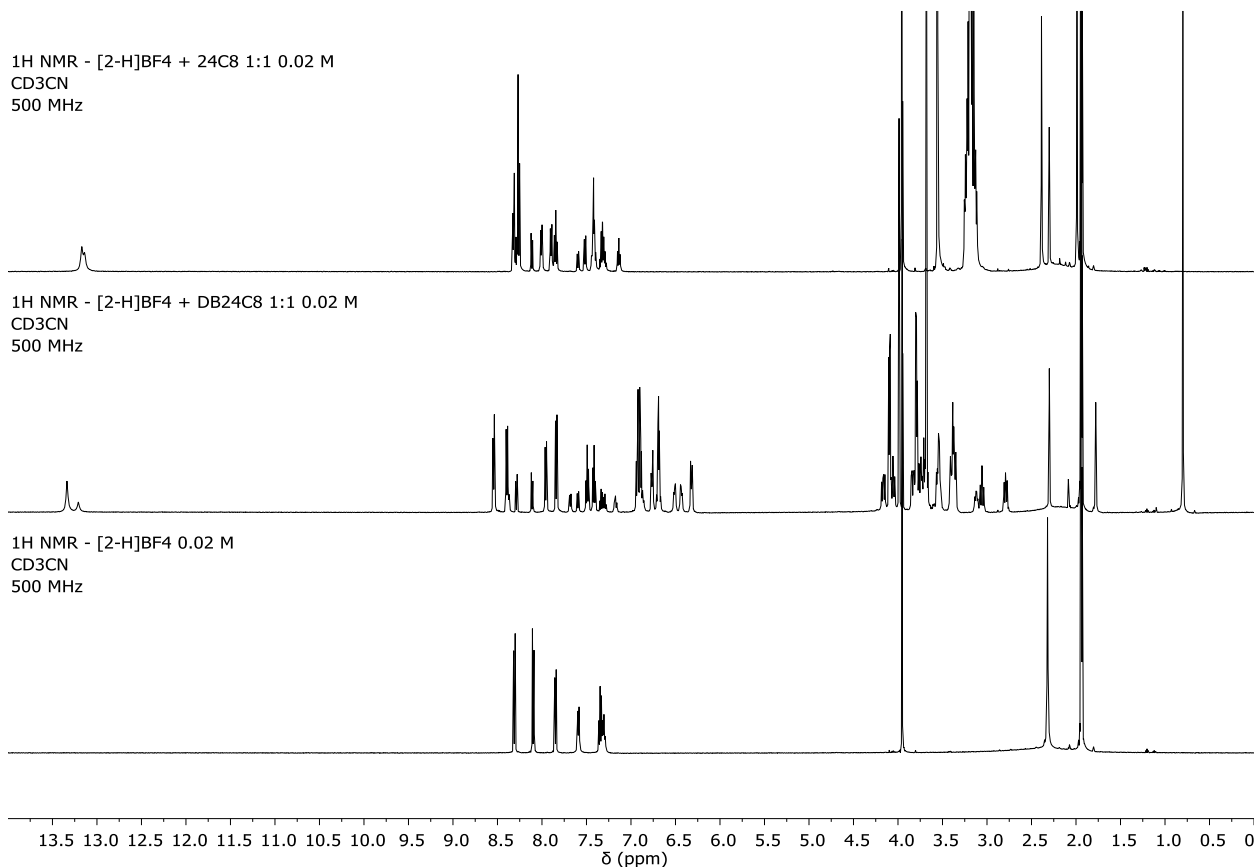
Figure S16. ^{1}H NMR spectra of [**2o**–H]BF$_4$ (bottom), [**2o**–H⊂**DB24C8**]BF$_4$ (middle), and [**2o**–H⊂**24C8**]BF$_4$ (top) (CD$_3$CN, 500 MHz, 298 K).

1H NMR - [3-H]BF4 + 24C8 1:1 0.02 M
CD3CN
500 MHz

1H NMR - [3-H]BF4 + DB24C8 1:1 0.02 M
CD3CN
500 MHz

1H NMR - [3-H]BF4 0.02 M
CD3CN
500 MHz
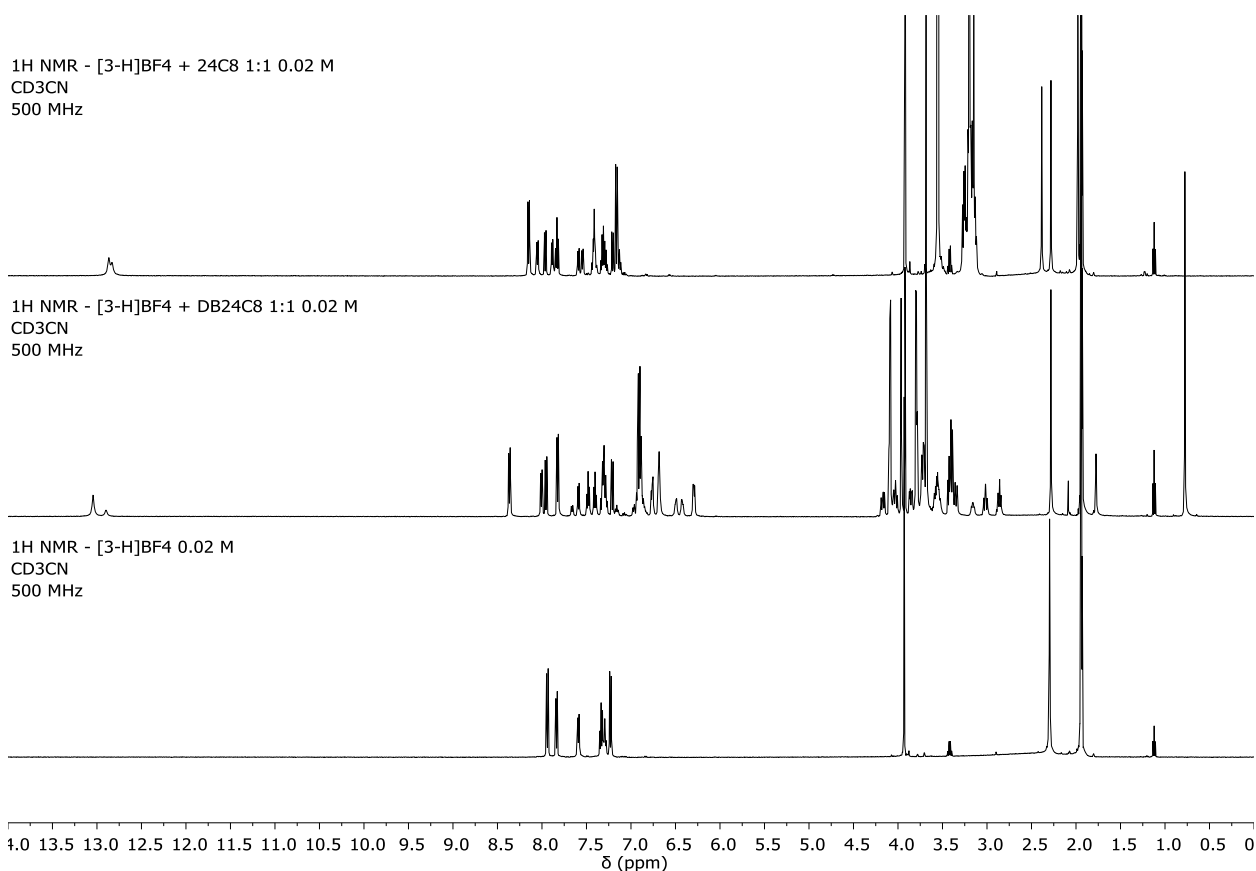
Figure S17. ^{1}H NMR spectra of [**3o**–H]BF$_4$ (bottom), [**3o**–H⊂**DB24C8**]BF$_4$ (middle), and [**3o**–H⊂**24C8**]BF$_4$ (top) (CD$_3$CN, 500 MHz, 298 K).

	DB24C8	**24C8**
[**1o**–H]BF$_4$	300 M^{-1}	380 M^{-1}
[**2o**–H]BF$_4$	800 M^{-1}	910 M^{-1}
[**3o**–H]BF$_4$	200 M^{-1}	290 M^{-1}

Table S4. Ka values for the formation of [2]pseudorotaxanes measured from single-point ^{1}H NMR titrations in CD$_3$CN (0.02 M, 298 K).

Variable temperature ^{1}H NMR of the axle [1o–H]BF$_4$

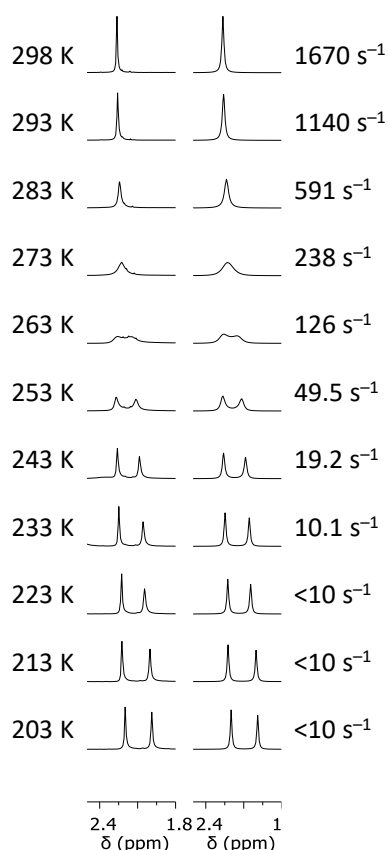Variable temperature ^{1}H NMR experiment was performed on a 10 mM solution of axle [**1o**–H]BF$_4$ in CD$_2$Cl$_2$ to determine the exchange rate between parallel and anti-parallel conformers of the bis(benzothienyl)imidazolium unit. ^{1}H NMR spectra of the sample were recorded in the range 203-298 K (10 K steps), and the methyl protons *h* and *h'* were selected to be used as the probe:
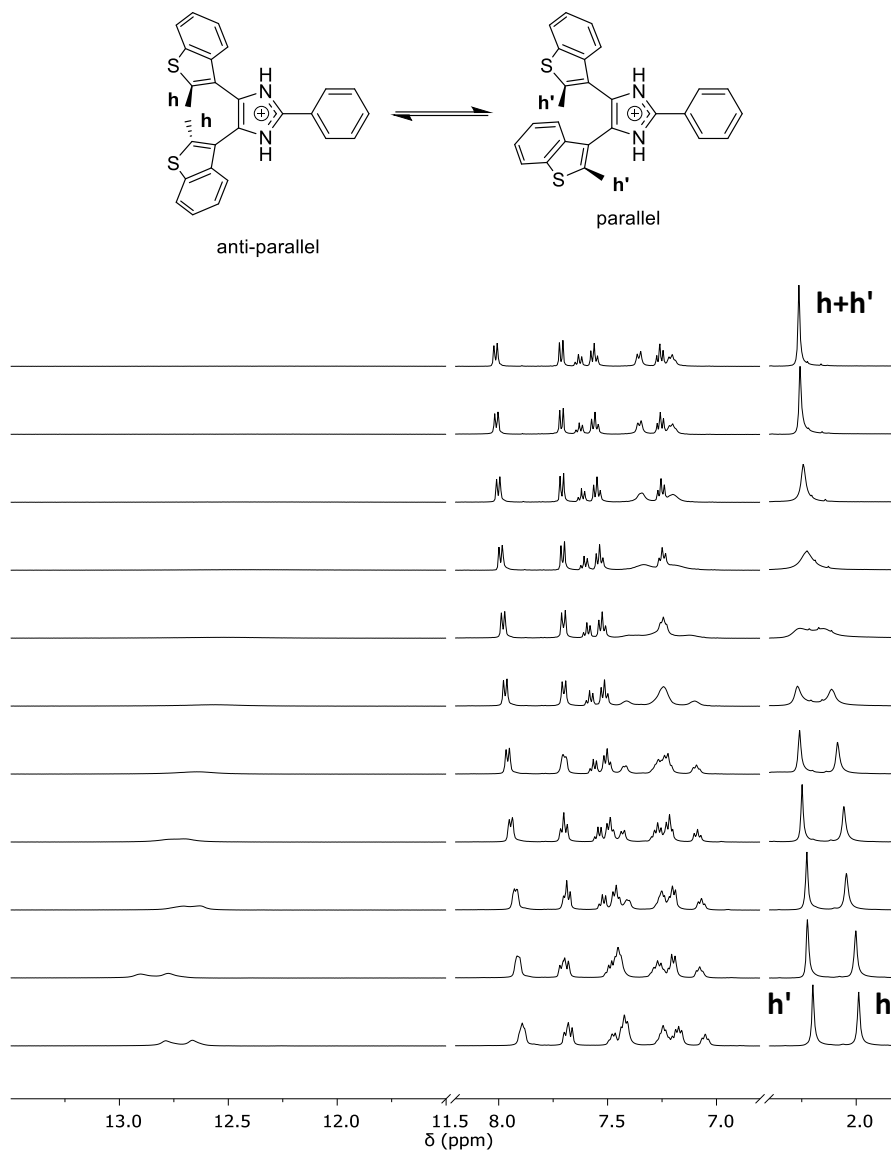
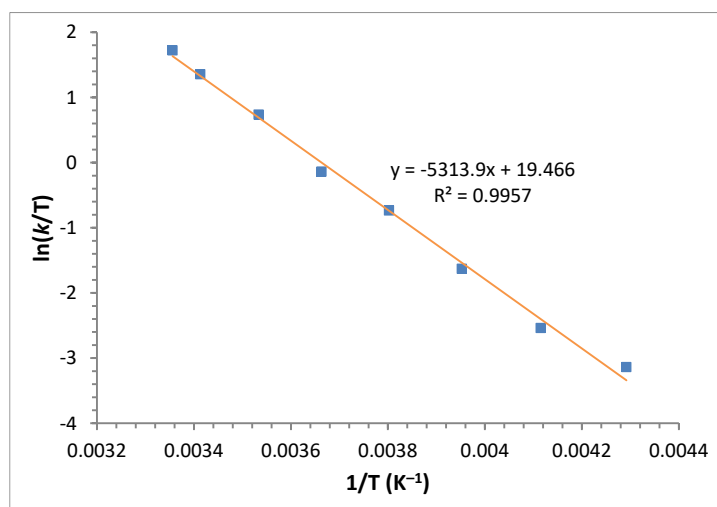**Figure S18.** Partial VT ^{1}H NMR spectra of [**1o**–H]BF$_4$ (CD$_2$Cl$_2$, 500 MHz, 10 mM)

Dynamic exchange lineshape analysis was carried out with the DNMR structure analysis tool included in Bruker's TopSpin software package.[S8] Simulations were performed at 500 MHz with exchange between signals at 2.20 and 1.99 ppm assuming a Gaussian lineshape. A static line width at half maximum of 5.4 Hz was estimated from measurements carried out at the lowest temperature (203 K). The chemical shift δ dependence on the temperature T was determined by plotting log δ versus 1/T, using δ values from spectra recorded at sufficiently low temperatures (203-253 K), and the predicted δ values at higher temperatures were used for the subsequent simulations. The ratio of parallel versus anti-parallel conformers was determined to be independent from the temperature and

equal to 53:47 by peak integration in spectra recorded at the lowest temperatures. The exchange rate constant k was refined for each spectrum with the DNMR tool until a best fit was obtained:

Temperature		Rate constant
298 K		1670 s^{-1}
293 K		1140 s^{-1}
283 K		591 s^{-1}
273 K		238 s^{-1}
263 K		126 s^{-1}
253 K		49.5 s^{-1}
243 K		19.2 s^{-1}
233 K		10.1 s^{-1}
223 K		<10 s^{-1}
213 K		<10 s^{-1}
203 K		<10 s^{-1}

2.4   1.8 2.4   1
δ (ppm)   δ (ppm)

Figure S19. Experimental (left) and simulated (right) VT ^{1}H NMR spectra of [**1o**–H]BF$_4$ (CD$_2$Cl$_2$, 500 MHz, 10 mM) accompanied by temperature of the experiment and simulated rate constants.

The k values obtained from the simulations were used to build an Eyring plot and extrapolate the activation parameters (R = 1.987 cal K^{-1} mol^{-1}, k_B = 3.30×10^{-24} cal K^{-1}, h = 1.58×10^{-34} cal s):

y = -5313.9x + 19.466
R² = 0.9957

$$\ln\frac{\boldsymbol{k}}{T} = \frac{-\Delta H^{\ddagger}}{R} \cdot \frac{1}{T} + \ln\frac{k_B}{h} + \frac{\Delta S^{\ddagger}}{R}$$

$$\boldsymbol{\Delta G^{\ddagger}} = -RT \ln\frac{\boldsymbol{k}h}{k_B T}$$

$\Delta H^{\ddagger} = 10.6$ kcal mol^{-1}

$\Delta S^{\ddagger} = -8.54$ cal mol^{-1} K^{-1}

$\Delta G^{\ddagger}_{298} = 13.1$ kcal mol^{-1}

Figure S20. Eyring plot to determine the activation parameters of the exchange between parallel and anti-parallel conformers of [**1o**–H]BF$_4$.

^{1}H-^{1}H EXSY NMR of [2]pseudorotaxane [1o–H⊂DB24C8]BF$_4$

^{1}H-^{1}H EXSY NMR experiments were performed on a 10 mM solution of [2]pseudorotaxane [**1o**–H⊂**DB24C8**]BF$_4$ in CD$_2$Cl$_2$ at 298 K to determine the exchange rate between parallel and anti-parallel conformers of the bis(benzothienyl)imidazolium unit of the threaded axle. Exchange rates were calculated using the computer program EXSYCalc.[S9] For the calculation of rate constants, the program requires the experimental amplitudes of separated NMR peaks in slow chemical exchange, obtained in two different EXSY experiments acquired and processed under identical conditions: one EXSY experiment must be acquired at mixing time (τ_m) large enough for the magnetization exchange process to take place, and the other EXSY experiment must be acquired at very short mixing time (reference experiment). In this particular case, experiments were performed at two different mixing times τ_m = 800 and 5 ms:
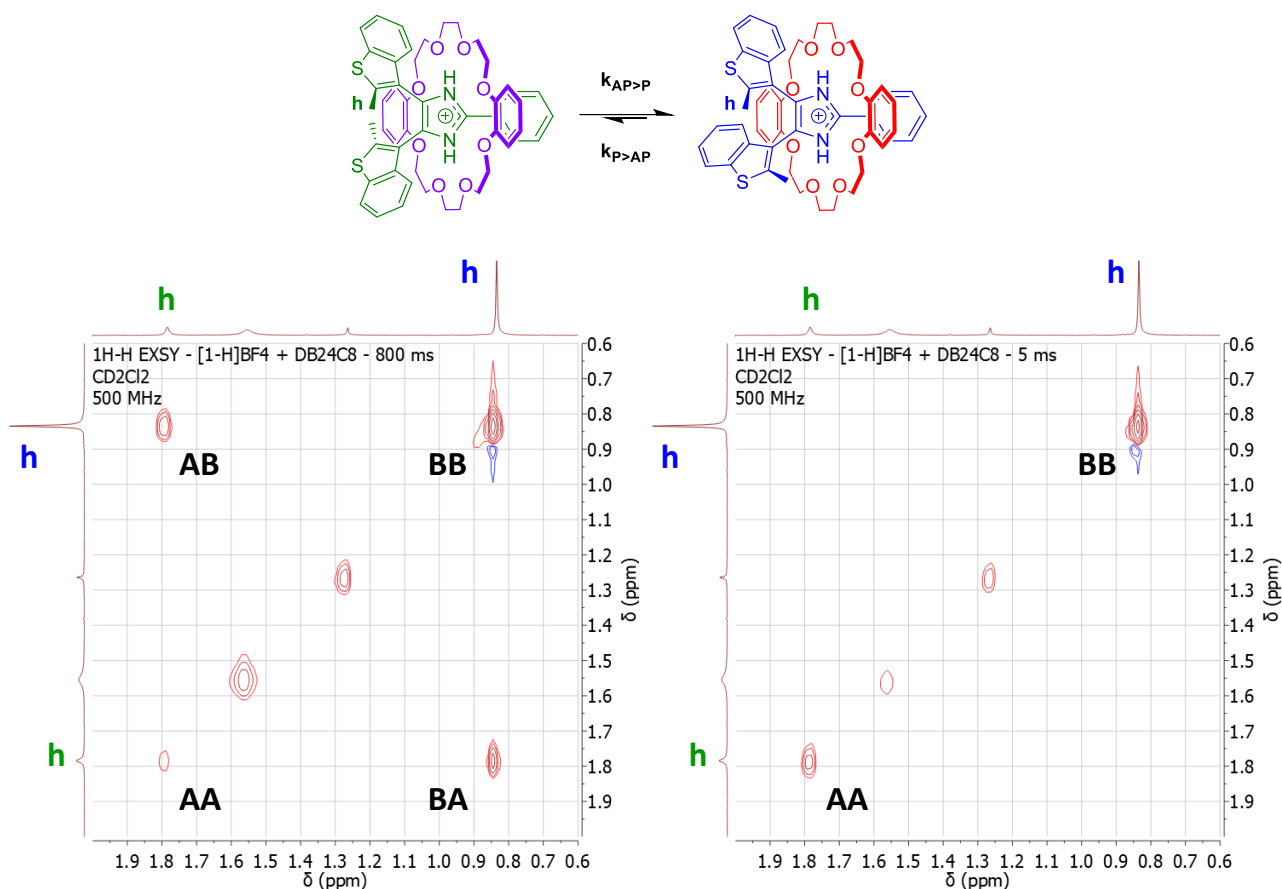
Figure S21. ^{1}H-^{1}H EXSY NMR spectra of [**1o**–H⊂**DB24C8**]BF$_4$ (CD$_2$Cl$_2$, 500 MHz, 298 K, 10 mM) recorded with mixing times τ_m = 800 ms (left) and 5 ms (right).

The intensities of signals in exchange were quantified for both diagonal (AA, BB) and cross peaks (AB, BA) for the experiment with long mixing time, while only the intensities of diagonal peaks were measured for the EXSY reference experiment. The raw intensities were introduced in the EXSYCalc program to obtain the exchange rate matrix, which includes the the exchange rate constants ($k_{AP \to P}$ and $k_{P \to AP}$) and the longitudinal relaxation rates (R_1 and R_2):
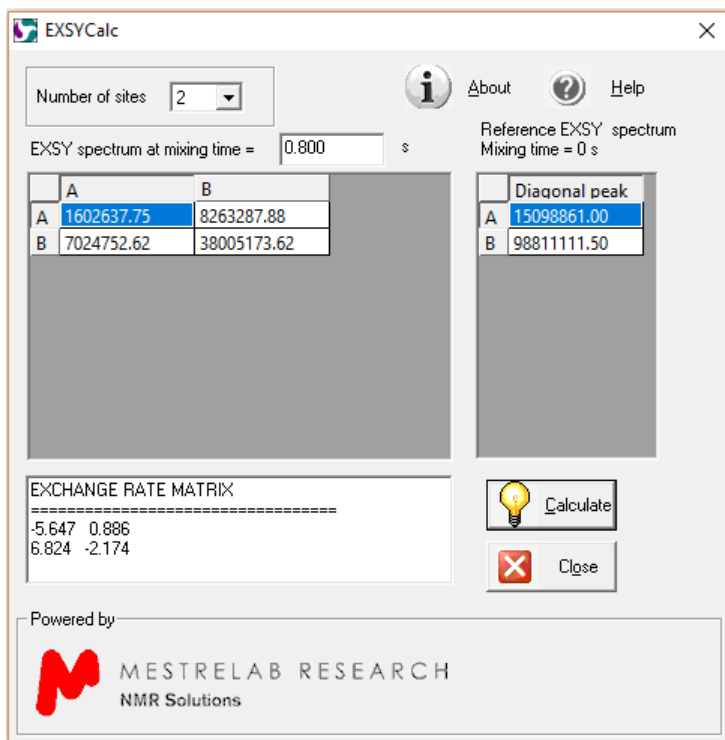
$\tau_m = 800$ ms $\tau_m = 5$ ms

$I_{AA} = 1602637.75$ $I_{AA} = 15098861.00$

$I_{BB} = 38005173.62$ $I_{BB} = 98811111.50$

$I_{AB} = 7024752.62$

$I_{BA} = 8263287.88$

$$R = \begin{vmatrix} -R_1 - k_{AP \to P} & k_{P \to AP} \\ k_{AP \to P} & -R_2 - k_{P \to AP} \end{vmatrix}$$

$k_{AP \to P} = 6.824$ s^{-1}

$k_{P \to AP} = 0.886$ s^{-1}

Figure S22. EXSYCalc software interface showing the raw intensities obtained from EXSY experiments and the resulting exchange rate matrix containing the exchange rates between parallel and anti-parallel conformers of [2]pseudorotaxane [**1o**–H⊂**DB24C8**]BF$_4$.

Axles photochromism and fatigue resistance

Irradiation experiments for all the following ^{1}H NMR studies were performed on samples (20 mM in CD$_2$Cl$_2$) contained in quartz NMR tubes, placed in a Luzchem LZC-ICH2 photoreactor equipped with 16 UV fluorescent lamps of the opportune wavelength (UVB for free axles, or UVC for pseudorotaxanes), for a total intensity of 4.8 mW/cm^2.

Due to the fast cycloreversion of the closed isomers, full kinetic studies of the thermal cycloreversion of axles [**1-3c**–H]$^+$ by ^{1}H NMR were not feasible. Nevertheless, the closed isomer [**1c**–H]$^+$ could be detected by irradiating, freezing, and subsequently thawing the sample right before the ^{1}H NMR spectrum was recorded.
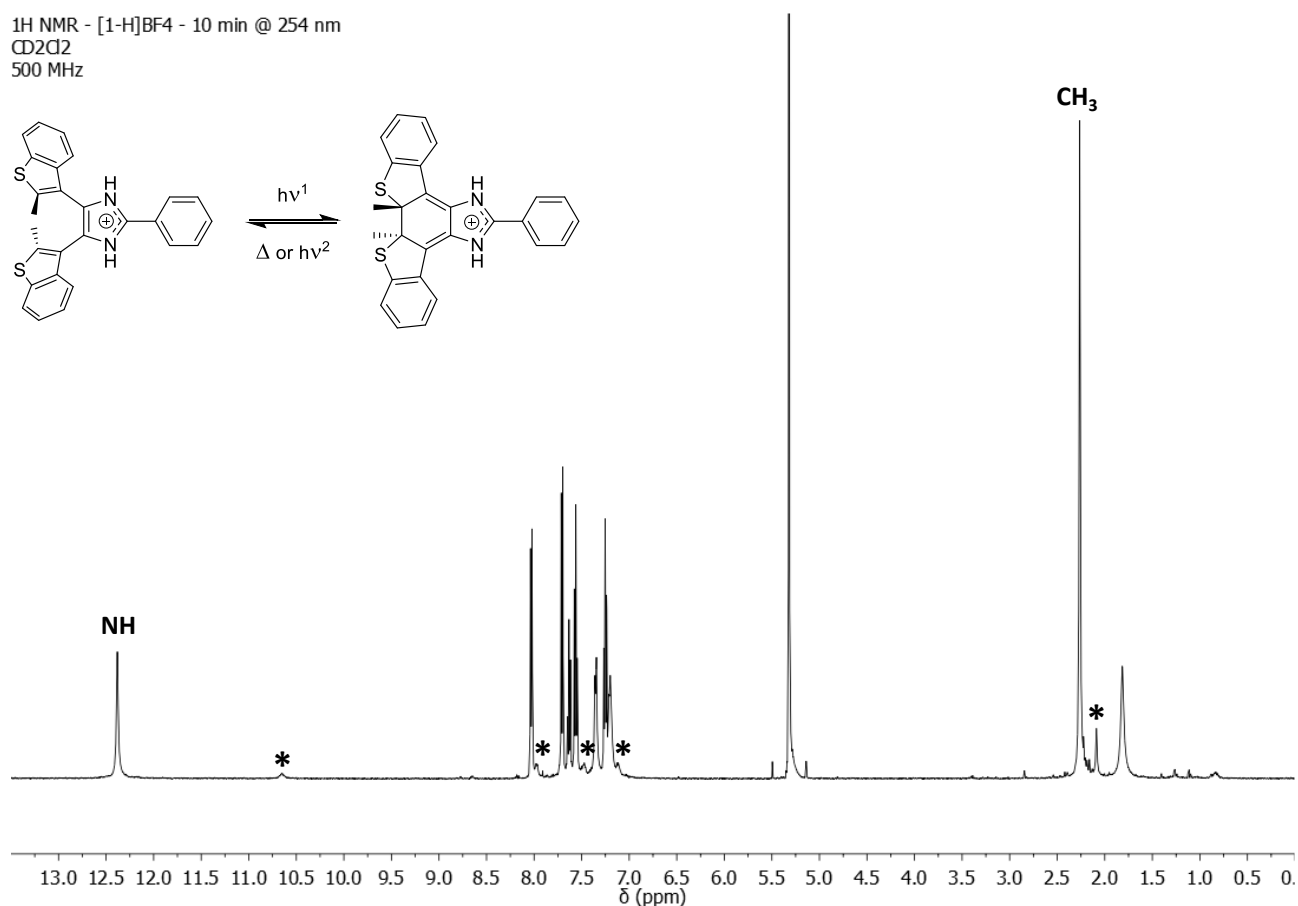
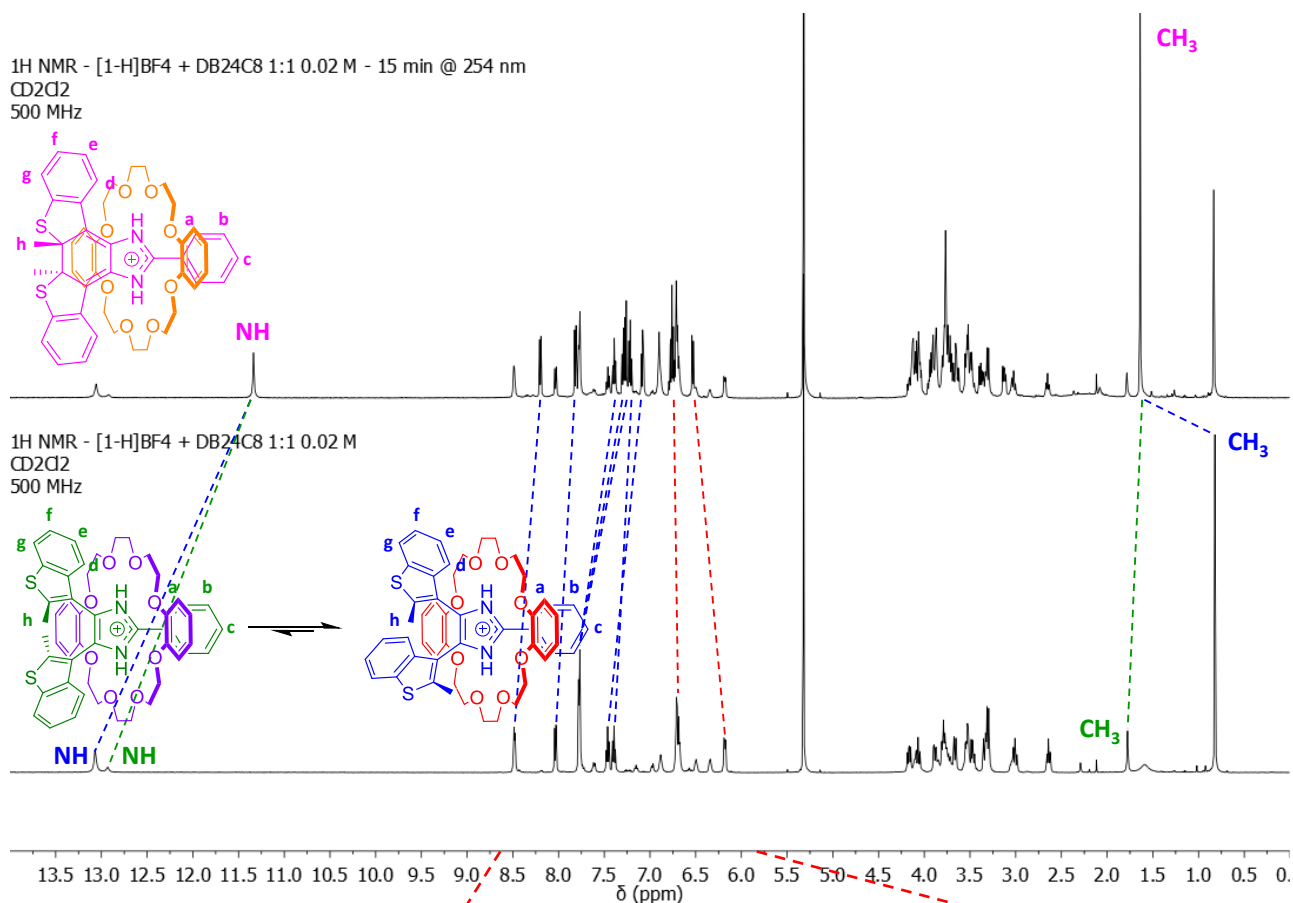**Figure S23.** ^{1}H NMR spectra of [**1c**–H]BF$_4$ (CD$_2$Cl$_2$, 500 MHz, 298 K) obtained by irradiation of a [**1o**–H]BF$_4$ solution at 313 nm for 10 minutes. Due to the fast thermal cycloreversion of the closed isomer, the peaks of [**1c**–H]$^+$ (highlighted by asterisks) are barely detectable.

Fatigue resistance of the axles [**1-3o**–H]BF$_4$ was investigated by alternating irradiation at 313 nm for 15 min and subsequently with white visible light for few seconds over five cycles. The percentage of open isomer was determined after every cycle (UV+Vis) by comparison of the integral of the *a* protons with a dibromomethane internal standard (4.97 ppm in CD$_2$Cl$_2$).
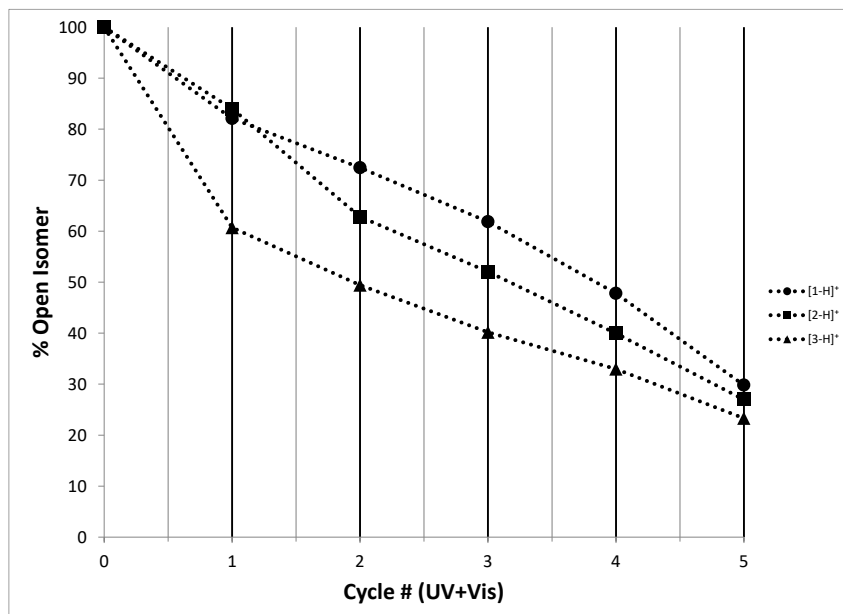
Chart S1. Fatigue resistance of axles [**1o**–H]BF$_4$ (●), [**2o**–H]BF$_4$ (■), and [**3o**–H]BF$_4$ (▲) determined by ^{1}H NMR experiments (CD$_2$Cl$_2$, 0.02 M, 500 MHz, 298 K).

**[2]Pseudorotaxane photochromism, thermal cycloreversion, and fatigue resistance**

Figure S24. ^{1}H NMR spectra of [**1o**–H⊂**DB24C8**]BF$_4$ (CD$_2$Cl$_2$, 500 MHz, 298 K) before (bottom) and after (top) irradiation of the solution at 254 nm for 15 minutes. The peaks of [**1o**–H⊂**DB24C8**]$^+$ are matched to the corresponding peaks of the closed form [**1c**–H⊂**DB24C8**]$^+$ by dashed lines (blue and green for parallel and anti-parallel axle, respectively, and red for DB24C8). The axle peaks of [**1o**–H⊂**DB24C8**]$^+$ are labelled in blue and green color, corresponding to the major parallel and the minor anti-parallel conformations, respectively; the same applies to the aromatic crown ether peaks, highlighted by red and purple asterisks, respectively. The axle and aromatic crown ether peaks of the closed form [**1c**–H⊂**DB24C8**]$^+$ are labelled in fuchsia and orange, respectively.

COSY 1H-1H NMR - [1-H]BF4 + DB24C8 1:1 0.02 M - 15 min @ 254 nm
CD2Cl2
500 MHz
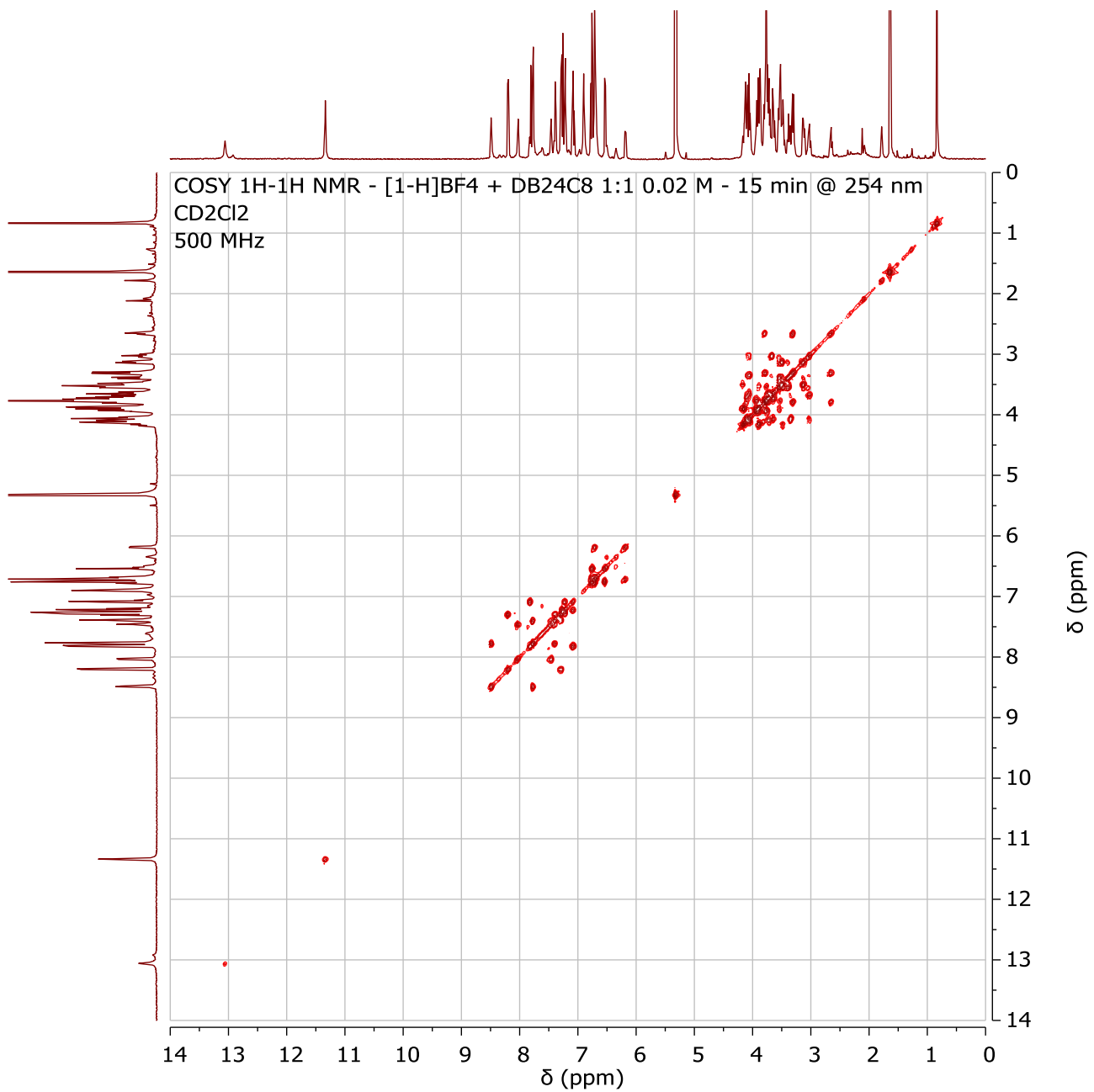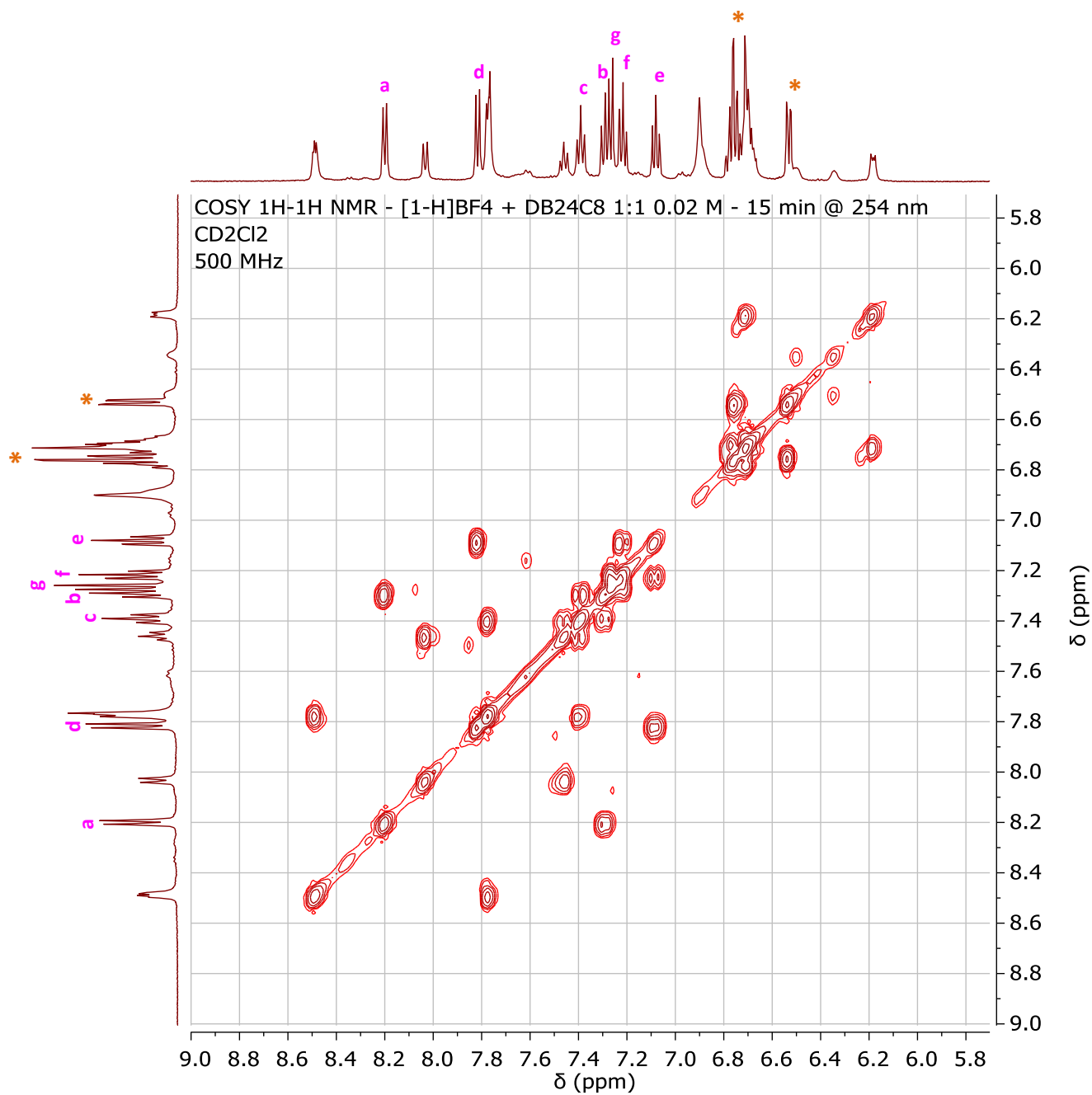
Figure S25. ^{1}H-^{1}H COSY NMR spectrum of [**1o**–H⊂**DB24C8**]BF$_4$ after irradiation of the solution at 254 nm for 15 minutes (CD$_2$Cl$_2$, 500 MHz, 298 K).
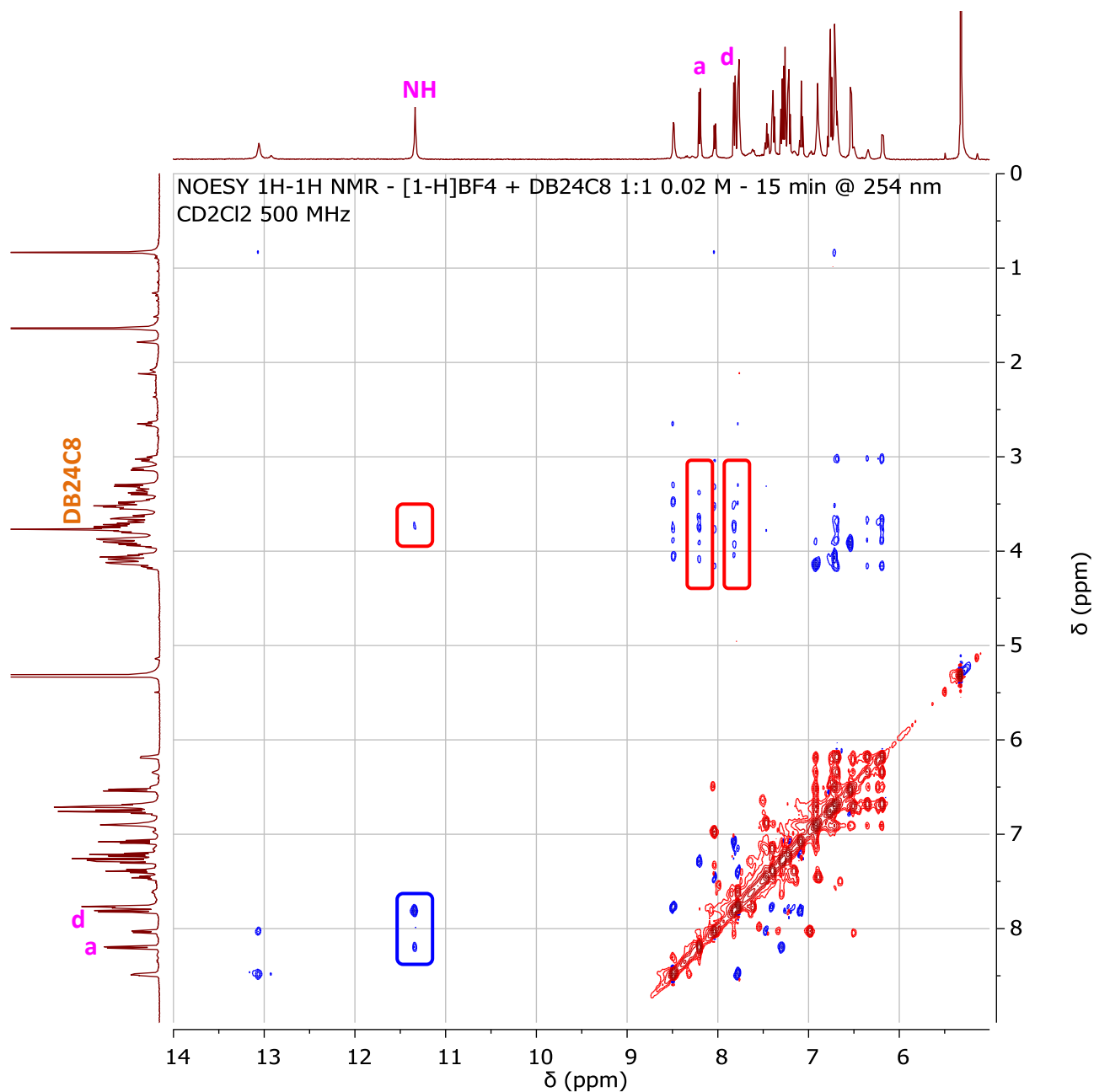
Figure S26. ^{1}H-^{1}H NOESY NMR spectrum of [**1o**–H⊂**DB24C8**]BF$_4$ (CD$_2$Cl$_2$, 500 MHz, 298 K) after irradiation of the solution at 254 nm for 15 minutes (CD$_2$Cl$_2$, 500 MHz, 298 K). Circled in blue, cross peaks useful for peak assignment and conformational analysis (key correlations: *NH* with *a* and *d*). Circled in red, cross peaks which confirm the persistence of the [2]pseudorotaxane after UV irradiation (key correlations: *NH, a,* and *d* with *aliphatic* **DB24C8** *protons*).
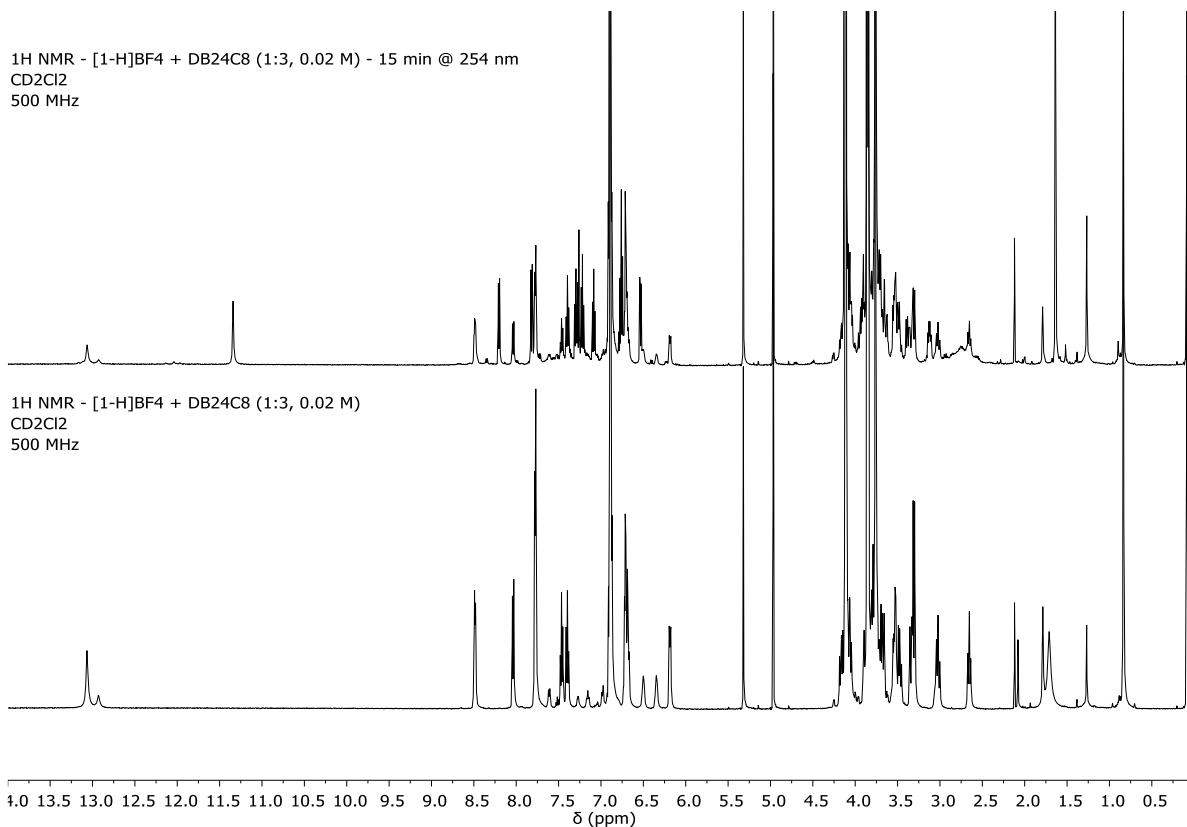
Figure S27. ¹H NMR spectra of [**1o**–H⊂**DB24C8**]BF₄, before (bottom) and after (top) irradiation of the solution at 254 nm for 15 minutes (CD₂Cl₂, 500 MHz, 298 K).
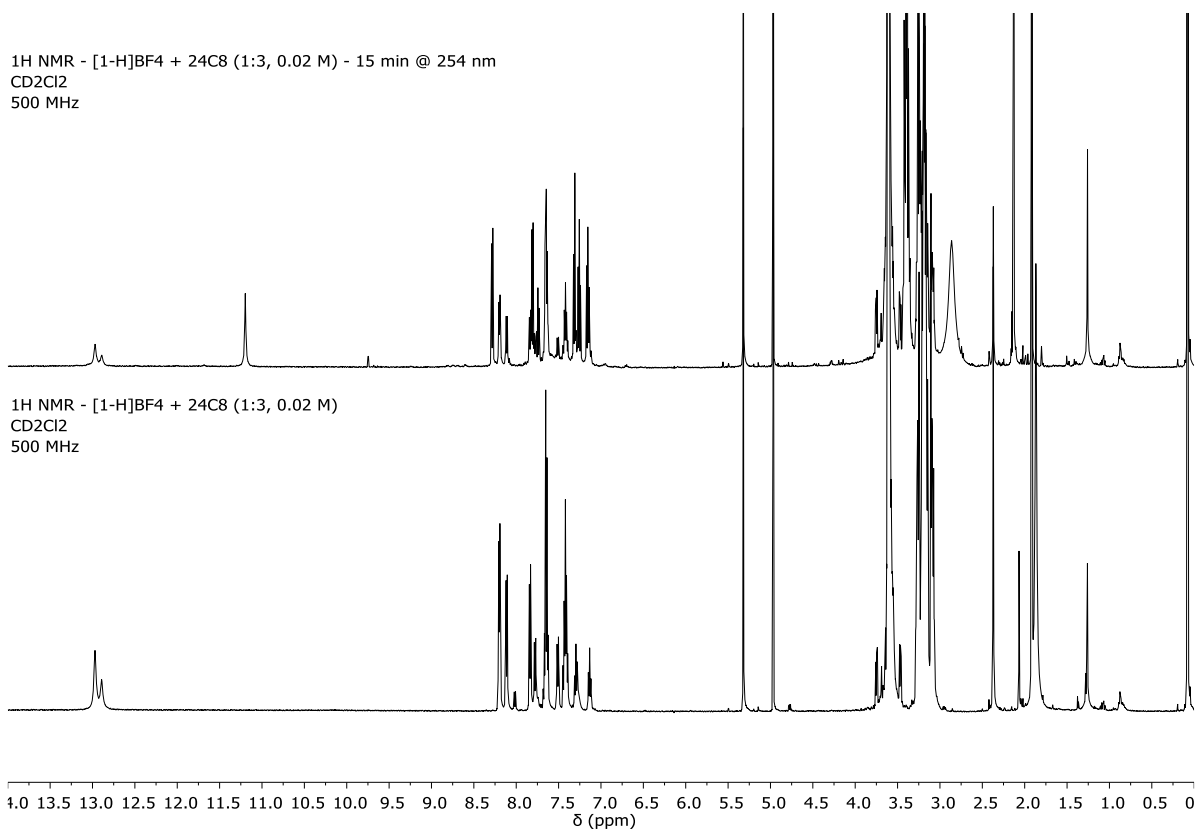
Figure S28. ¹H NMR spectra of [**1o**–H⊂**24C8**]BF₄, before (bottom) and after (top) irradiation of the solution at 254 nm for 15 minutes (CD₂Cl₂, 500 MHz, 298 K).

Figure S29. ¹H NMR spectra of [**2o**–H⊂**DB24C8**]BF₄, before (bottom) and after (top) irradiation of the solution at 254 nm for 15 minutes (CD₂Cl₂, 500 MHz, 298 K).

Figure S30. ¹H NMR spectra of [**2o**–H⊂**24C8**]BF₄, before (bottom) and after (top) irradiation of the solution at 254 nm for 15 minutes (CD₂Cl₂, 500 MHz, 298 K).

1H NMR - [3-H]BF4 + DB24C8 (1:3, 0.02 M) - 15 min @ 254 nm
CD2Cl2
500 MHz

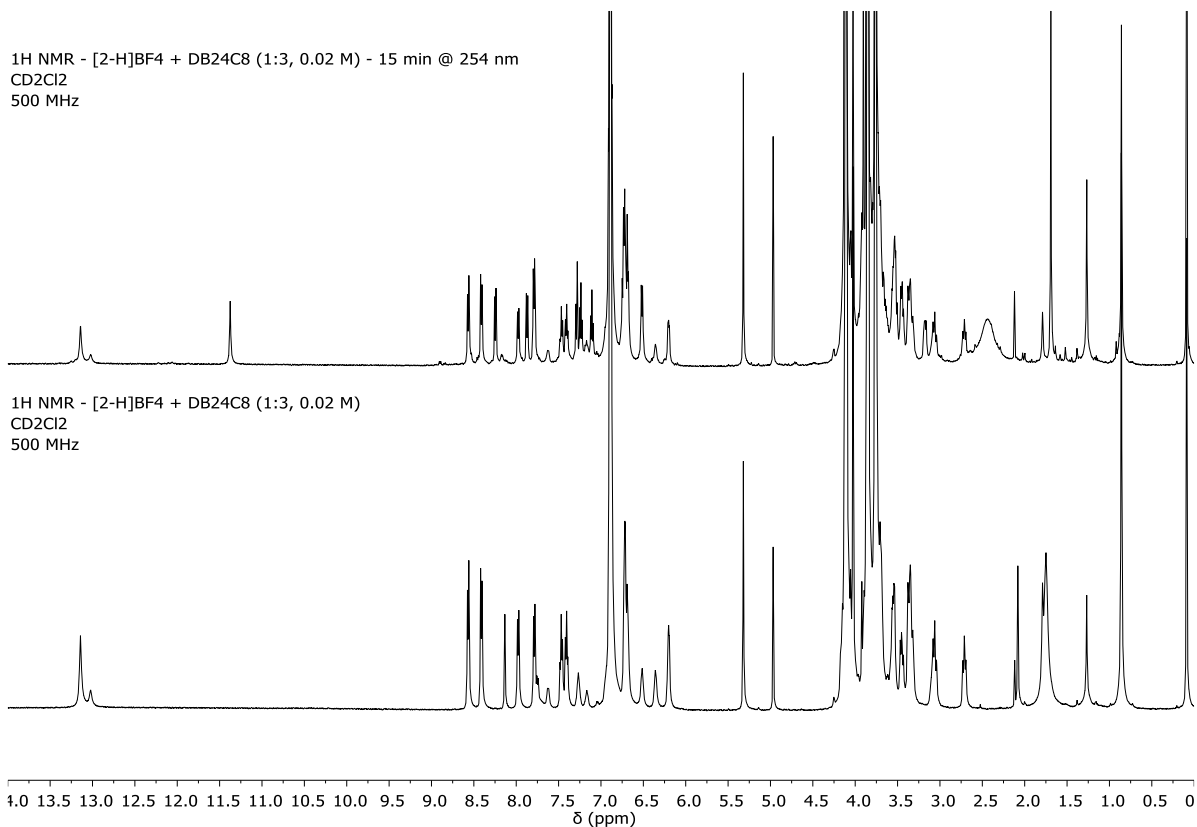1H NMR - [3-H]BF4 + DB24C8 (1:3, 0.02 M)
CD2Cl2
500 MHz

Figure S31. ^{1}H NMR spectra of [**3o**–H⊂**DB24C8**]BF$_4$, before (bottom) and after (top) irradiation of the solution at 254 nm for 15 minutes (CD$_2$Cl$_2$, 500 MHz, 298 K).

1H NMR - [3-H]BF4 + 24C8 (1:3, 0.02 M) - 15 min @ 254 nm
CD2Cl2
500 MHz

1H NMR - [3-H]BF4 + 24C8 (1:3, 0.02 M)
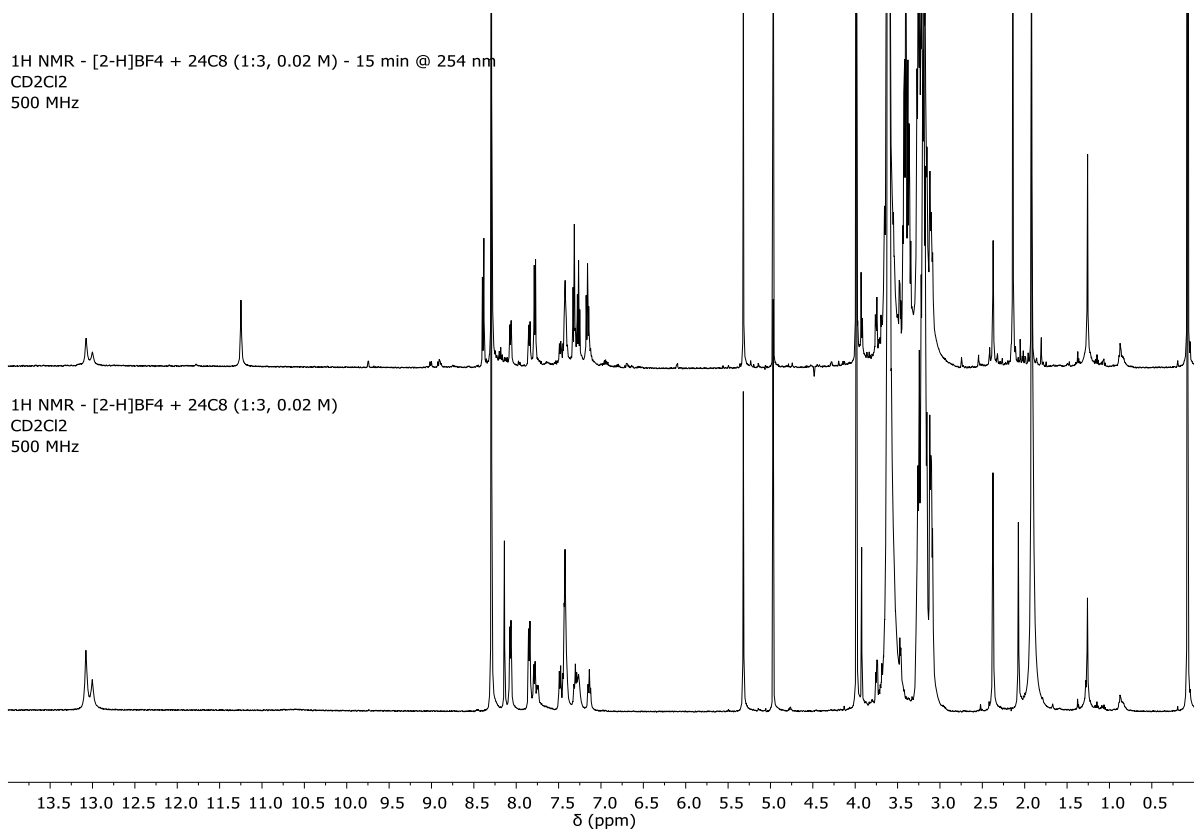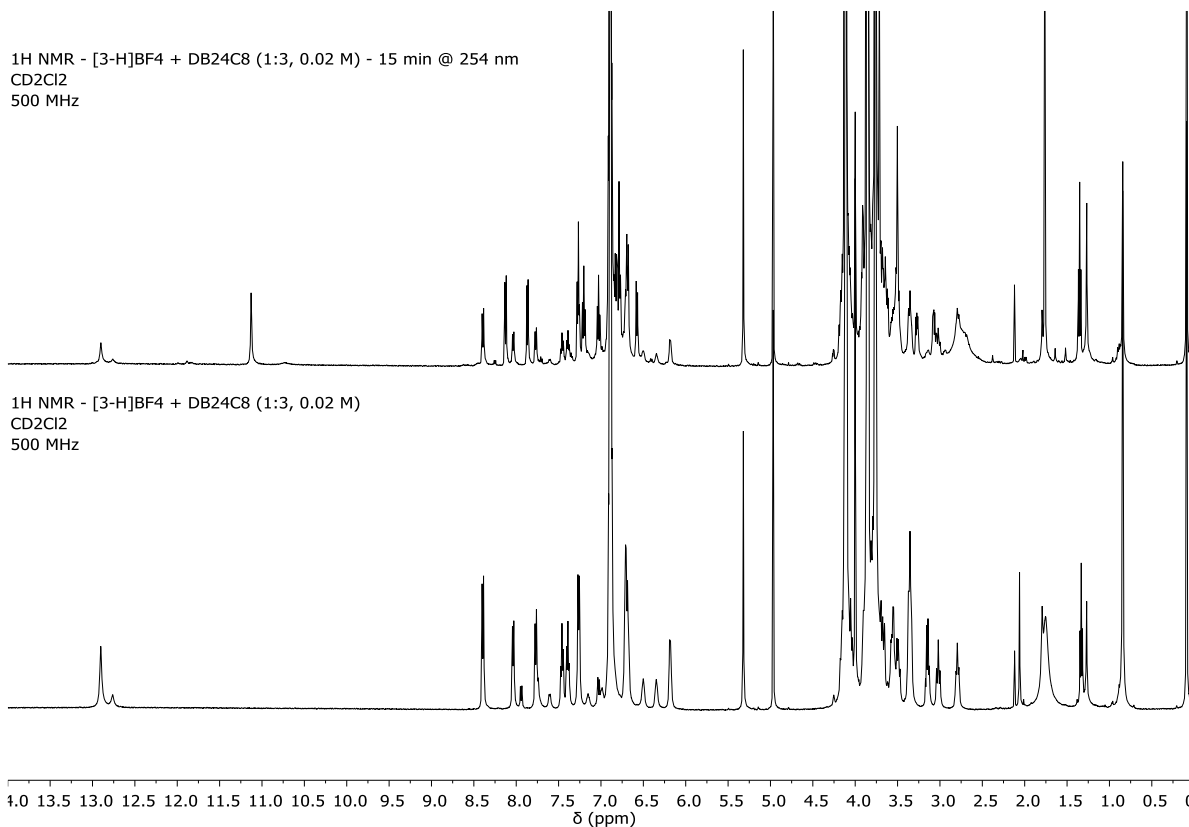CD2Cl2
500 MHz

Figure S32. ^{1}H NMR spectra of [**3o**–H⊂**24C8**]BF$_4$, before (bottom) and after (top) irradiation of the solution at 254 nm for 15 minutes (CD$_2$Cl$_2$, 500 MHz, 298 K).
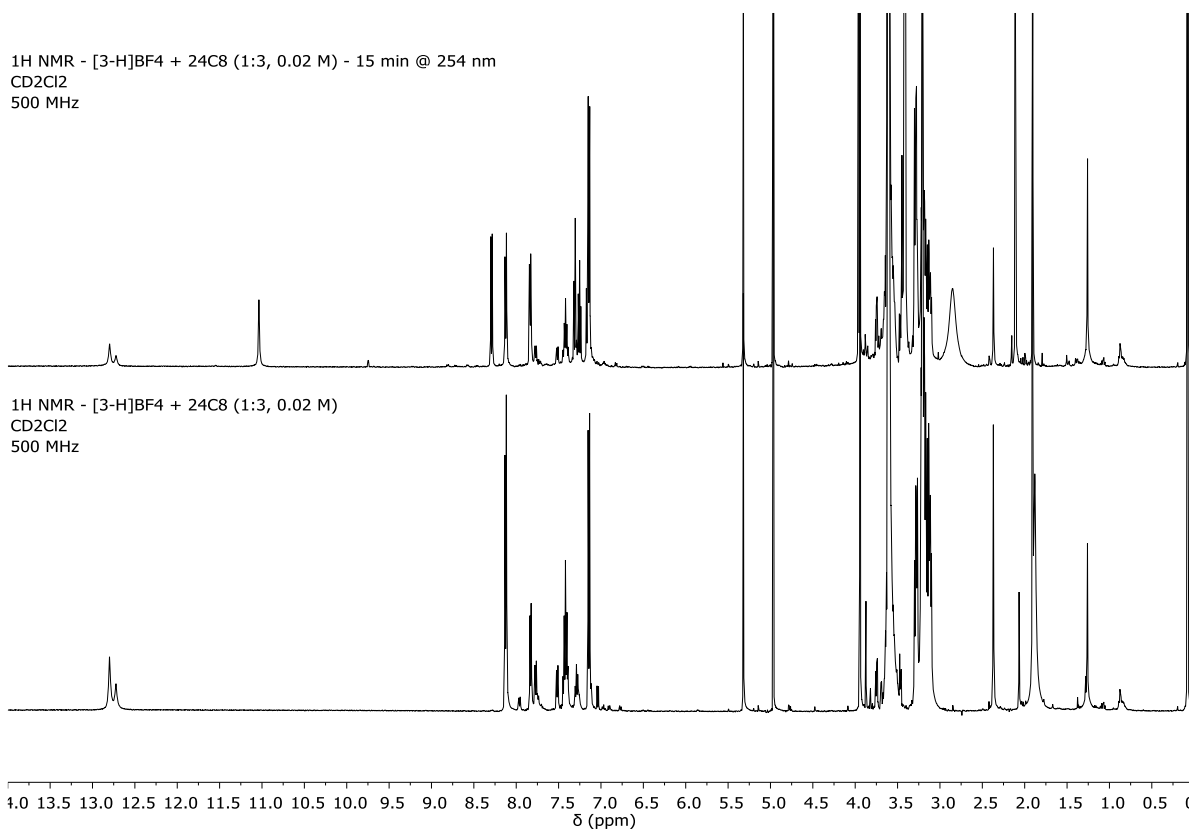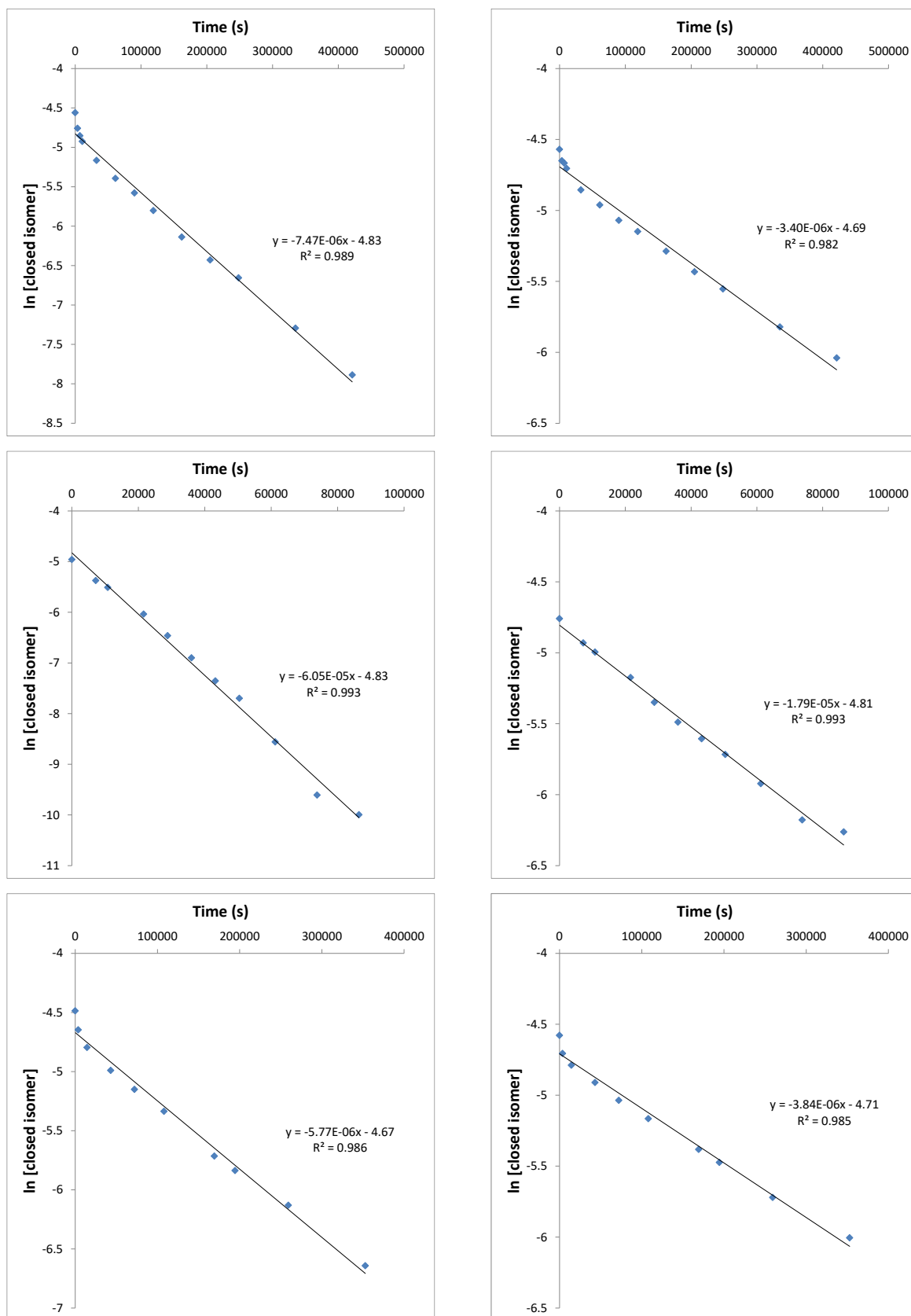
Kinetic studies of the thermal cycloreversion of the closed isomers of [2]pseudorotaxanes [**1-3c**– H⊂(**crown ether**)]BF$_4$ were performed by irradiating 0.02 M samples of axle and excess crown ether (3 equivalents) in CD$_2$Cl$_2$ for 15 minutes at 254 nm, in order to reach the maximum photoconversion, and then recording ^{1}H NMR spectra at increasing time intervals, while keeping the samples in the dark between measurements. The active concentration of the closed isomer of [2]pseudorotaxanes was determined by comparing the integral of the N*H* protons with a dibromomethane internal standard (4.97 ppm in CD$_2$Cl$_2$), and the rate constants were determined by linear fitting of the data into the integrated rate law of a first-order reaction.
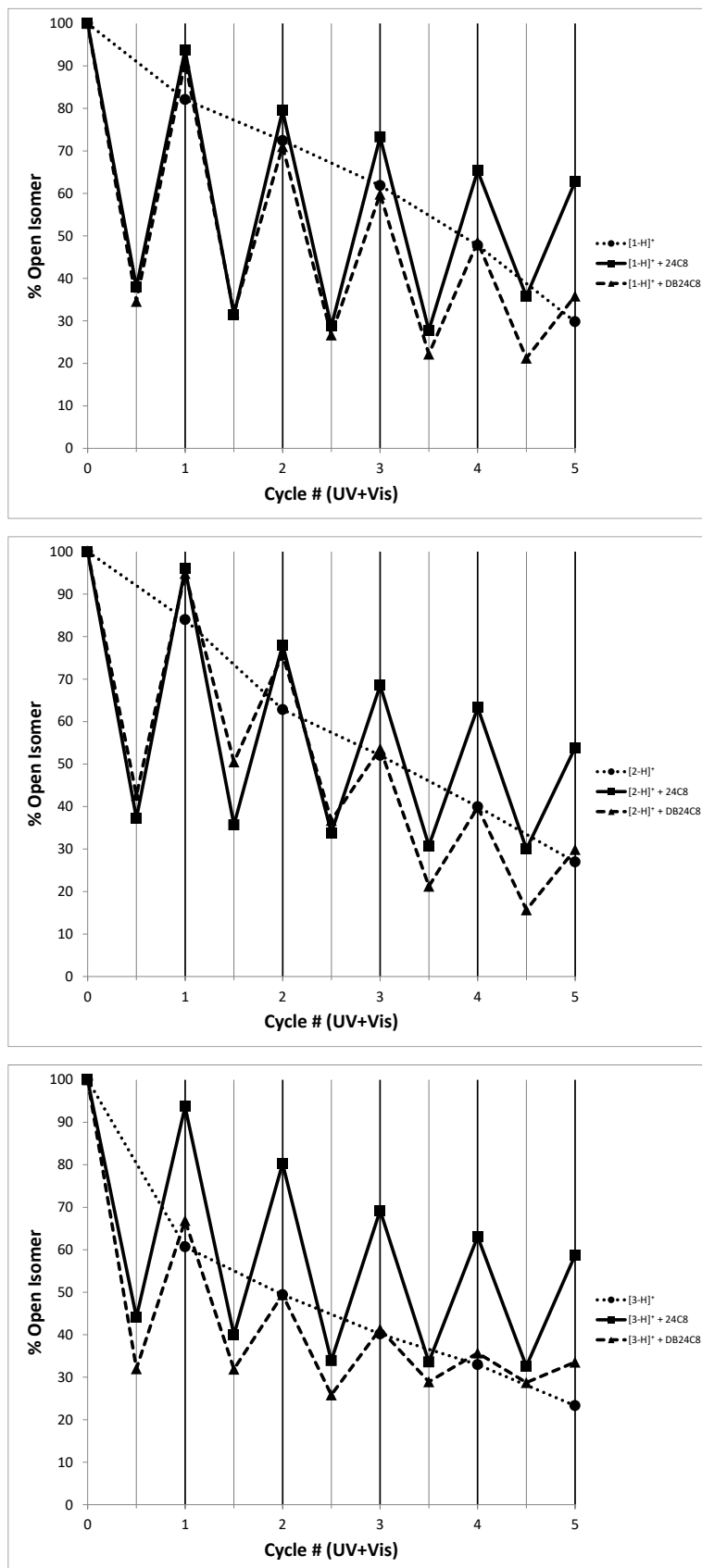
Fatigue resistance of the [2]pseudorotaxanes [**1-3o**–H⊂(**crown ether**)]BF$_4$ was investigated by alternating irradiation at 254 nm for 15 min and subsequently with white visible light for one minute over five cycles. The percentage of open isomer was determined after every irradiation event by comparison of the integral of the N*H* protons with a dibromomethane internal standard (4.97 ppm in CD$_2$Cl$_2$).

Axle	Macrocycle	% PC	$k\,(\text{s}^{-1})$	Half-life (h)
[**1o**–H]$^+$	**DB24C8**	52	7.47×10^{-6}	25.8
	24C8	52	3.40×10^{-6}	56.7
[**2o**–H]$^+$	**DB24C8**	43	6.05×10^{-5}	3.2
	24C8	38	1.79×10^{-5}	10.7
[**3o**–H]$^+$	**DB24C8**	51	5.77×10^{-6}	33.3
	24C8	56	3.84×10^{-6}	50.1

Table S5. Photoconversion percentages (% PC) of [2]pseudorotaxanes reached after irradiation with 254 nm light for 15 minutes, and first order cycloreversion rates (k) with corresponding half-life in hours measured by ^{1}H NMR experiments (CD$_2$Cl$_2$, axle and crown ether mixed in 1:3 ratio, 0.02 M, 298 K).

Chart S2. Linear fitting into the integrated first-order rate law of the thermal cycloreversion ^{1}H NMR data (CD$_2$Cl$_2$, 0.02 M, 500 MHz, 298 K) of the closed isomers of [2]pseudorotaxanes [**1o**–H⊂**DB24C8**]BF$_4$ (top left), [**1o**–H⊂**24C8**]BF$_4$ (top right), [**2o**–H⊂**DB24C8**]BF$_4$ (middle left), [**2o**–H⊂**24C8**]BF$_4$ (middle right), [**3o**–H⊂**DB24C8**]BF$_4$ (bottom left), and [**3o**–H⊂**24C8**]BF$_4$ (bottom right).

Chart S3. Fatigue resistance of [2]pseudorotaxanes [**1o**–H⊂(**crown ether**)]BF$_4$ (top), [**2o**–H⊂(**crown ether**)]BF$_4$ (middle), and [**3o**–H⊂(**crown ether**)]BF$_4$ (bottom) (●, dotted line: free axle; ▲, dashed line: **DB24C8**; ■, solid line: **24C8**) determined by ¹H NMR experiments (CD$_2$Cl$_2$, 0.02 M, 500 MHz, 298 K).

6. UV-VIS EXPERIMENTS

All spectroscopic measurements were performed in quartz cuvettes on air-equilibrated DCM (Uvasol) solutions at room temperature. UV-vis spectra were recorded either with Perkin Elmer Lambda750, Perkin Elmer Lambda650, Agilent Technologies Cary 300 or Varian Cary 50 Bio spectrophotometers. Emission spectra were recorded on Varian Cary Eclipse or Edinburgh FLS980 fluorescence spectrometers. Fluorescence lifetimes were measured with a time-correlated single photon counting, using a laser diode (320 nm, 340 nm, 360 nm) as excitation source.

Irradiation experiments were performed on air-equilibrated solutions, thoroughly stirred, at room temperature. A Hanau Q400 mercury medium pressure lamp (125 W), with an appropriate interference filter, or a fluorometer were used as sources of irradiation.

Stability considerations

Compounds [**1-3o**–H]BF$_4$ appeared to be unstable in the conditions of the UV-Vis spectroscopic experiments, *i.e.* UV grade dichloromethane, concentrations ranging from 10^{-4} to 10^{-6} M. In particular, the absorption changes observed during time suggest that the imidazolium unit undergoes a deprotonation reaction. In order to overcome this issue, neutral compounds **1-3o** were used, and protonated by means of trifluoromethanesulfonic acid (TfOH) as necessary. The clean and sharp absorption changes associated with the protonation reaction enable a full control on the protonation state of the compounds. Therefore, compounds [**1-3o**–H]OTf were prepared in situ just before performing the experiments, by adding a stoichiometric amount of trifluoromethanesulfonic acid (TfOH) to solutions of **1-3o**.

UV-Vis titrations

Spectrophotometric titrations were performed adding a concentrated solution of the host to a more diluted solution of the guest. The binding thermodynamic constants were obtained by fitting the absorbance changes at a single wavelength with software Bindfit,[S10] according to a 1:1 binding model.
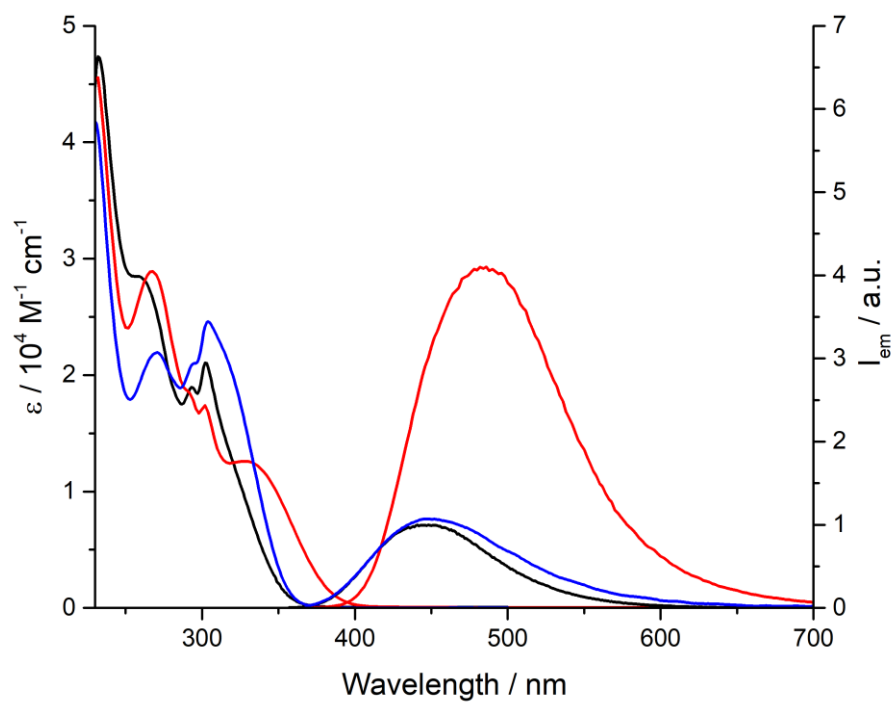
Figure S33. Absorption and emission spectra of compounds [**1o**–H]OTf (black), [**2o**–H]OTf (red), and [**3o**–H]OTf (blue) in CH_2Cl_2.
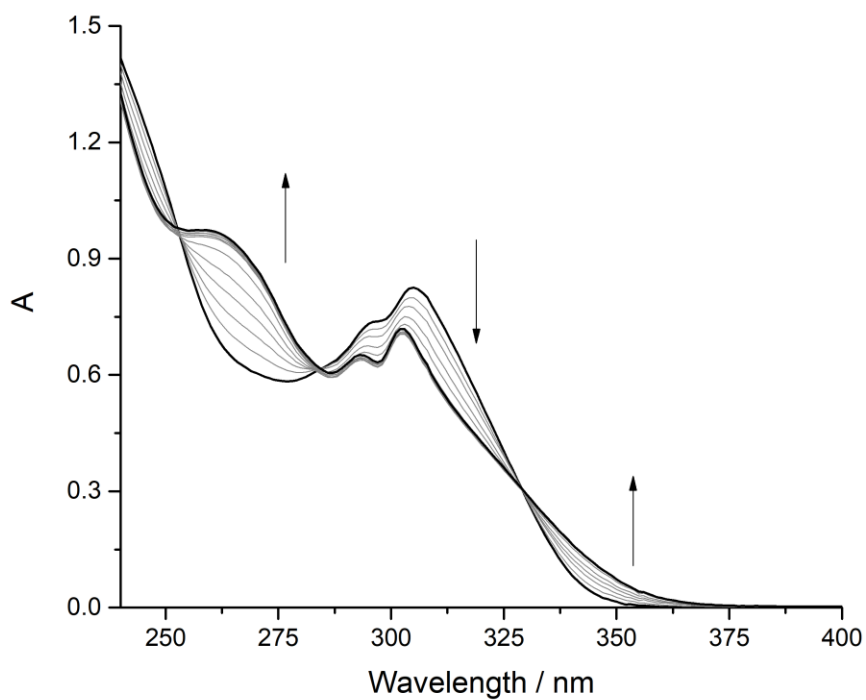
Figure S34. Absorption changes upon titration of a 3.0×10^{-5} M solution of **1o** with TfOH.
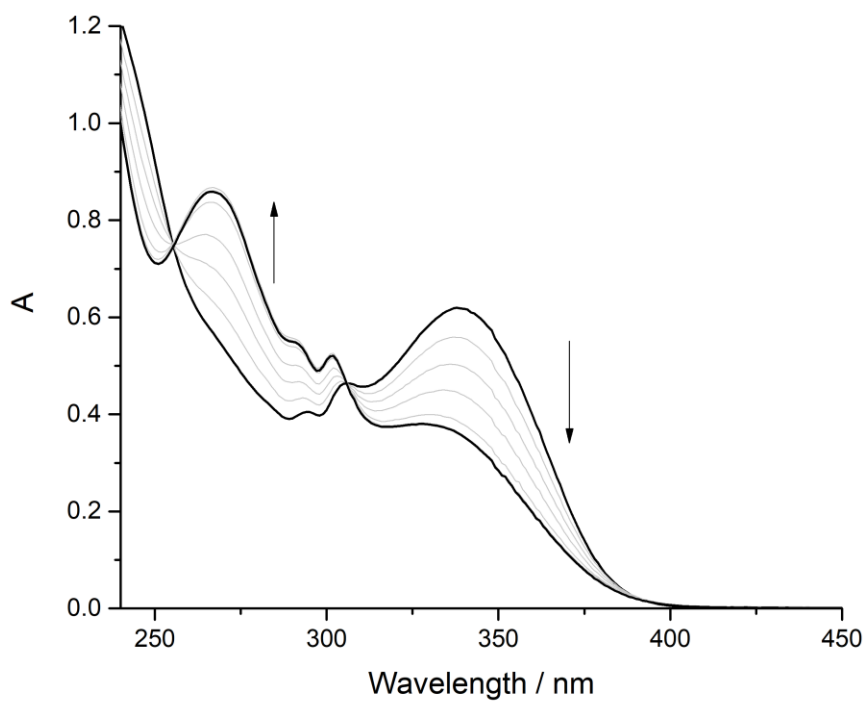
Figure S35. Absorption changes upon titration of a 4.5×10^{-5} M solution of **2o** with TfOH.

Figure S36. Absorption changes upon titration of a 6.0×10^{-5} M solution of **3o** with TfOH.

The formation of [2]pseudorotaxanes with the crown ethers **24C8** and **DB24C8** in CH_2Cl_2 solution was investigated by means of UV-Vis absorption spectroscopy. In all cases, similar absorption changes consistent with the formation of a complex between the axles and the macrocycles were observed. In some instances, the absorption changes are the opposite of the changes observed upon protonation of the neutral co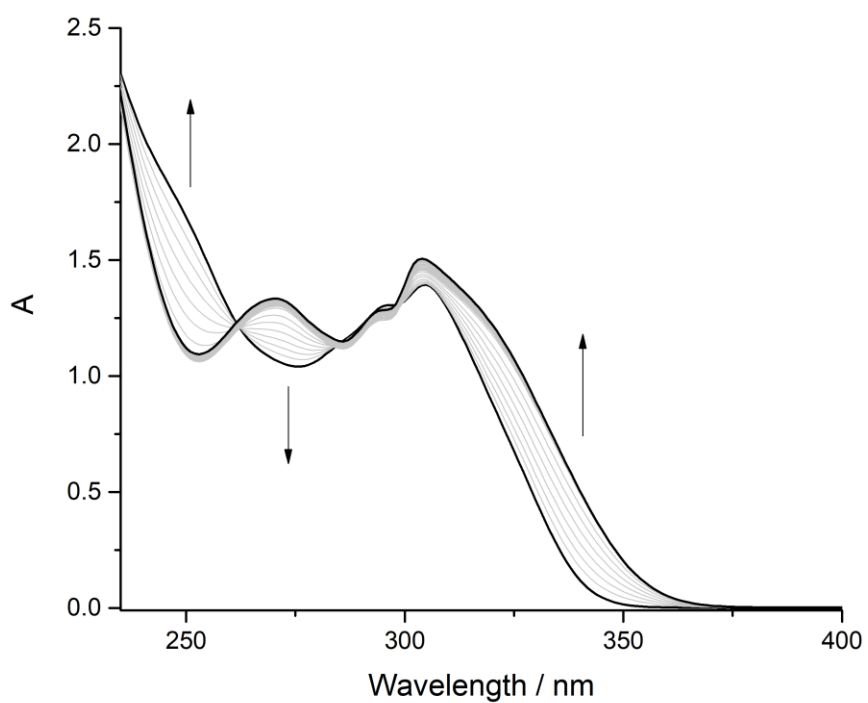mpounds with TfOH: this suggests that the proton on the imidazolium is now shared between the axle and the macrocycle. The emission bands of the open isomers are generally quenched and blue shifted upon complexation by the crown ethers.

A global analysis of the absorption spectra upon titration with crown ethers shows different trends at different wavelengths. This result would suggest that more complex equilibria might be involved, besides the 1:1 association process, *e.g.* the formation of adducts with more complex stoichiometry, or a competition between the crown and the axle for the proton. Nevertheless, these findings are not backed by the results of ^1H NMR experiments, which unequivocally evidence only the formation of a 1:1 complex. In order to reproduce the conditions of the ^1H NMR experiments, UV-Vis titrations were repeated on more concentrated solutions ($\sim 10^{-4}$ M), but no significant discrepancies were observed. In absence of other experimental evidence supporting the presence of other species involved in more complex equilibria, the simplest model was used to fit the data in the lower energy region of the absorption spectra, where the titration profiles are consistent with a 1:1 model.

For compounds [**1o**–H]$^+$ and [**3o**–H]$^+$, the values of the equilibrium constants follow the same trend observed in CH_3CN with ^1H NMR experiments: the most stable complex is formed between [**1o**–H]OTf and **24C8**, whereas the electron donating group on compound **3** reduces its acidity and weakens the hydrogen bonding interactions with the crown ethers. Compound [**2o**–H]OTf shows a different behavior with respect to the other compounds: first, the absorption changes associated to the protonation reaction of **2o** follow a different trend with respect to the other compounds, *i.e.* the lower energy band decreases upon addition of TfOH (Figure S35). As for the titration with crown ethers, the absorption changes are qualitatively similar to the ones of the other compounds, but it is not possible to find any region in the absorption spectrum where the titration can be fitted with a 1:1 model, therefore it is not possible to estimate the association constant (Figures S39-40). From a qualitative point of view, the [2]pseudorotaxanes containing compound [**2o**–H]$^+$ appear to be less stable than the other complexes. This observation is in contrast with the results obtained by ^1H NMR experiments, and is quite surprising in light of the electron-withdrawing nature of the methyl ester substituent. On the other hand, as also suggested by titrations with TfOH, the stronger acidity of [**2o**–H]OTf could promote other competing equilibria, in which the proton is either shared in higher stoichiometries complexes or captured by the crown ether.
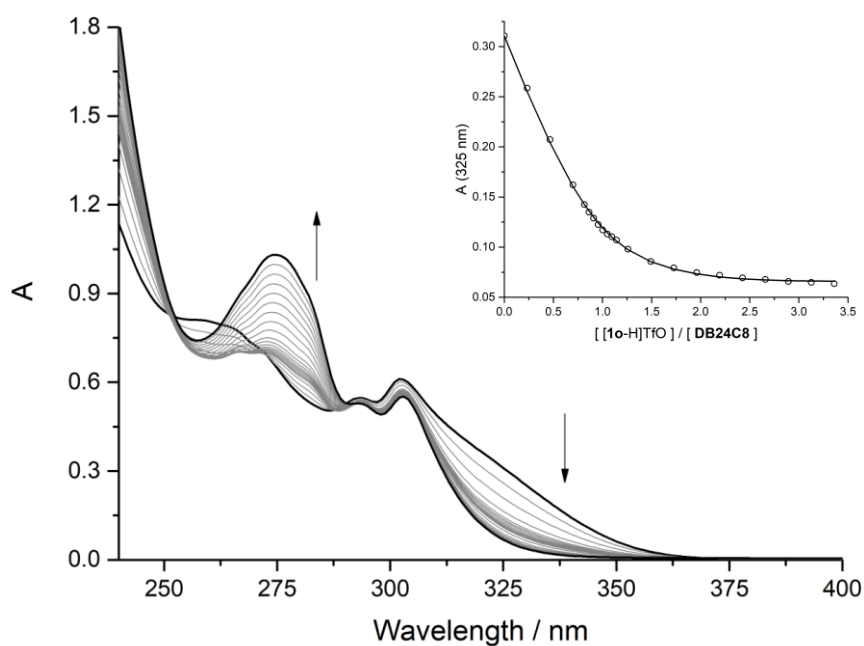
Figure S37. Absorption changes upon titration of a 3.0×10^{-5} M solution of [**1o**–H]OTf with **DB24C8**. The inset shows the titration profile in the lower energy region of the spectrum (empty circles) and the fitting of the experimental data with a 1:1 model (solid line).
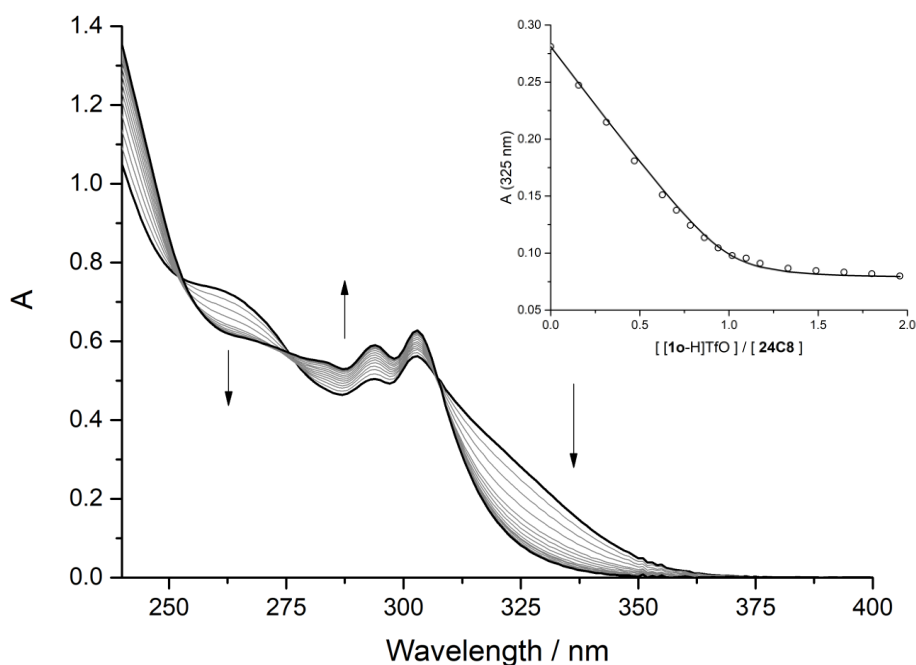
Figure S38. Absorption changes upon titration of a 2.6×10^{-5} M solution of [**1o**–H]OTf with **24C8**. The inset shows the titration profile in the lower energy region of the spectrum (empty circles) and the fitting of the experimental data with a 1:1 model (solid line).
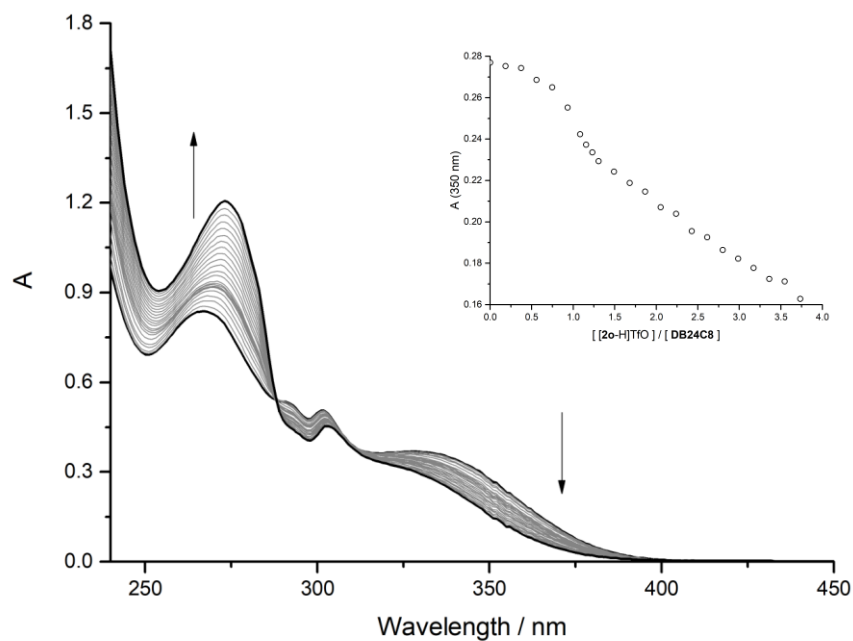
Figure S39. Absorption changes upon titration of a 3.0×10^{-5} M solution of [**2o**–H]OTf with **DB24C8**. The inset shows the titration profile in the lower energy region of the spectrum (empty circles).

Figure S40. Absorption changes upon titration of a 4.5×10^{-5} M solution of [**2o**–H]OTf with **24C8**. The inset shows the titration profile in the lower energy region of the spectrum (empty circles).
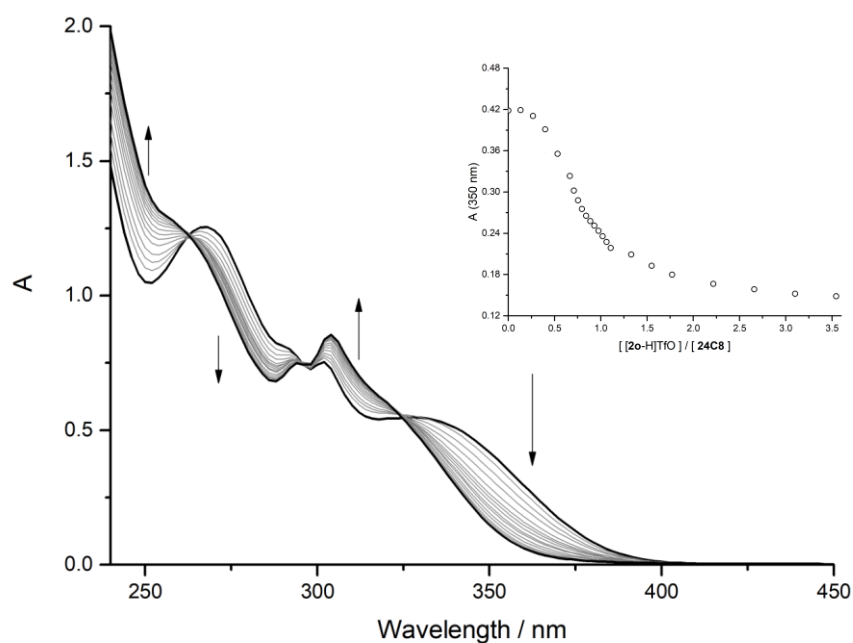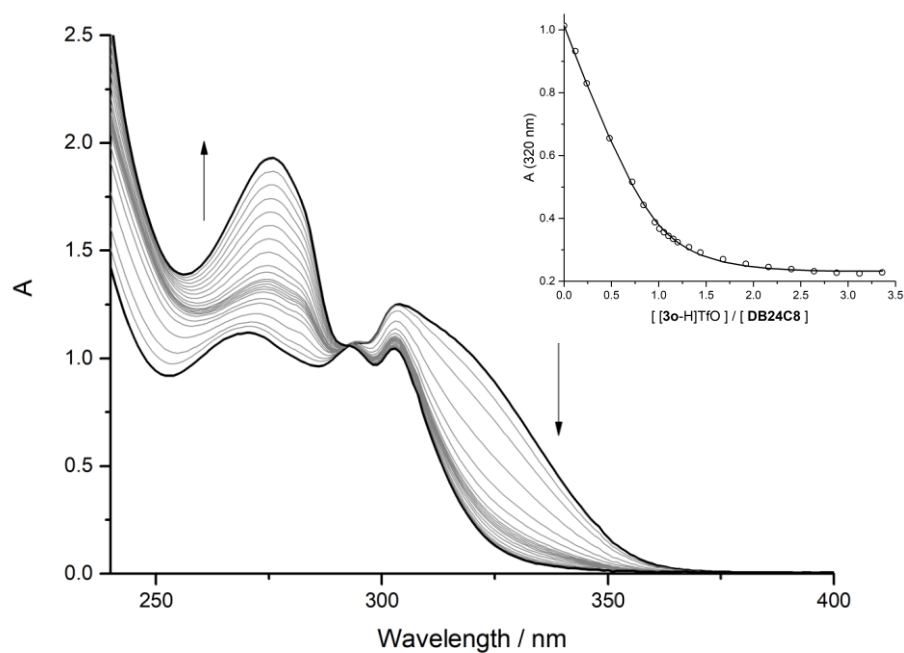
Figure S41. Absorption changes upon titration of a 6.0×10^{-5} M solution of [**3o**–H]OTf with **DB24C8**. The inset shows the titration profile in the lower energy region of the spectrum (empty circles) and the fitting of the experimental data with a 1:1 model (solid line).

Figure S42. Absorption changes upon titration of a 6.0×10^{-5} M solution of [**3o**–H]OTf with **24C8**. The inset shows the titration profile in the lower energy region of the spectrum (empty circles) and the fitting of the experimental data with a 1:1 model (solid line).
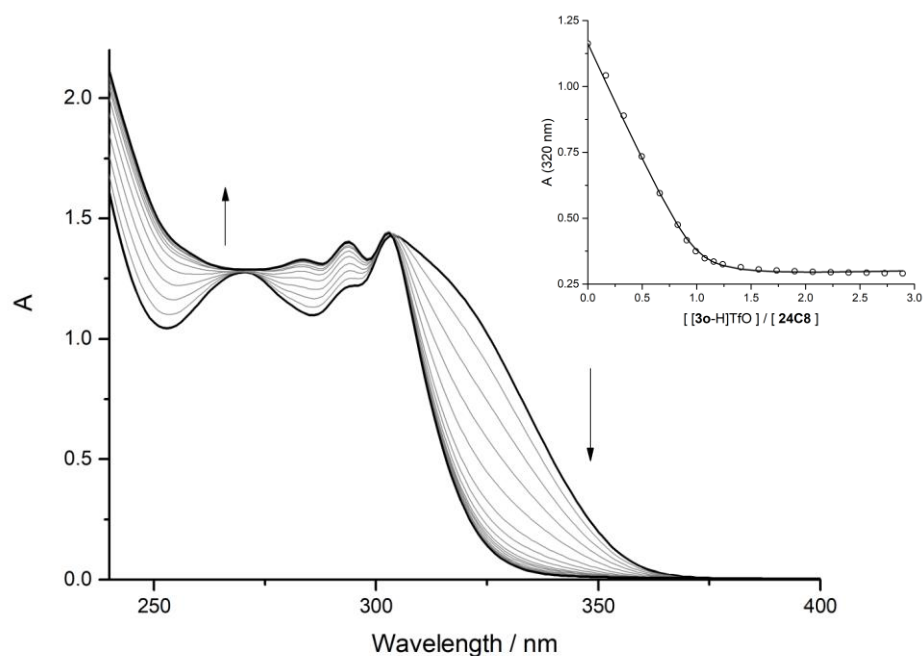
	DB24C8	24C8
$[\mathbf{1o}-H]^+$	2.9×10^5 M^{-1}	2.3×10^6 M^{-1}
$[\mathbf{2o}-H]^+$	NA	NA
$[\mathbf{3o}-H]^+$	2.5×10^5 M^{-1}	9.7×10^5 M^{-1}

Table S6. K_a values determined by UV-Vis titrations in CH$_2$Cl$_2$ (2.6-6.0 $\times$ 10^{-5} M, 298 K) assuming a 1:1 host-guest association model.


Irradiation experiments

All the axles [**1-3**–H]$^+$ exhibit low fatigue resistance: after prolonged irradiation the shape of the absorption spectra changes and the isosbestic points are not maintained anymore. It is likely that on prolonged irradiation a photoproduct of the closed isomer is formed, which absorbs in the visible region and is still present after the cycloreversion reactions. In general, the irradiation time that enables to reach the maximum extent of photoconversion (t$_{max}$) is determined by irradiating the samples for short intervals and checking the absorption spectrum after each interval.

The maximum percentage of photoconversion was estimated by measuring the extent of quenching of the luminescence of the open isomer upon isomerization from the open to the closed isomer. In order to evaluate the photoconversion percentage the samples were irradiated for t$_{max}$ and the emission spectra was measured before and after irradiation. Two experimental setups were used, depending on the rate of the thermal cycloreversion reactions: for the majority of the experiments two samples of the same compound were irradiated for t$_{max}$ with a medium pressure Hg lamp with the appropriate interference filter, and absorption or luminescence spectra were recorded before and after irradiation on the two samples, respectively. For compound [**2o**–H]OTf, which reverts too fast to collect the spectra after irradiation, the sample was irradiated directly inside the spectrofluorimeter, and the emission spectra was recorded simultaneously. The cycloreversion kinetics were fitted according to a zero-order or first-order kinetic model.
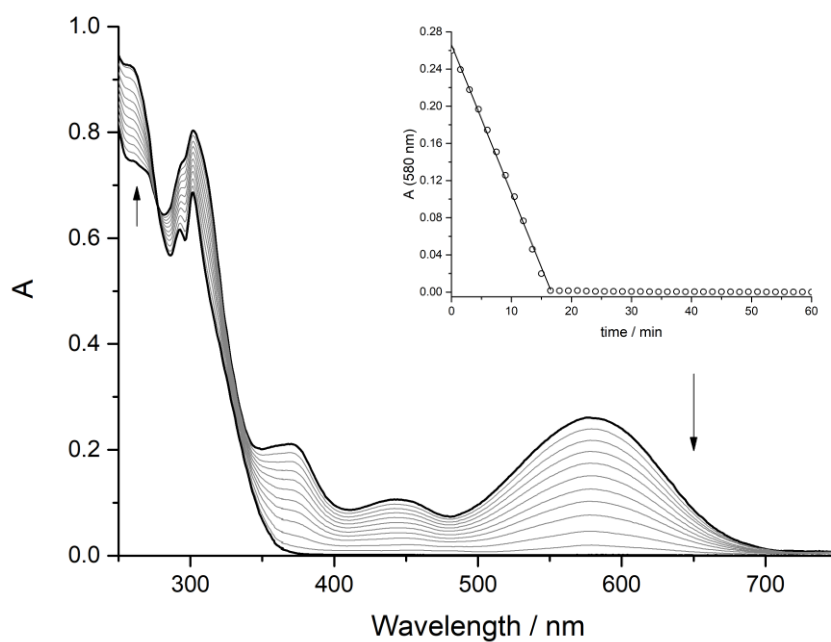
Figure S43. Absorption spectra showing the thermal cycloreversion of [**1c**–H]OTf, obtained after irradiation at 313 nm of a 3.2×10^{-5} M solution of [**1o**–H]OTf. The inset shows the plot of the absorption changes at 580 nm in time (white circles) and the fitting of the experimental data with a zero order kinetic model (solid line).
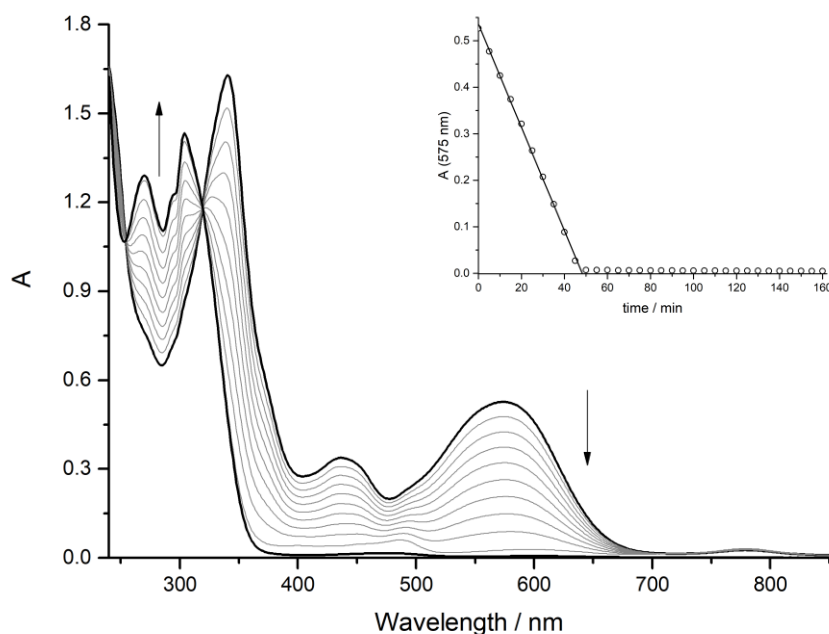
Figure S44. Absorption spectra showing the thermal cycloreversion of [**3c**–H]OTf, obtained after irradiation at 313 nm of a 6.0×10^{-5} M solution of [**3o**–H]OTf. The inset shows the plot of the absorption changes at 575 nm in time (white circles) and the fitting of the experimental data with a zero order kinetic model (solid line).

Mixtures of axles and crown ethers were irradiated with UV light in order to assess if and how the [2]pseudorotaxane formation affects the photoisomerization of the terarylenes and the thermal stability of the closed isomers, and, conversely, if the photoisomerization of the terarylenes affects the stability of the complexes. UV-Vis studies were performed on 1:1 mixtures of axles and crown ethers, which were irradiated with UV light, and the thermal cycloreversion reaction was followed at room temperature. In all cases, the same stability issues of the free axles were observed, *i.e.* degradation occurs upon prolonged irradiation. Therefore, the same precautions as for the free axles were taken when irradiating the pseudorotaxane solutions: the irradiation was kept up to the maximum conversion and stopped before any significant photodegradation occurred. The results of UV-Vis spectroscopic studies of [2]pseudorotaxanes are summarized in Table S7.

Pseudorotaxanes [**1o**–H⊂**24C8**]$^+$ and [**1o**–H⊂**DB24C8**]$^+$ photoisomerize to the closed forms with percentages of conversion similar to those observed for the free axles. The bands in the visible region ascribed to the closed isomers are slightly different from the corresponding bands of the free axles, suggesting that the closed isomers are still associated with the crown ethers. In the case of [**1o**–H⊂**24C8**]$^+$, the thermal cycloreversion reaction was completed within 30 minutes, and the kinetic profile was fitted with a first order model. In the case of [**1o**–H⊂**DB4C8**]$^+$ the thermal cycloreversion reaction follows a zero order kinetics at any concentration, but it is slowed down with respect to the free axle; the same results are obtained in presence of an excess of **DB24C8** up to 3 equivalents. Similar results were obtained with [**3o**–H⊂**24C8**]$^+$ and [**3o**–H⊂**DB24C8**]$^+$, *i.e.* the thermal cycloreversion reactions follow zero order kinetics, with rate constants slightly lower than the free axle and similar percentage of conversion to the free axle. On the other hand, compound [**2o**–H]$^+$ underwent a significant improvement in photochemical properties upon complexation: both [**2o**–H⊂**24C8**]$^+$ and [**2o**–H⊂**DB24C8**]$^+$ could be photoisomerized to the respective closed forms, which were fairly stable, and the photoconversion percentage increased from 30% up to 75%. The back thermal cycloreversion reactions are completed after 2 and 4 hours, respectively, and are compatible with a first order mechanism (Figures S47-48).

Some of the irradiation experiments were repeated at larger concentrations, in order to mimic the ^{1}H NMR experimental conditions as much as possible: the thermal cycloreversion reaction of a 4×10^{-4} M solution of [**1o**–H⊂**24C8**]$^+$ was shown to follow a zero order kinetic. In the case of [**2o**–H⊂**DB24C8**]$^+$, better results were obtained in presence of an excess of **DB24C8** (>3 equivalents), *i.e.* the fitting of the kinetic curve is better with respect to a 1:1 mixture of axle and macrocycle. This finding is not surprising, considering the shape of the titration curve of [**2o**–H]$^+$ with **DB24C8** (Figure S39), suggesting that the formation of this complex is heavily affected by the intrinsic higher acidity of the methyl ester-substituted [**2o**–H]$^+$, if compared to the other axles. Particularly, the dissociation of [**2o**–H]$^+$ to yield the free base **2o** cannot be neglected at the low concentrations

utilized in these UV-Vis experimental conditions. It is possible that, at lower ratios of crown ether to axle, a complete association cannot be achieved, and contributions from free [**2o**–H]OTf and **2o** cannot be completely ruled out.

The fact that the thermal cycloreversion reactions of the [2]pseudorotaxanes depend on the absolute concentration and/or on the relative ratio of the molecular components supports the hypothesis that multiple processes occur in the complexation reaction. In particular, these processes could involve the competition of the crown ethers with imidazolium and/or imidazolinium for the proton. It is worth recalling that in the imidazolinium moiety, which is formed upon isomerization, the positive charge is more confined than in the imidazolium: therefore, the protons should be more acidic, and the hydrogen bonding more efficient. On the other hand, at the low concentrations utilized for the UV-Vis experiments, other competing processes could arise, such as ion pairing, or, as mentioned above, more complex equilibria, wherein the proton is either shared in higher-stoichiometry complexes or taken-up by the crown ethers. All these competing equilibria are concentration dependent and could also be influenced by the nature of the counterions.
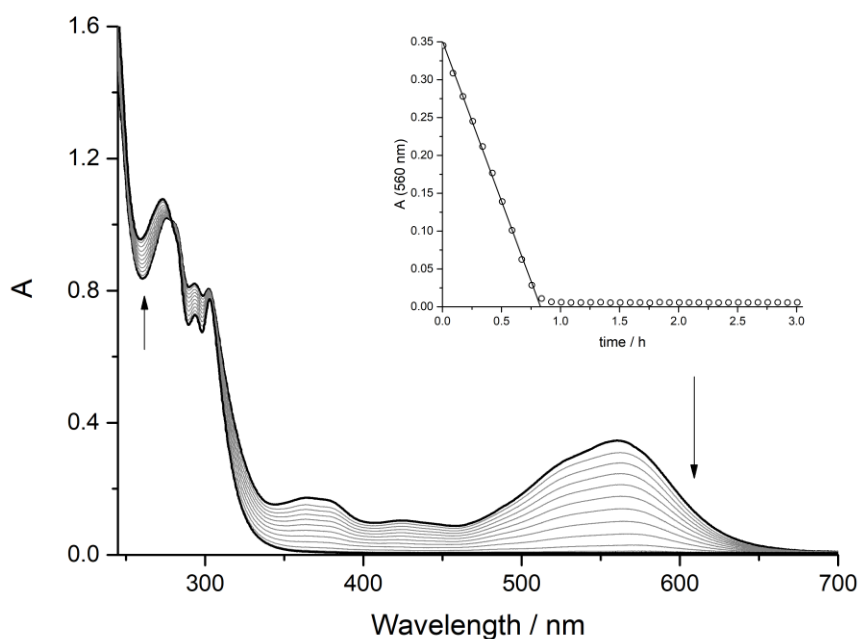
Figure S45. Absorption spectra showing the thermal cycloreversion of [**1c**–H]OTf in presence of **DB24C8**, obtained after irradiation at 313 nm of a 3.5×10^{-5} M solution of a 1:1 mixture of [**1o**–H]OTf and **DB24C8**. The inset shows the plot of the absorption changes at 560 nm in time (white circles) and the fitting of the experimental data with a zero order kinetic model (solid line).
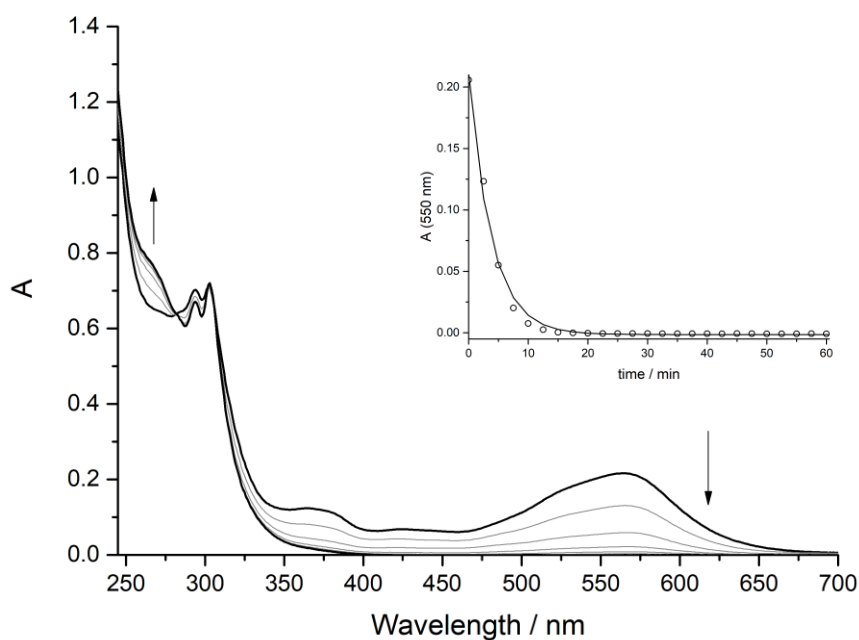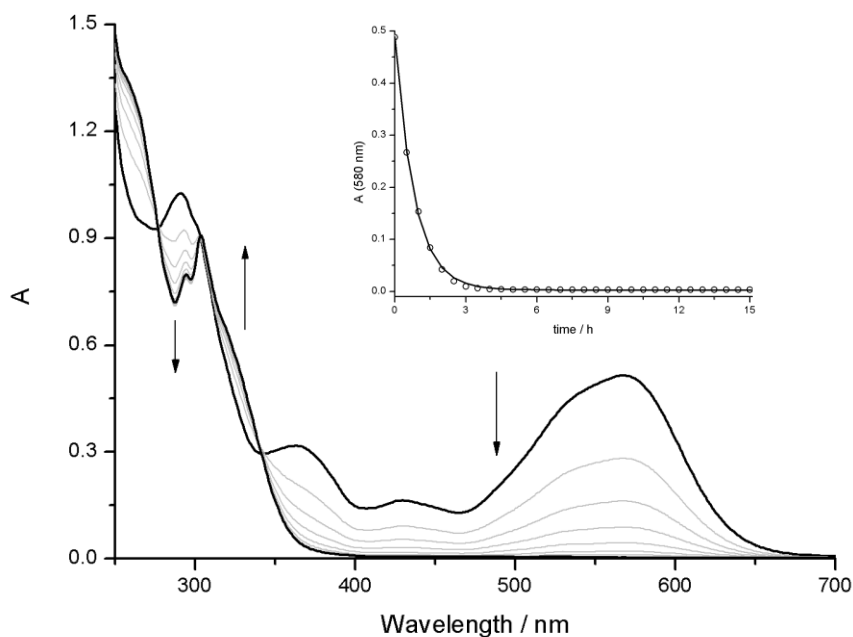
Figure S46. Absorption spectra showing the thermal cycloreversion of [**1c**–H]OTf in presence of **24C8**, obtained after irradiation at 313 nm of a 3.0×10^{-5} M solution of a 1:1 mixture of [**1o**–H]OTf and **24C8**. The inset shows the plot of the absorption changes at 550 nm in time (white circles) and the fitting of the experimental data with a first order kinetic model (solid line).
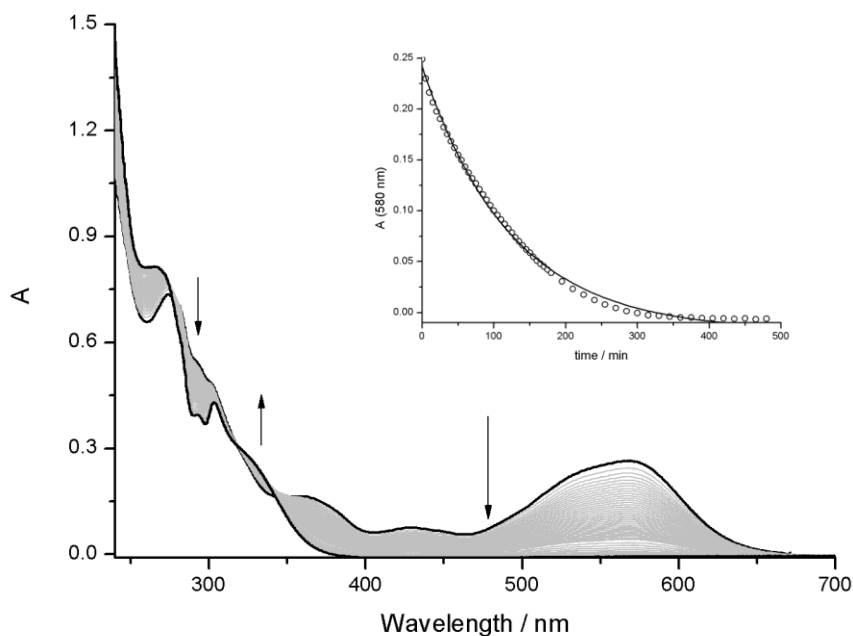
Figure S47. Absorption spectra showing the thermal cycloreversion of [**2c**–H]OTf in presence of **DB24C8**, obtained after irradiation at 313 nm of a 3.0×10^{-5} M solution of a 1:1 mixture of [**2o**–H]OTf and **DB24C8**. The inset shows the plot of the absorption changes at 580 nm in time (white circles) and the fitting of the experimental data with a first order kinetic model (solid line).
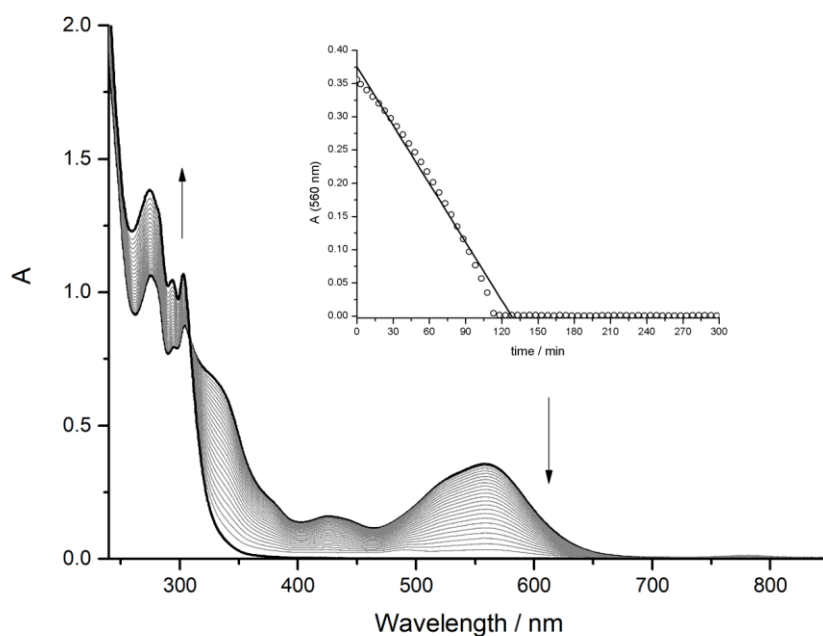
Figure S48. Absorption spectra showing the thermal cycloreversion of [**2c**–H]OTf in presence of **24C8**, obtained after irradiation at 313 nm of a 4.5×10^{-5} M solution of a 1:1 mixture of [**2o**–H]OTf and **24C8**. The inset shows the plot of the absorption changes at 580 nm in time (white circles) and the fitting of the experimental data with a first order kinetic model (solid line).
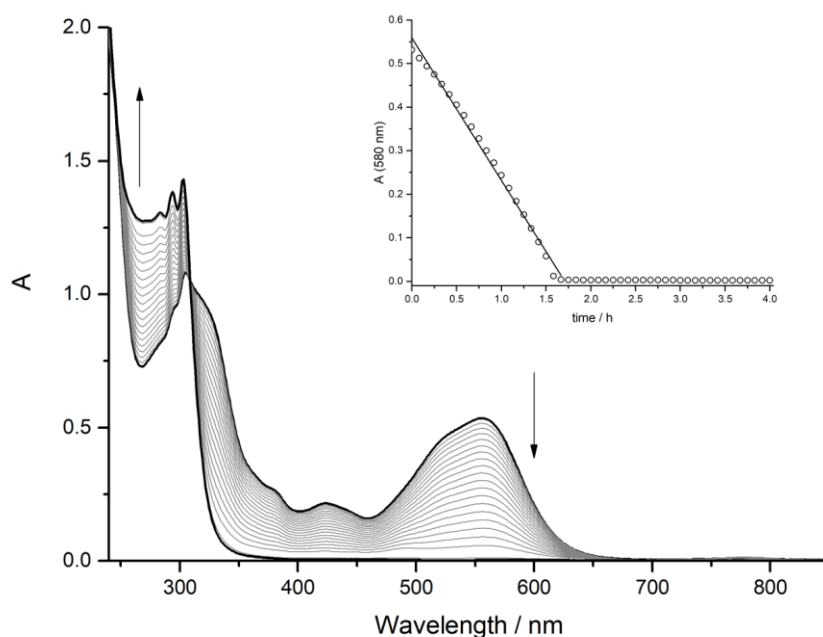

Figure S49. Absorption spectra showing the thermal cycloreversion of [**3c**–H]OTf in presence of **DB24C8**, obtained after irradiation at 313 nm of a 6.0×10^{-5} M solution of a 1:1 mixture of [**3o**–H]OTf and **DB24C8**. The inset shows the plot of the absorption changes at 560 nm in time (white circles) and the fitting of the experimental data with a zero order kinetic model (solid line).

Figure S50. Absorption spectra showing the thermal cycloreversion of [**3c**–H]OTf in presence of **24C8**, obtained after irradiation at 313 nm of a 6.0×10^{-5} M solution of a 1:1 mixture of [**3o**–H]OTf and **24C8**. The inset shows the plot of the absorption changes at 580 nm in time (white circles) and the fitting of the experimental data with a zero order kinetic model (solid line).

Axle	Macrocycle	$\lambda_{abs}{}^a$, $\varepsilon/M^{-1}cm^{-1}$	$\lambda_{em}{}^b$, Φ^c	% PC^d	$k_{tc}{}^e$ (reaction order)
	—	302, 21000	450, 0.10	56	1.8×10^{-8} Ms^{-1} (0)
[**1o**–H]$^+$	**24C8**		440, 0.05	48	4.3×10^{-3} s^{-1} (1)
	DB24C8		400, 0.41	53	8.3×10^{-9} Ms^{-1} (0)
	—	328, 12600	480, 0.41	30	NA^f
[**2o**–H]$^+$	**24C8**		450, 0.16	74	3.4×10^{-4} s^{-1} (1)
	DB24C8		470, 0.17	50	1.3×10^{-4} s^{-1} (1)
	—	304, 24600	430, 0.11	80	1.7×10^{-8} Ms^{-1} (0)
[**3o**–H]$^+$	**24C8**		370, 0.07	76	7.9×10^{-9} Ms^{-1} (0)
	DB24C8		430, 0.10	61	4.5×10^{-9} Ms^{-1} (0)

Table S7. Summary of irradiation studies: ^{a} maximum absorption wavelength of the lower energy band; ^{b} emission wavelength; ^{c} emission quantum yield; ^{d} maximum percentage of conversion upon photoisomerization; ^{e} rate constant of the thermal cycloreversion reactions; ^{f} not available.

7. REFERENCES

[S1] Kawai, S.; Nakashima, T.; Kutsunugi, Y.; Nakagawa H.; Nakanob, H.; Kawai, T. *J. Mater. Chem.* **2009**, *19*, 3606–3611.

[S2] El Yahyaoui, A.; Felix, G.; Heynderickx, A.; Moustrou, C.; Samat A. *Tetrahedron* **2007**, 63, 9482–9487.

[S3] Williams, D. B. G.; Lawton, M. *J. Org. Chem.* **2010**, *75*, 8351–8354.

[S4] Bruker, SAINT+ and SADABS. Bruker AXS Inc., Madison, Wisconsin, USA, 2012.

[S5] O. V. Dolomanov, L. J. Bourhis, R. J. Gildea, J. A. K. Howard, H. Puschmann, *J. Appl. Cryst.* **2009**, *42*, 339–341.

[S6] G. M. Sheldrick, *Acta Cryst.* **2015**, *C71*, 3–8.

[S7] Diamond® - Crystal and Molecular Structure Visualization - Crystal Impact - Dr. H. Putz & Dr. K. Brandenburg GbR, Kreuzherrenstr. 102, 53227 Bonn, Germany (http://www.crystalimpact.com/diamond).

[S8] Bruker, TopSpin 3.5. Bruker BioSpin GmbH, Rheinstetten, Germany.

[S9] J. C. Cobas, M. Martin-Pastor, EXSYCalc Ver 1.0; Mestrelab Research, Coruña, Spain, 2007.

[S10] http://supramolecular.org.